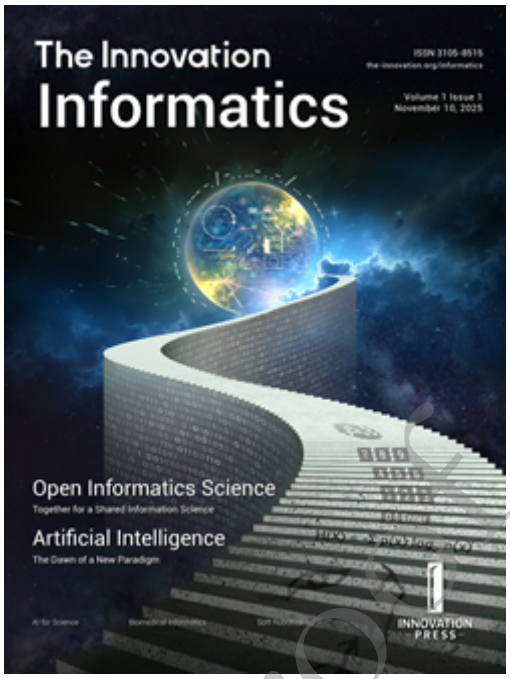

A dual-role solid calibration strategy for Chang'E-7 LUWA: Onboard CO_2 referencing and ground-based $H_2O/\delta D$ validation

Journal:	*The Innovation Informatics*
Manuscript ID	TII-2026-0006.R3
Manuscript Type:	Article
Keywords:	Chang'E-7, LUnar soil Water molecule Analyzer (LUWA), Hydrogen isotope measurement, Multi-payload detection framework, Lunar polar water ice
Speciality:	Spectroscopic Informatics < Optics and Optoelectronics, Remote Sensing Sensors < Optics and Optoelectronics

A dual-role solid calibration strategy for Chang'E-7 LUWA: Onboard CO_2 referencing and ground-based H_2O/δD validation

Rui Chen,[1,2,8] Xiang Li,[2,8] Wenzhen Lu,[1,2] Yi Xu,[1] Nailiang Cao,[2] Hejiu Hui,[3] Qiquan Yang,[4] Waikei Ng,[1] Xiaoping Zhang,[1] Kan Chen,[2] Zhenping Sui,[2,5] Zhenyu Xu,[2] Xindong Meng,[1] Renrui Liu,[1] Honkuan Wong,[1] Rongji Li,[2] Yun Qin,[1] Ling Zhang,[6] Ruifeng Kan,[2] Meiru Guo,[7] and Rui Gao[6]

*Correspondence: yixu@must.edu.mo (Y.X.); nlcao@aiofm.ac.cn (C.N.)

(The title should contain no more than **130** characters, including spaces.)

GRAPHICAL ABSTRACT

PUBLIC SUMMARY

- Chang'E-7's LUnar soil Water molecule Analyzer (LUWA) will measure lunar polar water and hydrogen isotopes.
- Solid materials were developed to release CO_2 or H_2O under vacuum with modest heating.
- Ag_2CO_3 enables repeated onboard CO_2 referencing through controlled partial gas release.
- Traceable $Cu(OH)_2$ provides an H_2O and hydrogen-isotope reference for ground calibration.
- These solid references support calibration of LUWA water and hydrogen-isotope measurements.

Key Words： Chang'E-7, LUnar soil Water molecule Analyzer (LUWA), Hydrogen isotope measurement, Multi-payload detection framework; Lunar polar water ice

A dual-role solid calibration strategy for Chang'E-7 LUWA: Onboard CO_2 referencing and ground-based H_2O/δD validation

Rui Chen,[1,2,8] Xiang Li,[2,8] Wenzhen Lu,[1,2] Yi Xu,[1] Nailiang Cao,[2] Hejiu Hui,[3] Qiquan Yang,[4] Waikei Ng,[1] Xiaoping Zhang,[1] Kan Chen,[2] Zhenping Sui,[2,5] Zhenyu Xu,[2] Xindong Meng,[1] Renrui Liu,[1] Honkuan Wong,[1] Rongji Li,[2] Yun Qin,[1] Ling Zhang,[6] Ruifeng Kan,[2] Meiru Guo,[7] and Rui Gao[6]

[1]The State Key Laboratory of Lunar and Planetary Science/Space Science Institute, Macau University of Science and Technology, Macau 999078, China
[2]Anhui Institute of Optics and Fine Mechanics, Hefei Institutes of Physical Science, Chinese Academy of Sciences, Hefei 230031, China
[3]The State Key Laboratory of Critical Earth Material Cycling and Mineral Deposits & Lunar and Planetary Science Institute, School of Earth Sciences and Engineering, Nanjing University, Nanjing 210023, China
[4]College of Surveying & Geo-Informatics, Tongji University, Shanghai 200092, China
[5]Jianghuai Advance Technology Center, Hefei 230000, China
[6]School of Earth Science and Engineering, Sun Yat-Sen University, Guangzhou 510275, China
[7]Lanzhou Institute of Physics, CAST, Lanzhou 730000, China
[8]The authors have the same contribution
[*]**Correspondence: yixu@must.edu.mo (Y.X.); nlcao@aiofm.ac.cn (C.N.)**

ABSTRACT

Lunar polar water ice is a key target of the Chang'E-7 mission because its abundance, physical state, and origin remain insufficiently constrained. Within the Chang'E-7 multi-payload framework, the LUnar soil Water molecule Analyzer (LUWA) is designed to measure H_2O abundance and hydrogen isotopic composition in permanently shadowed regions. Reliable measurements require calibration compatible with high vacuum, low power consumption, limited sealing capability, and restricted heating temperatures, conditions under which conventional gas- and liquid-phase standards are poorly suited. Here, we develop and validate two complementary solid reference materials for LUWA. Vacuum thermogravimetric analysis showed that Ag_2CO_3 and $Cu(OH)_2$ decompose at approximately 100-120 °C, releasing CO_2 and H_2O, respectively. Spectroscopic and mass-spectrometric measurements identified the expected dominant signals, with no obvious interfering gaseous species detected within the measured ranges. In the current LUWA implementation, Ag_2CO_3 was selected as the onboard CO_2 reference material for in situ calibration, whereas traceable $Cu(OH)_2$ was developed primarily for ground-based H_2O and δD calibration, prototype testing, end-to-end validation, and controlled regolith-simulant experiments. $Cu(OH)_2$ synthesized from precursor waters with known δD values preserved the mean isotopic information of the water source, with absolute differences between precursor-water and solid-derived vapor means within 10‰. Independent Cr-EA/IRMS measurements further supported the isotope-measurement workflow. Beyond its current role, traceable $Cu(OH)_2$ can serve as a solid isotope standard for validating heating, gas release, transfer, pressure measurement, and spectroscopic or mass-spectrometric detection. It also provides a controllable H_2O and δD source for regolith simulants with known water contents and for future characterization of adsorption–desorption memory effects, baseline drift, and pressure-dependent isotope response. With further storage, contamination-control, and flight-qualification studies, $Cu(OH)_2$-type materials may support future planetary payloads requiring controlled H_2O and hydrogen-isotope references. Together, these results establish a dual-role solid calibration strategy for LUWA.

-INTRODUCTION

The significance of lunar water exploration

Lunar water serves two fundamental roles. Scientifically, it provides critical insights into the Moon's evolutionary history. As a key volatile, water records the delivery of extraterrestrial materials from multiple sources and constrains the thermal and geochemical evolution of the lunar interior and surface. As a resource, it enables sustainable bases through in-situ resource utilization (ISRU), reduces the costs of deep-space mission, and promotes the development of a cislunar economy. The Moon

was initially regarded as a dry body.[1] However, subsequent studies demonstrated that the Moon's small obliquity allows certain polar regions to remain in permanent shadow, forming permanently shadowed regions (PSRs).[2] These regions maintain cryogenic temperatures low enough for water ice to persist over geological timescales.[3] Under such conditions, the sublimation rate of exposed water ice can be lower than 1 m per billion years. The scientific and resource potential of lunar polar water ice, however, can only be fully realized when its abundance, physical state, and origin are constrained.

The history of orbiter remote sensing exploration

Previous lunar missions have provided multiple lines of evidence for the presence and stability of water or hydrogen-bearing species in the lunar polar regions, but remote-sensing approaches have limitations. Thermal observations from the Diviner radiometer onboard the Lunar Reconnaissance Orbiter (LRO) demonstrate that temperatures in permanently shadowed regions (PSRs) can remain sufficiently low for water ice to be stable over geological timescales.[4] Radar observations also provided indications of possible polar ice. The Clementine bistatic radar experiment detected signals consistent with the presence of water ice within PSRs,[5] and subsequent polarimetric radar observations, such as Mini-RF, reported Circular Polarization Ratio (CPR) anomalies.[6] However, CPR is also affected by surface roughness, rock abundance, and viewing geometry, rendering radar anomalies alone insufficient for unambiguous water-ice identification.

Neutron spectroscopy has provided an additional constraint. The Lunar Exploration Neutron Detector (LEND) aboard LRO detected enhanced hydrogen abundances in polar regions,[7] but neutron data cannot discriminate between molecular water ice, hydroxyl-bearing minerals and solar-wind-implanted hydrogen. Spectral observations further reveal widespread hydration signatures: the Moon Mineralogy Mapper (M^3) aboard Chandrayaan-1 detected OH/H_2O-related absorption features in sunlit regions.[8,9] Molecular water detected near 6 μm has primarily been observed in illuminated terrains and is commonly associated with surface processes, limiting its direct relevance to PSR ice reservoirs.[10] The LCROSS impact experiment provided the most direct evidence for polar volatiles by detecting water in the ejecta plume from Cabeus crater,[11] yet impact-induced sublimation and excavation dynamics limit its ability to determine the undisturbed abundance and physical state of water ice in PSR regolith.

Therefore, although orbital and impact observations strongly support the presence of polar volatiles, they are insufficient to independently resolve the abundance, physical state, burial depth, stratification, and origin of lunar water ice. In particular, Mini-RF identifies dielectric or roughness anomalies but lacks the capability to constrain subsurface structure, ice-layer thickness, burial depth, and lateral continuity, which can be addressed by the Lunar Penetrating Radar (LPR).[12,13] These limitations highlight the necessity for in-situ measurements combined with multi-payload data integration, in which direct H_2O and hydrogen-isotope measurements are integrated with radar-derived structural constraints.

The rationale for in situ detection

The origin of lunar water remains a central scientific question and can be constrained through hydrogen isotopic analysis. Three major source mechanisms have been proposed: delivery by asteroidal impacts, particular carbonaceous chondrites;[14,15] contribution from cometary impacts;[16] and solar-wind hydrogen implantation followed by reactions with oxygen-bearing lunar surface materials.[17] These sources are expected to produce distinct hydrogen isotopic signatures. Terrestrial mantle water and many carbonaceous chondrites exhibit broadly similar D/H ratios, typically corresponding to intermediate, δD range (-126 to 46‰),[18,19] whereas solar-wind hydrogen is characterized by extremely low D/H ratios, with δD values lower than -980‰.[20] Accordingly, hydrogen isotope measurements provide a powerful diagnostic for constraining the relative contributions of different water sources.[14,17]

Previous isotope studies have mainly relied on returned samples and terrestrial laboratory analyses. Lunar sample measurements are commonly conducted using ion microprobe or secondary ion mass spectrometry methods,[16] while terrestrial materials can be measured through thermal extraction coupled with infrared spectroscopy and mass spectrometry.[21] However, returned lunar samples are susceptible to terrestrial contamination during collection, curation, transport, and laboratory processing, particularly for trace water and hydrogen isotopes. In addition, solar-wind-implanted hydrogen may interact with indigenous lunar materials, complicating the interpretation of returned-sample D/H data. These limitations highlight the importance of in-situ measurements for minimizing contamination and direct measurement of the isotopic composition of lunar polar volatiles.

Nevertheless, in-situ H_2O and δD measurements alone are insufficient to fully resolve the abundance, physical state, and origin of lunar polar water ice. Within the Chang'E-7 framework, LUWA provides calibrated point-scale measurements of water abundance and hydrogen isotopic composition,[22] while complementary constraints must be obtained from other payloads. Orbital Miniature Synthetic Aperture Radar (MSAR) can identify polarization anomalies and dielectric heterogeneity over broader polar terrains,[13,23] and rover-mounted LPR can further constrain local subsurface profiles, including possible burial depth, stratification, and lateral continuity. [24, 25] These observations, combined with mineralogical context from infrared and Raman spectroscopy, enable integrated interpretation of polar ice occurrence. In this context, LUWA-derived H_2O and δD

measurements function as traceable point-scale anchors within a broader Chang'E-7 multi-payload information chain, rather than as a standalone solution to the characterization of lunar water-ice.

The importance of Chang'E-7 and calibration materials

The Chang'E-7 mission targets PSRs in the lunar south polar region, where LUWA aboard a mini-flying probe will perform in-situ measurements of water abundance and hydrogen isotopic composition. These point-scale data require integration with observations from other Chang'E-7 payloads to constrain the distribution and origin of lunar polar water ice.

LUWA combines Tunable Diode Laser Absorption Spectroscopy (TDLAS) with mass spectrometry to achieve high-precision compositional analysis. [26] Its operational sequence includes system preparation, bake-out and purge, calibration, sample collection, sealed heating, gas analysis, and sample disposal. Operation in PSRs requires additional thermal control to ensure instrument stability. Because LUWA derives quantitative H_2O abundance and δD values from gases released during soil heating, accurate and traceable calibration is essential for ensuring the reliability of the entire measurement chain.

Conventional terrestrial calibration approaches are not well suited to lunar in-situ conditions. Standard gases are difficult to store and deliver under high vacuum, mass-limited, and sealing-constrained conditions, while also introducing potential leakage risks. Liquid water, although widely used for hydrogen-isotope calibration on Earth, requires sampling, vaporization, and transfer procedures that may introduce adsorption and isotope-fractionation effects.[27,28]These limitations are particularly critical under lunar operating conditions, where calibration opportunities, heating power, and operational time are limited.

Accordingly, LUWA requires compact, stable, and traceable solid calibration materials capable of releasing well-defined calibration gases under controlled heating. Such materials reduce storage and sealing risks, simplify the calibration procedure, and provide a metrological basis for converting LUWA spectral and mass-spectrometric signals into reliable in-situ water and isotope information. This study therefore focuses on the development, synthesis, and validation of solid calibration materials as a prerequisite for robust LUWA measurements within the Chang'E-7 multi-payload water-ice detection framework. Within this multi-payload framework, the scientific value of LUWA-derived measurements ultimately depends on the reliability of its calibration. Without traceable calibration materials compatible with lunar operational constraints, point-scale H_2O and δD data cannot be confidently integrated with radar-derived structural constraints or orbital observations for comprehensive water-ice interpretation. This requirement motivates the development of solid calibration materials described in this study.

The state-of-the-art and limitations of calibration material studies

Calibration for in-situ lunar water and isotope measurements faces multiple coupled constraints, including high vacuum, large temperature variations, limited sealing performance, restricted heating power, and short operational time. Under low-temperature conditions, polymer seals may lose elasticity and increase leakage risks, while elevated temperatures and vacuum conditions can reduce the effective volatilization or decomposition thresholds of calibration materials.[29] Over multi-week operations, even minor leakage or adsorption can alter the amount and isotopic composition of calibration gases. In addition, the limited battery budget and thermal-control capability of the mini-flying probe constrain calibration temperature to a relatively low range, typically around 80-120 °C.[30] These factors require calibration materials that are compact, vacuum-stable, chemically well defined, and capable of releasing calibration gases under modest heating.

Existing lunar volatile exploration payloads and calibration strategies do not fully satisfy these requirements for LUWA. For example, VIPER's Near Infrared Volatile Spectrometer Subsystem (NIRVSS) infers volatile content indirectly from reflectance spectra and cannot directly quantify hydrogen isotopic composition.[31, 32] Its Mass Spectrometer Observing Lunar Operations (MSolo) relies on pressurized gas standards stored in an onboard calibration gas system, which remain susceptible to leakage and temperature-dependent pressure fluctuations during long-duration spaceflight.[28,33,34] Luna-27's LASMA-LR laser ionization mass spectrometer is primarily designed for elemental and isotopic composition analysis of solid regolith, and does not employ calibration strategies optimized for in-situ water abundance and hydrogen-isotope measurement[35]. Although the accompanying DLS-L spectrometer targets D/H and oxygen isotope analysis via TDLAS, its calibration relies on liquid water and gaseous CO_2 standards that are susceptible to isotopic fractionation during long-duration spaceflight storage and transfer[36]. The PROSPECT/ProSPA package validates its evolved gas analysis using compounds such as $CaCO_3$, whose decomposition temperature of approximately 550–750°C is incompatible with the low-power and thermally constrained operating conditions required for LUWA in PSRs.[37,38]. LUMVI-X uses perfluorotributylamine as a calibrant, but its limited mass resolution restricts its ability to distinguish hydrogen isotopic signature relevant to D/H analysis.[39,40]

These limitations indicate that the key challenge lies not only in detecting water-related signals, but in converting such signals into traceable and quantitatively reliable water and isotope information under lunar operational constraints. For LUWA, an ideal calibration material should remain stable during storage, release a single and identifiable calibration gas under vacuum

at approximately 80-120 °C, minimize adsorption and isotope-fractionation effects, and provide a known reference for both spectroscopic and mass-spectrometric measurements. These requirements motivate the development of solid, traceable calibration materials for reliable in-situ water and isotope information acquisition.

1.6 The innovation and significance

The LUWA onboard Chang'E-7 is designed to provide direct in-situ information on water abundance and hydrogen isotopic composition in lunar polar environments. Prototype testing has demonstrated its capability for water-vapor pressure and hydrogen-isotope measurements under laboratory conditions.[41-43] However, the scientific value of LUWA-derived H_2O and δD data depends not only on instrument sensitivity, but also on the availability of calibration materials that are stable, traceable, and compatible with lunar operational constraints. Without reliable calibration, point-scale measurements from LUWA cannot be confidently integrated with other Chang'E-7 observations for broader water-ice interpretation.

The innovation of this study lies in developing traceable solid calibration materials that convert a difficult in-situ calibration problem into a controlled solid-to-gas release process. By screening candidate materials under vacuum, identifying Ag_2CO_3 and $Cu(OH)_2$ as low-temperature gas-release materials, characterizing the evolved CO_2 and H_2O signals using spectroscopic and mass-spectrometric measurements, and assessing the hydrogen-isotope fidelity of synthesized $Cu(OH)_2$, this work establishes a practical and traceable calibration basis for LUWA.

The significance of this work is twofold. From an engineering perspective, the proposed solid calibration materials offer compact, vacuum-compatible, and low-power calibration sources for a resource-constrained lunar payload. From lunar scientific perspective, they improve the reliability and traceability of LUWA-derived water and isotope information, allowing these point-scale measurements to serve as calibrated anchors in the Chang'E-7 multi-payload framework. When combined with regional hydrogen mapping, radar-derived subsurface structure, mineralogical and spectral context, and complementary volatile measurements, such calibrated LUWA data contribute to constraining the abundance, physical state, and potential origin of lunar polar water ice.

METHODS

Ground calibration platform

After the vacuum tank has been evacuated for 72 hours to below 10^{-5} Pa, the instrument is held at 35 °C. With the gas-extraction furnace sealed and valves 1 and 2 closed in Fig. 1c, the electronics unit issues a heating command to the calibration gas unit, raising and maintaining its temperature at 100 °C. The mass spectrometer selects its intake path according to the measured pressure. If the pressure is below 100 Pa, open self-locking valve 2 and draw gas through the black pipeline. The main pipeline pressure is then checked with the vacuum gauge. If the main pipeline pressure rises above 200 Pa, close the self-locking valve 2 and switch sampling to the gray pipeline.

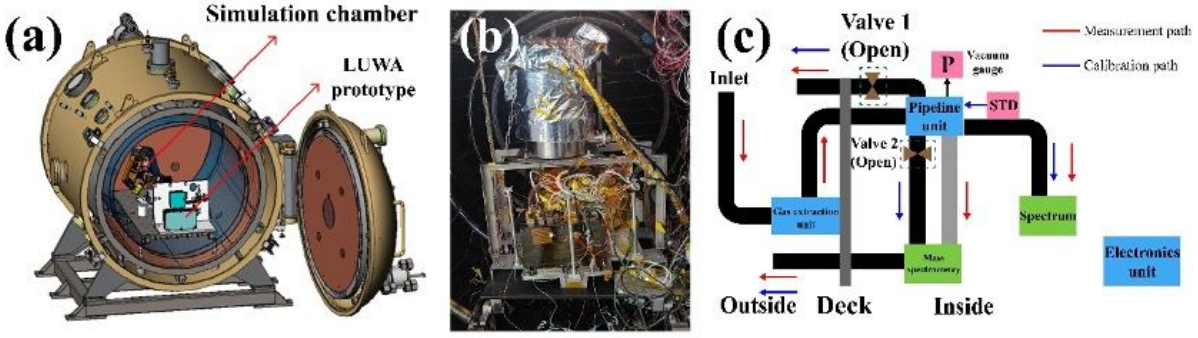

Figure 1. Ground calibration platform and LUWA prototype (A) LUWA prototype in the simulation chamber; (B) photograph of the prototype; and (C) internal pipeline configuration.

Standard material selection

LUWA incorporates two independent calibration units to support repeated calibration during lunar operation. An initial calibration is performed after landing to verify the instrument response following launch, transit, and landing, and additional calibrations can be conducted before individual in-situ measurements to establish contemporaneous references under the prevailing vacuum and thermal conditions. Each calibration unit can release the reference gas multiple times through controlled heating rather than being limited to a single use. During each calibration, an appropriate amount of gas is introduced into the analytical pathway, after which the gas is vented, and the calibration unit is isolated until the next calibration cycle.

Table 1. Decomposition temperatures of common carbonates.

Carbonate	Ag_2CO_3	$CdCO_3$	$ZnCO_3$	$MgCO_3$	$CaCO_3$	$SrCO_3$	$BaCO_3$
Td (℃)	147	240	250	441	661	615	942

Considering the complexity of binary systems [44] and the interaction between carbonate and metallic inner surfaces, the calibration materials were restricted to substances expected to release predominantly a single target gas upon heating (excluding bicarbonates, oxalates, etc.). Referring to the design specifications of the spectrometer and mass spectrometer in the analyzer, CO_2 and H_2O were selected as the target calibration gases and used in ground-based pre-experiments. [26] Because CO_2-releasing solid calibrants were of primary interest for onboard referencing, the initial screening focused on carbonates. Thermal decomposition temperatures of common carbonates at atmospheric pressure are listed in Table 1.[45]

Accounting for chemical-kinetic effects in vacuum, the onset temperature for thermal decomposition shifts downward;[46] Therefore, we targeted carbonates with vacuum-decomposition temperatures between 80 °C and 120 °C. In practice, this criterion encompasses minerals whose atmospheric-pressure decomposition occurs between 100 °C and 300 °C—such as magnesium carbonate ($MgCO_3$) and calcium carbonate ($CaCO_3$). Based on their thermal profiles (Table 1), the carbonates of cobalt ($CoCO_3$), zinc ($ZnCO_3$), cadmium ($CdCO_3$), and silver (Ag_2CO_3) emerged as the most promising candidates.

Among these candidates, zinc carbonate predominantly occurs as the basic hydrated form $2ZnCO_3{\cdot}3Zn(OH)_2{\cdot}H_2O$, making it difficult to obtain pure $ZnCO_3$.[47] Its thermal decomposition releases both H_2O and CO_2, which would complicate calibration. Given the toxicity concerns associated with cobalt and cadmium compounds,[48,49] silver carbonate (Ag_2CO_3) was therefore chosen as the solid calibration substance for this temperature range.

CO_2 is suitable for pressure, spectroscopic, and mass-spectrometric referencing, but it cannot provide a hydrogen-isotope reference. We therefore additionally evaluated a water-releasing calibrant with a known hydrogen isotopic composition.

Therefore, we evaluated solid materials that release water upon heating, specifically hydrates and weakly basic compounds. However, common hydrates typically decompose below the 80-120 °C range, rendering them unsuitable for our in-situ calibration needs ,[50,51] and their decomposition onset shifts even lower in vacuum, making them unsuitable for in-orbit storage. Among weak bases, the readily available copper hydroxide ($Cu(OH)_2$) was selected, as it decomposes at approximately 150 °C under ambient pressure [52], and it is a practical candidate for producing a controlled water release for calibration.

Vacuum thermogravimetric analysis

Conventional thermogravimetric analysis (TGA) is typically conducted in controlled gas atmospheres (e.g., high-purity N_2 or O_2). The presence of a gas phase can influence the diffusion of decomposition products, modify reaction pathways, or chemically interact with the sample, thereby introducing confounding factors. To eliminate these confounding effects, vacuum thermogravimetric analysis (TGA) is required, since prior studies have shown that TGA curves obtained under inert-gas atmospheres can differ substantially from those measured in vacuum.[46]

To determine the decomposition temperatures of candidate calibration materials under orbital conditions and to establish the heating power and duration required for in-situ calibration, we performed vacuum TGA on $CaCO_3$, $MgCO_3$, Ag_2CO_3, and $Cu(OH)_2$. Measurements were carried out on a NETZSCH STA 2500 vacuum thermogravimetric analyzer (Supplementary Figure S2a), with the analysis chamber maintained below 1 Pa. The heating protocol applied a rate of 1 °C min^{-1}, including isothermal holds at 25 °C, 50 °C, and 70 °C for 20 min each to assess stability, followed by continuous heating to 150 °C. Each experiment was repeated twice, and the averaged results are reported. We then conducted end-to-end experiments with the two selected calibration materials, following the protocol detailed in Section 2.1. Before each sample measurement, the calibration routine described therein was executed to ensure consistency.

Approximately 50 mg of each material was used for each vacuum thermogravimetric measurement. Each material was measured twice under identical vacuum and heating conditions. The sample mass was normalized to its initial value, and the

normalized curves from the two runs were averaged for data presentation.

Chemical synthesis

For CO_2 referencing, a carbonate with well-characterized composition and predominantly CO_2 release is required. In contrast, water-based calibration demands a reference material with a known hydrogen isotopic ratio to evaluate instrument performance and calibrate its isotope-measurement capability. We tested two samples (A and B) from the same batch of analytical-grade $Cu(OH)_2$. Each sample was vacuum-heated, and the released gases were introduced into a TDLAS spectrometer pre-calibrated with a liquid-water standard. The spectrometer recorded at 5 Hz, yielding over 500 δD measurements per sample. The mean δD values (Figure. 2) differ by approximately 50‰. This variability, attributable to untraceable hydrogen sources in $Cu(OH)_2$, indicates that commercially available analytical-grade copper hydroxide is unsuitable for direct use as an isotopic calibration standard.

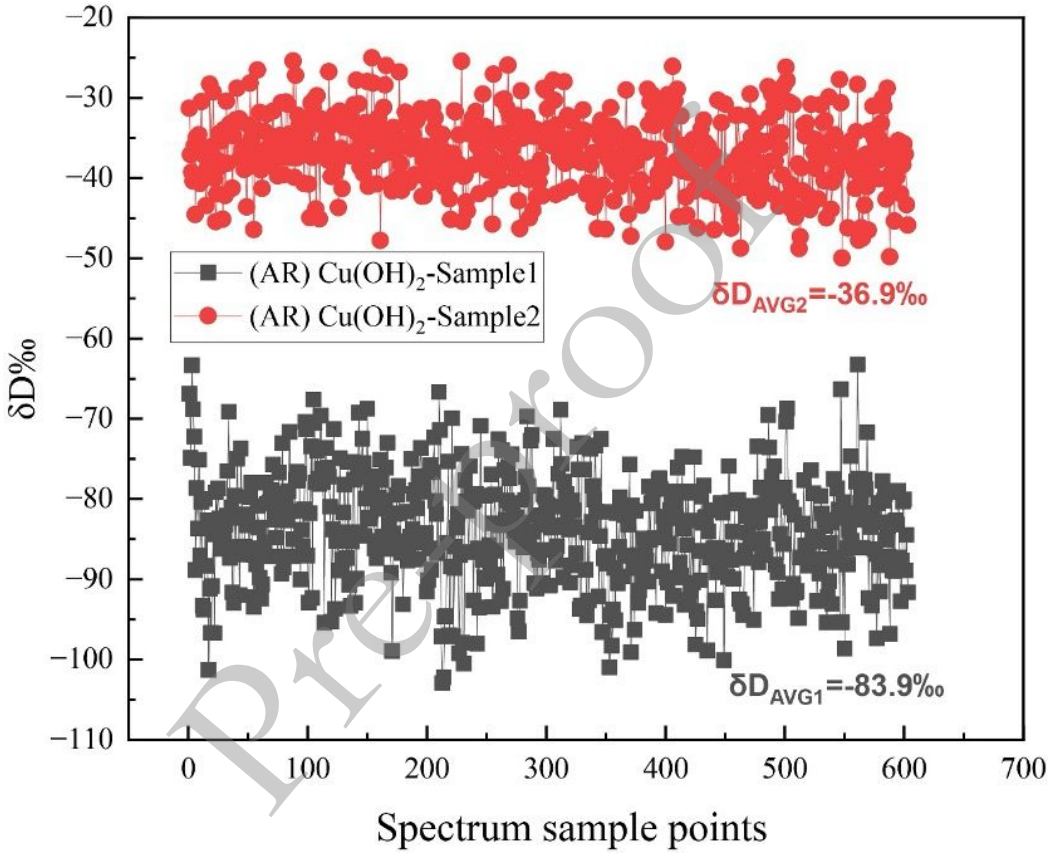

Figure 2. Time-resolved δD measurements of H_2O released from two commercial analytical-grade $Cu(OH)_2$ samples obtained from the same batch.

To address this issue, we developed a simple method for preparing $Cu(OH)_2$ with a traceable hydrogen isotopic composition as a solid reference material. A schematic overview of the synthesis procedure is provided in Supplementary Figure S1.[53]

The preparation method is guided by chemical reaction kinetics, the thermal stability of the products, and is designed according to the following chemical equations:

$$CuSO_4 + Na_2O + H_2O = Cu(OH)_2\downarrow + Na_2SO_4 (1)$$

During synthesis, we exploit the fact that chemical reaction rates are significantly faster than those of physical thermal fractionation processes.[28,54] Hydrogen sources were tightly controlled through elemental bookkeeping: copper was introduced as anhydrous copper sulfate, the base as high-purity sodium oxide, and all hydrogen in the product was derived from the added precursor water. During precipitation, hydrogen from the precursor water was incorporated into the structural hydroxyl groups

of $Cu(OH)_2$. The final product was therefore a solid $Cu(OH)_2$ reference material with a traceable hydrogen isotopic composition. All operations were conducted in a glovebox under a high-purity nitrogen atmosphere.

We performed the entire preparation inside a high-purity nitrogen glovebox, ensuring that deionized water was the sole hydrogen source. The procedure comprised the following steps:

Prepare the copper solution: In the glove box, dissolve anhydrous copper sulfate (analytical grade) in deionized water to obtain a 0.1–0.3 mol/L solution.

Precipitate formation: Add high-purity Na_2O gradually in small portions until no further precipitate forms, yielding a mixed reaction suspension. Maintain the mass ratio of Na_2O to anhydrous copper sulfate at 1:(2–2.5).

Filtration and washing: Filter the suspension by suction. Wash the collected residue with anhydrous ethanol to remove soluble impurities. Use deionized water or anhydrous ethanol as required to assist the suction filtration.

Drying and storage: Dry the filtered precipitate under vacuum and then seal it in bottles inside the glove box under an inert gas atmosphere. After vacuum drying, a light-blue $Cu(OH)_2$ powder was obtained, as illustrated in Supplementary Figure S1.

To strictly control the hydrogen source to originate solely from precursor deionized water, analytical-grade anhydrous copper sulfate and high-purity Na_2O (containing ~20 wt% Na_2O_2 impurity) were used. To minimize adventitious hydrogen incorporation, all reagents and equipment were degassed in the glove box transition chamber prior to use. Heat-resistant apparatus was degassed at 150–200°C; other items were evacuated naturally for 1–2 days following the vacuum-degassing protocol.[27] All experimental operations were conducted in an inert gas glove box, and required reagents were opened and handled within the glove box.

Although chemical reaction rates are much higher than those of physical processes such as phase changes, thereby minimizing D/H fractionation associated with phase transitions, the mass difference between H and D leads to slightly different bond energies. In other words, compared to D, H is more likely to be incorporated into the product.[55]

This phenomenon can be calculated using Rayleigh fractionation:[55]

$$R_w = R_0 \cdot f^{\alpha-1} (2)$$

Here, R_w is the isotopic value in the water. R_0 is the isotopic value in the initial reactant. f is the proportion of residual reactant, which is approximately equal to 1 due to the reaction being in the liquid water. α is the fractionation factor.[55] During precipitation, the liquid water reservoir was substantially larger than the amount of water (-OH) incorporated into the precipitate, such that the residual water fraction remained close to unity. According to the Rayleigh fractionation relationship, the isotopic composition of the residual water therefore changed only slightly throughout precipitation. Consequently, precipitates formed at different stages interacted with a water reservoir of nearly constant isotopic composition, limiting progressive Rayleigh-type fractionation and intraprecipitate isotopic heterogeneity. The bulk isotopic composition of the precipitate should thus mainly reflect the initial solid–water fractionation rather than substantial amplification caused by progressive depletion of the water reservoir.

However, kinetic equilibrium has not yet been reached. Before product filtration and drying, evaporation of the liquid phase will cause continuous isotopic changes.[28]These changes in the liquid phase isotope composition will further exchange with the product.[56] The influence of post-reaction kinetic equilibrium will be verified experimentally.

After preparation, the solid calibration material was subjected to a suite of compositional and performance tests; the details of these analyses are given in the next section.

Tests

Scanning electron microscopy was used to characterize the morphology and surface features of the synthesized $Cu(OH)_2$ particles. Measurements were performed using a ZEISS GeminiSEM 500 scanning electron microscope (Figure S2B). X-ray diffraction was used to identify the crystalline phases of the synthesized material. Measurements were performed using a Rigaku SmartLab diffractometer (Supplementary Figure S2C) over a 2θ range of 20–80°, and the measured diffraction pattern was compared with the reference pattern of $Cu(OH)_2$. SEM was used for morphological characterization, whereas XRD provided qualitative crystalline-phase identification.

The critical test for the calibration material is the hydrogen isotopic analysis, which verifies whether the synthesized solid can serve as a hydrogen-isotope calibrant. Before synthesis, 100 mL of each precursor water was reserved for hydrogen-isotope analysis. The detailed procedures for precursor-water calibration, solid-derived vapor measurement, and independent Cr-EA/IRMS validation are described in Section 2.6.

Because the isotope measurement system analyzes gaseous H_2O rather than the solid material directly, the LUWA

prototype was modified to accommodate thermal release from solid samples (Figure 3). $Cu(OH)_2$ powders were synthesized from three precursor waters with distinct hydrogen isotopic compositions.

Before isotope measurement, the synthesized $Cu(OH)_2$ samples were stored in sealed containers inside the glovebox under an inert atmosphere for 7 days. The measurement assembly was placed in a vacuum chamber and valves 1 and 2 were opened. The chamber was evacuated for 72 hours until the vacuum gauge read $<10^{-5}$ Pa. Valve 1 was then closed, and the gas-generation/calibration component was heated to release the sample's water vapor for analysis. To avoid concentration-dependent isotope effects,[57,58] the gas pressure in the measurement line was kept below 250 Pa. The hydrogen isotopic composition of the evolved gas was then recorded.

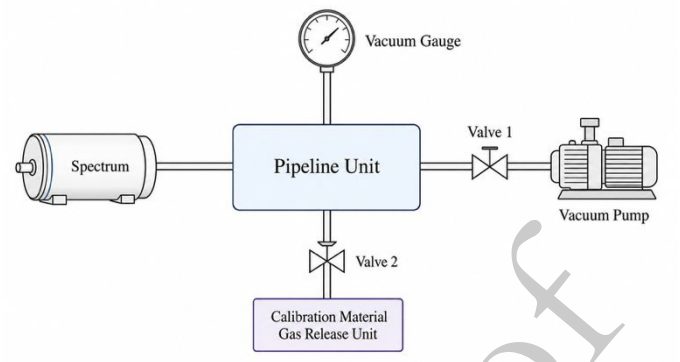

Figure 3. Solid-isotope measurement platform based on the LUWA prototype.

Hydrogen isotope analysis protocol

Hydrogen isotope compositions are reported as δD values relative to the VSMOW scale, defined as $\delta D = [(D/H)_{sample}/(D/H)_{VSMOW} - 1] \times 1000‰$. The isotope protocol comprised three analytical steps: determination of the δD values of precursor waters using a Picarro L2130i system, gas-phase δD measurement of H_2O released from synthesized $Cu(OH)_2$ using the LUWA prototype TDLAS system, and independent Cr-EA/IRMS validation of representative synthesized $Cu(OH)_2$ solid standards.

The hydrogen isotopic compositions of the precursor waters were determined using a Picarro L2130i cavity ring-down spectrometer (Figure S2D) coupled with an automated PAL LSI liquid sample injector (Figure S2E). The analytical procedure followed the laser absorption spectroscopy protocol for hydrogen and oxygen isotope analysis of water samples specified in DZ/T 0184.36—2024. For each analytical batch, the Picarro analyzer was calibrated immediately before sample measurements using three national certified reference waters with distinct δD values: GBW04458, GBW04459, and GBW04460. Their certified δD values are −1.7 ± 0.4‰, −63.4 ± 0.6‰, and −144.0 ± 0.8‰, respectively (Table 2). According to the certificates, these reference waters are traceable to international isotope standards, including VSMOW2 and SLAP2, and their δ values are reported relative to the VSMOW scale. A batch-specific linear calibration was established between the raw instrumental values and the certified values, and this calibration was applied to the precursor-water measurements.

Each precursor-water sample was measured by ten consecutive injections. To minimize carryover and memory effects, the first six injections were excluded, and the reported value was calculated from the final four injections. The same procedure was applied to both reference waters and unknown precursor-water samples. Short-term instrumental precision was evaluated from repeated measurements of the reference waters immediately before sample analysis. Under the analytical conditions used in this study, the δD repeatability was better than 0.1‰. This calibration and replicate-measurement procedure provided the traceability and analytical precision required for evaluating the isotopic offsets between the precursor waters and the synthesized $Cu(OH)_2$-derived water.

For gas-phase measurements of the synthesized solid standards, $Cu(OH)_2$ samples were heated to release H_2O vapor, which was then introduced into the LUWA prototype TDLAS system for isotope analysis. In the solid-standard measurements, H_2O vapor was first generated by thermal decomposition of $Cu(OH)_2$ and then analyzed by the same laser absorption spectroscopic principle. For each synthesized $Cu(OH)_2$ sample, one independent thermal release was performed. The mean δD value and standard deviation were calculated from the accepted time resolved measurements collected during the continuous release. The resulting standard deviation represents within-release temporal variability under evolving gas pressure conditions and should not be interpreted as analytical uncertainty or release-to-release reproducibility. This procedure allowed the isotopic composition of water vapor released from the synthesized solid standard to be evaluated on the same VSMOW-referenced

scale. The LUWA prototype TDLAS system was independently calibrated using standard waters, and the precursor waters were also measured to verify consistency between the Picarro and TDLAS measurement scales.

To independently evaluate the isotope consistency of the synthesized $Cu(OH)_2$ solid standards, representative samples prepared using the same synthesis protocol were analyzed by Cr-EA/IRMS.[59] This analysis was designed to provide an orthogonal mass-spectrometric validation of the TDLAS-based gas-phase measurement of H_2O vapor released from the solid standards. Continuous-flow analyses were carried out using a Flash 2000HT elemental analyzer with a MAS 200R autosampler coupled to a Delta V Advantage isotope ratio mass spectrometer via a ConFlo IV interface. Approximately 4–5 mg of each solid sample was reacted with chromium chips and chromium powder at 1050 °C to generate H_2, which was then carried by helium into the isotope ratio mass spectrometer for analysis. USGS57 and USGS58 were used for data linear regression, and the analytical accuracy was better than 2‰. This Cr-EA/IRMS procedure provided an independent check on the hydrogen isotopic composition of the synthesized $Cu(OH)_2$ standards and on the reliability of the solid-derived vapor isotope measurement workflow.

Table 2. Certified reference waters used for δD calibration.

Reference water	Certified δD value	Uncertainty	Scale
GBW04458	−1.7‰	±0.4‰	VSMOW
GBW04459	−63.4‰	±0.6‰	VSMOW
GBW04460	−144.0‰	±0.8‰	VSMOW

RESULTS

Figure 4 presents the averaged vacuum thermogravimetric curves obtained from two independent measurements of each candidate material, with an initial sample mass of approximately 50 mg in each experiment. The two measurements showed nearly overlapping thermal behavior, indicating good repeatability under the applied vacuum and heating conditions.

Under vacuum, $Cu(OH)_2$ underwent its principal mass loss between approximately 100 °C and 120 °C. The measured mass loss was approximately 18.2 wt%, consistent with the theoretical H_2O mass fraction of 18.47 wt% for complete decomposition to CuO and H_2O. This agreement indicates that $Cu(OH)_2$ was nearly completely decomposed within the investigated temperature range.

Ag_2CO_3 began to decompose gradually at approximately 100 °C and continued to lose mass up to the maximum investigated temperature of 150 °C, without reaching a clear plateau. Therefore, a decomposition completion temperature could not be assigned. The theoretical mass loss for complete conversion of Ag_2CO_3 to Ag_2O and CO_2 is 15.96 wt%. The reaction remained incomplete within the investigated temperature range.

$MgCO_3$ began to decompose slowly at approximately 70 °C, indicating insufficient thermal stability, whereas $CaCO_3$ showed no identifiable decomposition within the investigated temperature range. Based on the criteria outlined in Section 2.2, Ag_2CO_3 and $Cu(OH)_2$ were selected for subsequent full process tests as candidate CO_2 and H_2O reference materials, respectively.

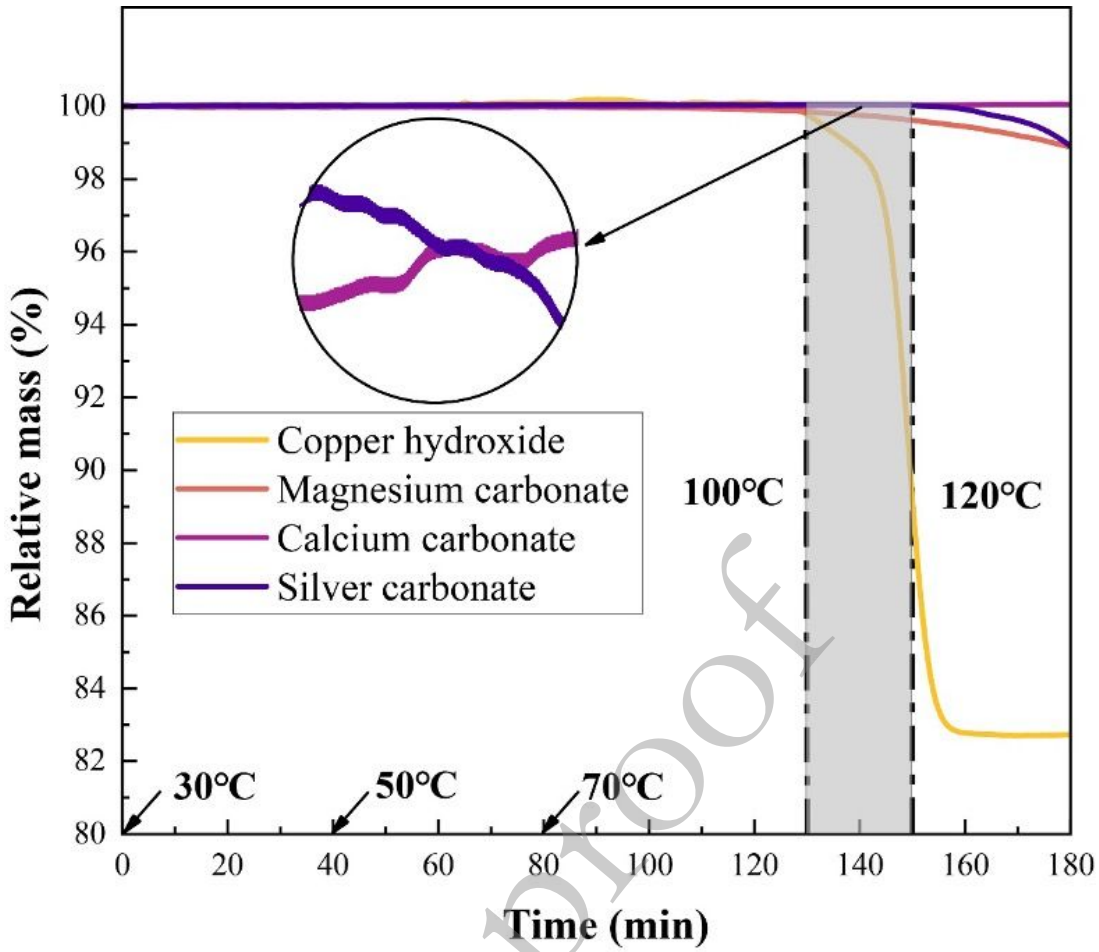

Figure 4. Averaged vacuum thermogravimetric curves obtained from two independent measurements of $CaCO_3$, $MgCO_3$, Ag_2CO_3, and $Cu(OH)_2$.

During the full process tests, Ag_2CO_3 and $Cu(OH)_2$ were used as the CO_2- and H_2O-releasing materials, respectively. Figure 5 shows the spectroscopic and mass-spectrometric results obtained from the evolved gases at a vacuum-gauge pressure of approximately 137 Pa. The spectroscopic measurements show clear absorption features attributable to CO_2 and H_2O vapor. The mass spectra likewise display the expected dominant molecular-ion signals, together with fragment signals at m/z 16 and 17 for H_2O. These fragment peaks arise from facile H–O bond cleavage during ionization, producing O (mass number of 16) and OH (mass number of 17) species. No obvious interfering gaseous species were observed within the measured spectroscopic and mass-to-charge ranges. These results demonstrate the feasibility of using Ag_2CO_3 and $Cu(OH)_2$ as controlled sources of CO_2 and H_2O reference signals for LUWA calibration and validation.

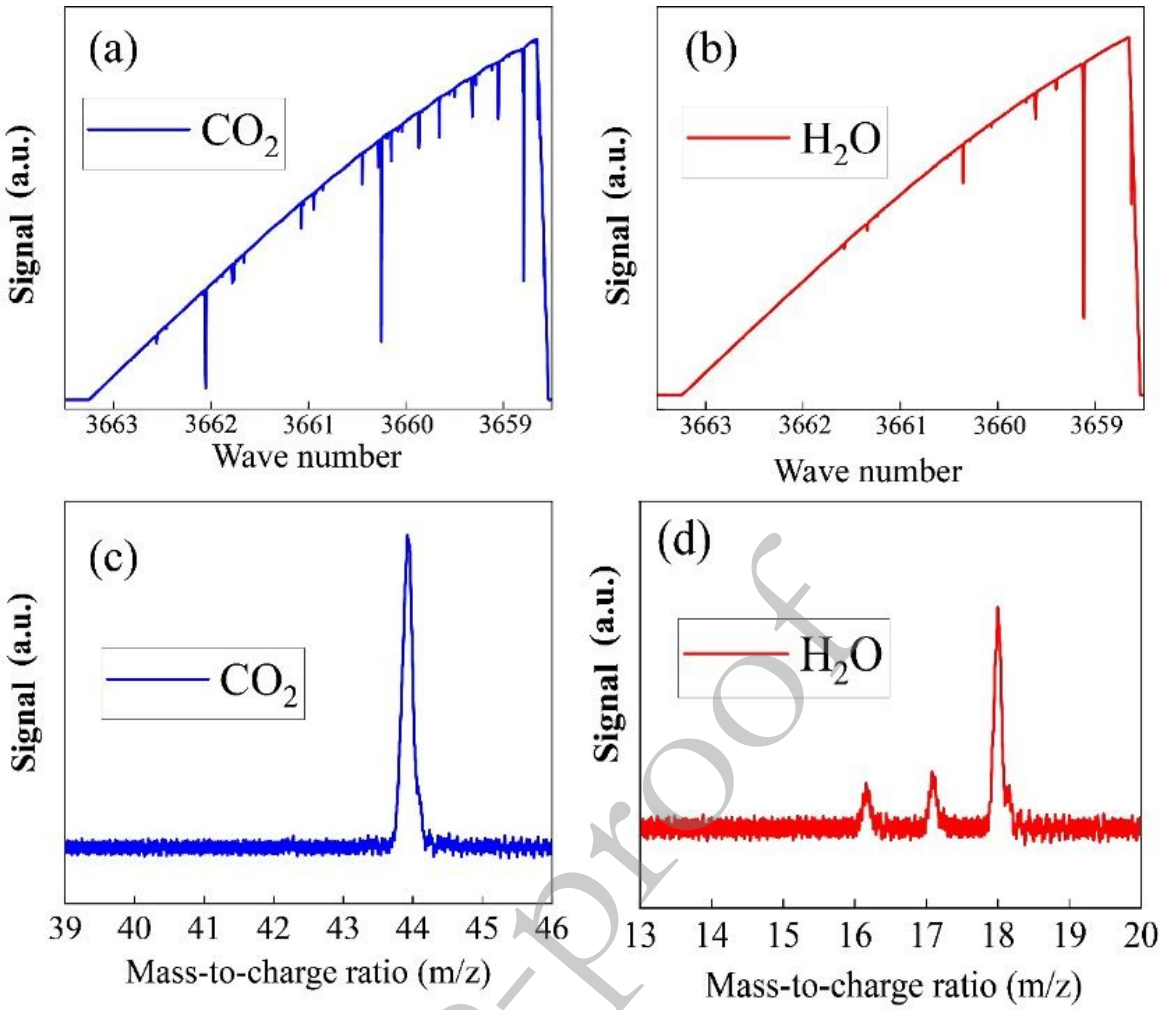

Figure 5. Spectroscopic and mass-spectrometric signals of gases evolved from Ag_2CO_3 and $Cu(OH)_2$ (A) CO_2 absorption spectrum from Ag_2CO_3; (B) H_2O absorption spectrum from $Cu(OH)_2$; (C) mass spectrum of gas evolved from Ag_2CO_3; and (D) mass spectrum of gas evolved from $Cu(OH)_2$.

During the full process tests, $Cu(OH)_2$ released H_2O rapidly and underwent nearly complete decomposition within the applied heating range. The amount of H_2O inferred from the measured partial pressure was consistent with the theoretical water content of $Cu(OH)_2$, approximately 18 wt%. Nearly complete decomposition ensured that the evolved H_2O represented the bulk hydrogen isotope composition of the material and minimized potential isotope fractionation associated with partial release.

Ag_2CO_3 exhibited a slower and more gradual CO_2 release. A pressure above approximately 50 Pa was sufficient to provide spectroscopic and mass spectrometric reference signals, after which the inlet valve was closed and gas introduction was terminated without requiring complete decomposition of the loaded material. No signal at m/z 32 was detected in the full mass scan (not shown), providing no evidence for substantial O_2 release or further decomposition of the Ag_2O product under the applied conditions. The remaining Ag_2CO_3 could therefore be retained for subsequent controlled gas releases.

The full process tests involved vibration, long-term storage (> 4 month) and thermal-cycling procedures. Following these procedures, the tested units remained operational and retained their ability to generate the target-gas reference signals required for calibration.

Considering the gas release characteristics observed in the full process tests together with the current LUWA mission requirements, Ag_2CO_3 was selected as the reference material for the two onboard calibration units. The pressure controlled partial release strategy allows the remaining material to be used in subsequent calibration cycles. With a nominal material loading volume of approximately 1 cm^3 per unit, the two calibration units are designed to support approximately four to five calibrations in total, including an initial calibration after landing and additional calibrations before individual in-situ measurements.

Traceable $Cu(OH)_2$ was assigned primarily to ground H_2O and δD calibration, prototype testing, full process validation, and controlled regolith simulant experiments. This assignment reflects the operational requirements and calibration strategy of

the current mission rather than an intrinsic restriction on the possible flight use of $Cu(OH)_2$.

Figure 6 presents SEM images of the synthesized $Cu(OH)_2$. The sample consists predominantly of plate-like and elongated particles with a heterogeneous particle-size distribution. Higher-magnification images reveal textured surface features on the particles. These observations characterize the morphology of the synthesized material.

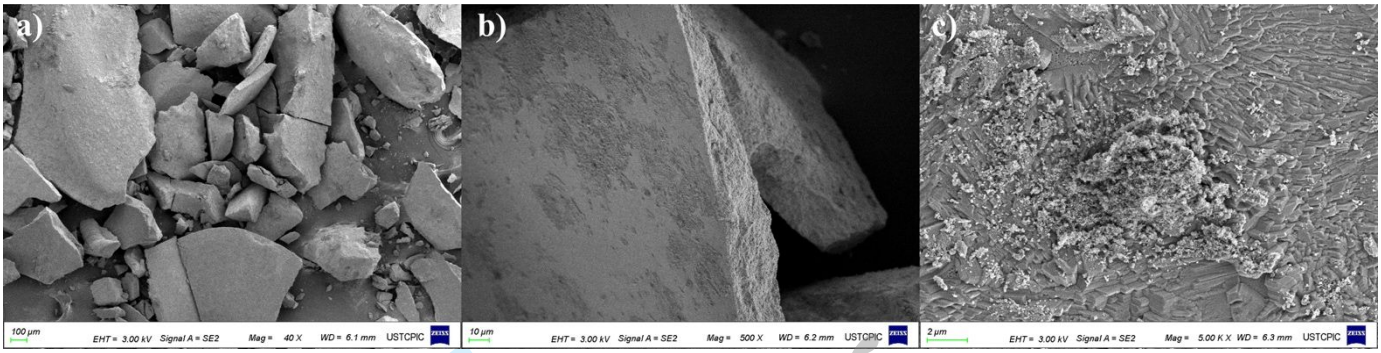

Figure 6. SEM images of synthesized $Cu(OH)_2$ at scale bars of (A) 100 µm, (B) 10 µm, and (C) 2 µm.

Figure 7 presents the XRD pattern of the synthesized material together with the reference pattern of $Cu(OH)_2$ (PDF#99-000-3468). The principal diffraction peaks at approximately 23.8°, 34.0°, and 53.3°, together with secondary peaks at approximately 35.9°, 38.1°, and 39.7°, are consistent with the reference peak positions of crystalline $Cu(OH)_2$. No prominent additional crystalline peaks were observed within the investigated 2θ range. These results identify $Cu(OH)_2$ as the dominant crystalline phase of the synthesized material.

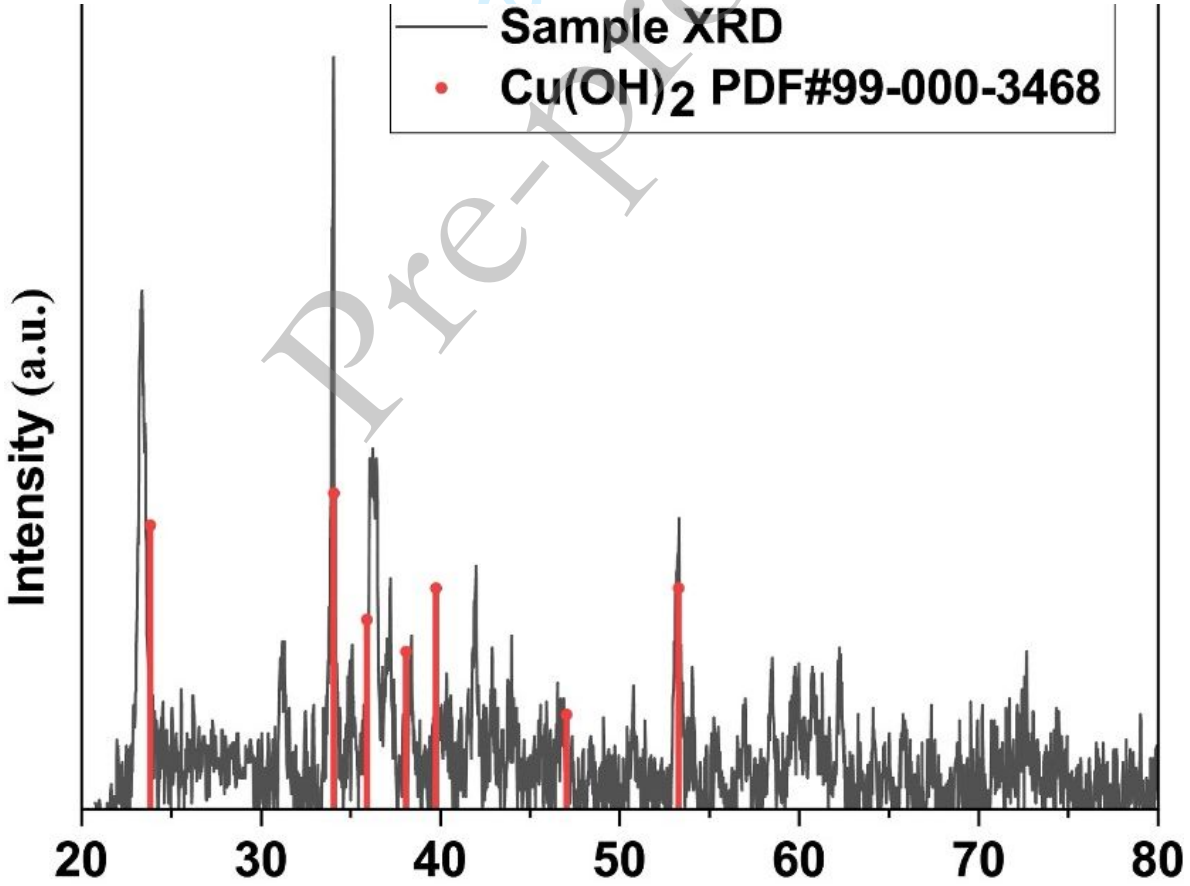

Figure 7. XRD pattern of the synthesized material compared with the reference diffraction pattern of $Cu(OH)_2$ (PDF#99-000-3468).

The spectroscopic isotope signal approached its lower detection limit at an H_2O partial pressure of approximately 150 Pa. The hydrogen isotope results are summarized in Supplementary Table S1. The precursor waters had δD values of +4.0‰, −74.0‰, and −24.0‰. The corresponding H_2O released from synthesized $Cu(OH)_2$ yielded mean δD values of −4.3 ± 25.30‰, −68.7 ± 19.64‰, and −16.4 ± 25.21‰, based on 116, 114, and 116 accepted time-resolved measurements, respectively (Fig. 8).

One independent thermal release was performed for each synthesized $Cu(OH)_2$ sample. The reported standard deviations therefore represent temporal variability during an individual dynamic release rather than release-to-release reproducibility. This variability reflects the continuously changing H_2O partial pressure and signal intensity during decomposition and may also include contributions from pressure-dependent isotope response, adsorption and desorption within the analytical pathway, and reduced signal quality near the isotope detection limit.

The absolute differences between the mean precursor-water and solid-derived vapor values were 8.3‰, 5.3‰, and 7.6‰, respectively. These differences remained within 10‰, indicating that the overall synthesis, drying, thermal release, gas-transfer, and measurement workflow preserved the mean isotope information of the precursor waters within the investigated accuracy range. Given the analytical uncertainty and within-release temporal variability, these differences should not be interpreted as a resolved or systematic isotope-fractionation factor.

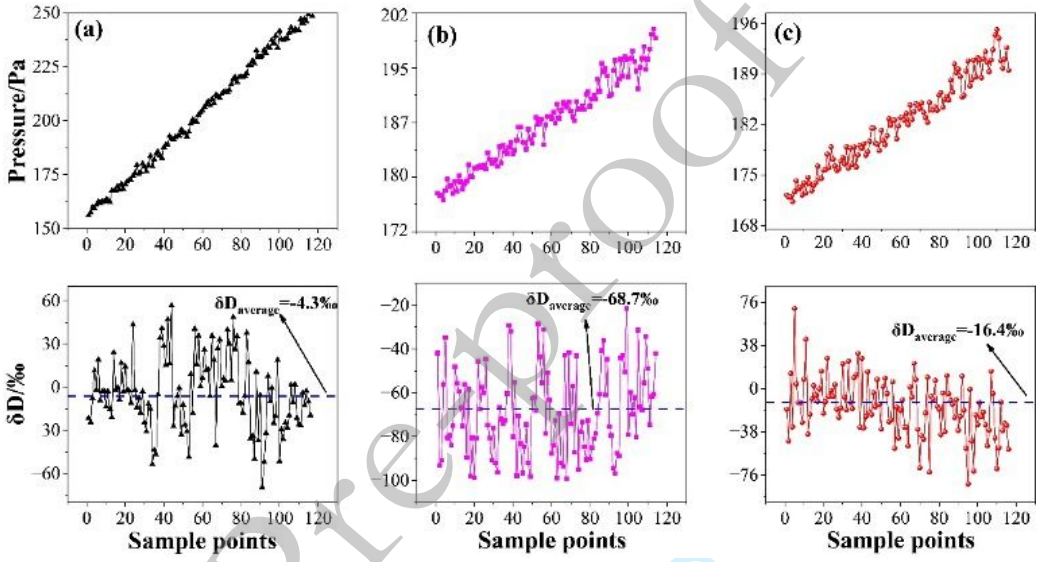

Figure 8. Time-resolved δD measurements of H_2O released from synthesized $Cu(OH)_2$ samples prepared using three precursor waters with different hydrogen isotopic compositions.

A separate batch of $Cu(OH)_2$ was synthesized using the same protocol for the Cr-EA/IRMS cross-method comparison. This cross-method comparison was designed to evaluate the consistency of the solid-derived vapor isotope measurement workflow against an independent mass-spectrometric method. The Cr-EA/IRMS measurements yielded a mean δD value of −113.98 ± 0.36‰ (n = 5), whereas the TDLAS gas-phase measurements yielded −121.45 ± 4.06‰ (n = 5). The mean difference between the two methods was approximately 7.47‰, which is substantially smaller than the current isotope precision of the LUWA prototype. This result supports the reliability of the gas-phase isotope measurement workflow for LUWA-related ground calibration and prototype testing.

DISCUSSION

Solid calibration materials provide a practical alternative to conventional gaseous or liquid isotope standards for in-situ planetary measurements. Their main advantage is the ability to generate calibration gases on demand through controlled thermal decomposition, thereby reducing the complexity of storing and handling volatile standards under spaceflight conditions.

Material selection was determined not only by decomposition temperature and gas composition, but also by the different operational requirements of onboard calibration and ground validation. Ag_2CO_3 and $Cu(OH)_2$ therefore serve complementary roles in the current LUWA calibration and validation framework.

Ag_2CO_3 was selected as the reference material for the two onboard calibration units. Its comparatively gradual CO_2 release is advantageous for controlled calibration because complete decomposition of the material is not required during a single operation. Instead, an appropriate amount of CO_2 can be released through controlled heating, and the calibration unit can be isolated after the required reference pressure is reached. The remaining material can then support subsequent calibration cycles. This operating mode enables an initial calibration after landing and additional calibrations before individual in-situ measurements.

Traceable $Cu(OH)_2$ is used primarily for ground H_2O and δD calibration, prototype testing, full process validation, and controlled regolith simulant experiments. Its low decomposition temperature, rapid H_2O release, and known stoichiometric water content make it suitable for evaluating the complete LUWA process, including sample heating, gas release, transfer, pressure measurement, and spectroscopic and mass spectrometric detection. The synthesis route developed in this study links the mean hydrogen isotope composition of the released H_2O to that of the precursor water, with absolute differences between the mean values remaining within 10‰.

The uncertainty measures associated with the precursor waters and the solid-derived vapor have different statistical meanings. The uncertainty of the precursor-water values reflects the consistency of repeated calibrated liquid injections under relatively stable analytical conditions. In contrast, the standard deviation of the solid-derived vapor reflects temporal variability during a single dynamic thermal release, in which H_2O pressure and signal intensity changed continuously. The present results therefore demonstrate consistency between the mean isotope values rather than release-to-release precision of the synthesized solid reference.

The observed differences between the mean precursor-water and solid-derived vapor values may represent the cumulative effects of precipitation, filtration, vacuum drying, thermal decomposition, gas transfer, adsorption and desorption, measurement memory, pressure-dependent spectroscopic response, and instrumental uncertainty. Because these stages were not evaluated independently, their individual contributions cannot be quantitatively separated in the present study. Nearly complete decomposition of $Cu(OH)_2$ was used to reduce additional isotope bias associated with selective partial H_2O release, but it does not eliminate possible fractionation or measurement effects during the other stages.

The current role assigned to $Cu(OH)_2$ reflects the mission configuration and calibration strategy adopted for LUWA rather than an intrinsic limitation of the material for spaceflight. Within its current ground-based role, synthesized $Cu(OH)_2$ offers several broader methodological advantages for water isotope measurements. First, it can serve as a solid isotope transfer reference by incorporating hydrogen from precursor water with a known δD value into a stable solid phase. This enables repeated evaluation of the complete solid sample measurement process, including heating, gas release, transfer, and detection. Second, it can support end to end validation of LUWA like analytical systems by allowing controlled assessment of release kinetics, gas pathway adsorption, pressure dependent isotope response, measurement memory, and consistency between spectroscopic and mass spectrometric measurements. Third, because the H_2O content of $Cu(OH)_2$ is defined by its stoichiometry, it provides a practical means of preparing regolith simulants with known and reproducible water contents, avoiding the uncontrolled sublimation and redistribution that can occur when real ice is handled under laboratory conditions.

These capabilities also indicate potential applications beyond the present LUWA ground validation program. With further optimization of storage, packaging, contamination and background control, operational procedures, and flight qualification, traceable $Cu(OH)_2$ type materials may provide controlled H_2O and δD references for future planetary payloads. In particular, a solid reference with known water content and isotope composition could provide an intermittent anchor for characterizing adsorption and desorption memory effects in carrier gas free isotope measurement systems. However, this application has not yet been implemented in the current LUWA configuration and will require further development and validation.

Known limitations include adsorption and surface exchange with atmospheric moisture, the propensity of copper hydroxide to react with CO_2 and form carbonates if stored improperly, potential kinetic isotope effects during partial equilibration or concentration-dependent release, and instrument detection limits (in our tests, the spectrometer isotope signal reached its lower detection limit when evolved H_2O partial pressure fell to ~150 Pa).

Another important advantage of traceable solid calibration materials is their ability to provide reference anchors for correcting isotope memory effects during repeated measurements. Water-isotope analyses are particularly susceptible to memory effects because residual H_2O can adsorb on chamber walls, valves, transfer lines, and optical cells, causing the isotope signal of one measurement to influence subsequent analyses. This problem may become more pronounced in spaceborne instruments, where repeated purge, bake-out, and full replacement of the gas-handling pathway are constrained by power, time, and mechanical resources. A solid calibrant with a known H_2O content and δD value can therefore serve as an intermittent truth anchor in the measurement sequence. By inserting calibration releases before, between, or after sample analyses, the residual contribution from previous measurements can be quantified, allowing correction of baseline drift, adsorption–desorption effects, and carryover-induced isotope bias. In this sense, traceable $Cu(OH)_2$ is not only a calibration source for absolute δD assignment, but also a practical tool for maintaining isotope-data consistency during repeated LUWA-related ground validation and, after

further qualification, for future planetary isotope-measurement workflows.

To mitigate these risks, calibration materials should be stored under inert, anhydrous conditions or in evacuated, gas-tight containers, and where practical, thermally pre-cleaned, with an aliquot reserved for isotopic verification. Before measurement, samples must be evacuated to high vacuum (for example, below 10^{-5} Pa) and then subjected to controlled heating, ensuring that the partial pressure of evolved gases remains under the threshold for concentration-dependent isotope effects (approximately 250 Pa). Rigorous monitoring of background levels and reproducibility through blanks and replicate releases further safeguards measurement integrity.

The isotope precision of LUWA also defines the level of source discrimination that can be realistically achieved. For a single dominant source, the designed δD precision of LUWA, approximately 50‰, is sufficient to distinguish the solar-wind end-member ($\delta D < -980‰$) from the more D-enriched asteroidal/cometary end-members, but is not sufficient to resolve asteroidal vs. cometary mixtures when the solar-wind contribution is minor. Here, the 5.3–8.3‰ isotopic offsets observed for the synthesized $Cu(OH)_2$ calibrants are smaller than the instrumental design precision and therefore are not expected to dominate the current isotope error budget. However, source interpretation becomes less straightforward when lunar water ice represents a mixture of multiple reservoirs. In particular, if the solar-wind component is absent or minor, mixed asteroidal and cometary contributions may become difficult to distinguish using δD alone because their effective isotopic signatures can overlap depending on the mixing proportion. In such cases, isotope data should be combined with quantitative mixing models, constrained by the impact history, cold-trap evolution, and thermal history of the Moon, as well as by the spatial and structural information provided by other Chang'E-7 payloads.

The solid form factor reduces leakage and handling risks relative to pressurized gas and liquid standards and is compatible with the restricted heating capability of LUWA. Ag_2CO_3 supports repeated pressure-controlled partial release for onboard referencing, whereas $Cu(OH)_2$ provides a consumable H_2O and δD reference for ground validation. The tested calibration units retained their functional calibration capability after vibration, thermal cycling, and storage for more than four months. These results support the robustness of the solid calibration approach under the tested conditions, although longer-duration stability, shelf life, and formal flight qualification require further systematic evaluation.

Overall, Ag_2CO_3 and traceable $Cu(OH)_2$ provide complementary reference functions within the LUWA calibration and validation framework. The present results demonstrate controlled target-gas generation, repeated onboard CO_2 referencing capability, and consistency between the mean isotope compositions of precursor waters and solid-derived H_2O. It provides LUWA with a traceable calibration reference for acquiring reliable H_2O and δD information, which can contribute critical isotopic constraints for interpreting the origin of lunar water ice, particularly when integrated with subsurface structural information from in-situ radar sounding, including possible ice layer boundaries, burial depth, ice layer continuity, and dielectric heterogeneity, as well as orbital remote-sensing constraints on the spatial distribution and geological context of potential ice-bearing deposits[60]. Further work should quantify release-to-release reproducibility, gas recovery and instrumental response, long-term storage stability, and the feasibility of memory-effect correction using traceable solid H_2O references.

CONCLUSIONS

Accurate in-situ detection of lunar water ice requires reliable measurements of both water abundance and hydrogen isotopic composition. Deep-space operating conditions, including ultra-high vacuum, tight energy constraints, limited sealing capability, and extreme temperature variations, challenge conventional gas- and liquid-phase calibration methods and require calibration strategies compatible with lunar operational constraints.

To meet these requirements for the Chang'E-7 LUWA, we evaluated silver carbonate and copper hydroxide as solid calibration materials. Vacuum thermogravimetric analysis showed that both materials release calibration gases within an operationally feasible temperature range under vacuum. Full-process prototype validation further confirmed that Ag_2CO_3 and $Cu(OH)_2$ can generate identifiable CO_2 and H_2O signals, respectively, for spectral and mass-spectrometric calibration. These results demonstrate the feasibility of using solid materials as compact calibration sources for LUWA under simulated space-environment constraints.

For hydrogen-isotope calibration, we developed a synthesis route for $Cu(OH)_2$ with a traceable hydrogen isotopic signature derived from precursor water. The synthesized $Cu(OH)_2$ largely preserved the isotopic information of the precursor water, providing a route toward traceable solid-phase δD calibration. We then integrated this material into a prototype water-molecule analyzer and established a solid-phase hydrogen-isotope measurement workflow, demonstrating its applicability for LUWA-related H_2O release and isotope-detection experiments.

The two materials serve different calibration roles. Ag_2CO_3 provides a stable CO_2 calibration source and is suitable for both ground-based testing and final mission calibration. The synthesized $Cu(OH)_2$ developed in this study provides a traceable solid H_2O source for hydrogen-isotope-related calibration and validation under laboratory conditions. Although our synthesis

strategy effectively controls the hydrogen source and overcomes the isotope-traceability issue of commercial $Cu(OH)_2$, introducing an additional H_2O-releasing material during in-situ lunar measurements could increase the background water signal and interfere with the analysis of indigenous lunar water. Therefore, $Cu(OH)_2$ is used primarily for LUWA ground calibration, prototype testing, and controlled regolith-simulant experiments.

In the ground-based regolith experiments, $Cu(OH)_2$ was used as a controllable analogue for ice-bearing or "dirty-ice" regolith. This strategy allows the preparation of regolith simulants with known and reproducible water contents, while avoiding uncontrolled water loss caused by sublimation during sample preparation and storage. Because the hydrogen in the synthesized $Cu(OH)_2$ is chemically incorporated from precursor water with a known isotopic composition, the material also minimizes sublimation-driven isotope fractionation before measurement. It therefore provides a stable and traceable solid H_2O source for testing the LUWA heating-release and detection process under controlled laboratory conditions.

By establishing a traceable solid-calibration route, this work improves the reliability of the first step in the Chang'E-7 water-ice information chain: the conversion of released gas signals into quantitative H_2O abundance and δD data. They can provide ground-truth-like point constraints for evaluating radar- and remote-sensing-based interpretations of polar ice deposits. For example, in-situ radar sounding can reveal subsurface layering, burial geometry, and dielectric contrasts along the rover traverse, while orbital observations can place these local measurements within the broader spatial and geological setting of candidate ice-bearing regions. In this way, calibrated LUWA data can strengthen the joint assessment of where lunar polar water ice occurs, how it is stored in the regolith, and which source reservoirs may have contributed to its formation.

REFERENCES

[1] Nakajima M. and Stevenson D.J. (2018). Inefficient volatile loss from the Moon-forming disk: Reconciling the giant impact hypothesis and a wet Moon. Earth Planet. Sci. Lett. 487:117-126. DOI:10.1016/j.epsl.2018.01.026

[2] Arnold J.R. (1979). Ice in the lunar polar regions. J. Geophys. Res. Solid Earth 84:5659-5668. DOI:10.1029/JB084iB10p05659

[3] Watson K., Murray B., and Brown H. (1961). On the possible presence of ice on the Moon. J. Geophys. Res. 66:1598-1600. DOI:10.1029/JZ066i005p01598

[4] Paige D.A., Siegler M.A., Zhang J.A., et al. (2010). Diviner lunar radiometer observations of cold traps in the Moon's south polar region. Science 330:479-482. DOI:10.1126/science.1187726

[5] Nozette S., Lichtenberg C.L., Spudis P.D., et al. (1996). The Clementine bistatic radar experiment. Science 274:1495-1498. DOI:10.1126/science.274.5292.1495

[6] Fa W. and Cai Y. (2013). Circular polarization ratio characteristics of impact craters from Mini-RF observations and implications for ice detection at the polar regions of the Moon. J. Geophys. Res. Planets 118:1582-1608. DOI:10.1002/jgre.20110

[7] Sanin A.B., Mitrofanov I.G., Litvak M.L., et al. (2017). Hydrogen distribution in the lunar polar regions. Icarus 283:20-30. DOI:10.1016/j.icarus.2016.06.002

[8] Li S. and Milliken R.E. (2017). Water on the surface of the Moon as seen by the Moon Mineralogy Mapper: Distribution, abundance, and origins. Sci. Adv. 3:e1701471. DOI:10.1126/sciadv.1701471

[9] Li S., Lucey P.G., Milliken R.E., et al. (2018). Direct evidence of surface exposed water ice in the lunar polar regions. Proc. Natl. Acad. Sci. U.S.A. 115:8907-8912. DOI:10.1073/pnas.1802345115

[10] Honniball C.I., Lucey P.G., Li S., et al. (2021). Molecular water detected on the sunlit Moon by SOFIA. Nat. Astron. 5:121-127. DOI:10.1038/s41550-020-01222-x

[11] Colaprete A., Schultz P.H., Heldmann J.L., et al. (2010). Detection of water in the LCROSS ejecta plume. Science 330:463-468. DOI:10.1126/science.1186986

[12] Spudis P.D., Bussey D.B.J., Baloga S.M., et al. (2013). Evidence for water ice on the Moon: Results for anomalous polar craters from the LRO Mini-RF imaging radar. J. Geophys. Res. Planets 118:2016-2029. DOI:10.1002/jgre.20156

[13] Mo L., Xu J., Dong Z., et al. (2025). Water ice and the shallow regolith structure of the Shackleton Crater, the Moon: Implications for future Chang'E-7 in situ radar observation. Space Sci. Technol. 5:0225. DOI:10.34133/space.0225

[14] Saal A.E., Hauri E.H., Van Orman J.A., et al. (2013). Hydrogen isotopes in lunar volcanic glasses and melt inclusions reveal a carbonaceous chondrite heritage. Science 340:1317-1320. DOI:10.1126/science.1235142

[15] Barnes J.J., Kring D.A., Tartèse R., et al. (2016). An asteroidal origin for water in the Moon.

Nat. Commun. 7:11684. DOI:10.1038/ncomms11684

[16] Greenwood J.P., Itoh S., Sakamoto N., et al. (2011). Hydrogen isotope ratios in lunar rocks indicate delivery of cometary water to the Moon. Nat. Geosci. 4:79-82. DOI:10.1038/ngeo1050

[17] Liu Y., Guan Y., Zhang Y., et al. (2012). Direct measurement of hydroxyl in the lunar regolith and the origin of lunar surface water. Nat. Geosci. 5:779-782. DOI:10.1038/ngeo1601

[18] Hallis L.J. (2017). D/H ratios of the inner Solar System. Philos. Trans. R. Soc. A 375:20150390. DOI:10.1098/rsta.2015.0390

[19] Piani L., Nagashima K., Kawasaki N., et al. (2023). Hydrogen isotopic composition of hydrous minerals in asteroid Ryugu. Astrophys. J. Lett. 946:L43. DOI:10.3847/2041-8213/acc393

[20] Wiens R.C., Bochsler P., Burnett D.S., et al. (2004). Solar and solar wind isotopic compositions. Earth Planet. Sci. Lett. 226:549-565. DOI:10.1016/j.epsl.2004.07.011

[21] Moine B., Bolfan-Casanova N., Radu I., et al. (2020). Molecular hydrogen in minerals as a clue to interpret D variations in the mantle. Nat. Commun. 11:3604. DOI:10.1038/s41467-020-17442-8

[22] Li Y., Shen S., Lu W., et al. (2026). Calibration method and implementation for the Lunar Penetrating Radar on Chang'E-7 mission (in Chinese). Chin. J. Space Sci. 46:507-519. DOI:10.11728/cjss2026.02.2025-0102

[23] Wang C., Jia Y., Xue C., et al. (2024). Scientific objectives and payload configuration of the Chang'E-7 mission. Natl. Sci. Rev. 11:nwad329. DOI:10.1093/nsr/nwad329

[24] Shen S., Tang C., Li Y., et al. (2025). The Lunar Penetrating Radar on the Chang'E-7 Rover. Space Sci. Rev. 221:98. DOI:10.1007/s11214-025-01223-0

[25] Feng J., Siegler M.A., and White M.N. (2022). Dielectric properties and stratigraphy of regolith in the lunar South Pole-Aitken basin: Observations from the Lunar Penetrating Radar. Astron. Astrophys. 661:A47. DOI:10.1051/0004-6361/202143015

[26] Li X., Cao N.L., Kan R.F., et al. (2025). Miniaturized tunable laser spectrometer for the simultaneous detection of water ice and hydrogen-oxygen isotopes for the Chang'E-7 Lunar Soil Water Molecule Analyzer. ACS Sens. 10:4679-4686. DOI:10.1021/acssensors.5c01115

[27] Pfeiffer Vacuum. (2008). The Vacuum Technology Book. Pfeiffer Vacuum.

[28] Cappa C.D., Hendricks M.B., DePaolo D.J., et al. (2003). Isotopic fractionation of water during evaporation. J. Geophys. Res. Atmos. 108:4525. DOI:10.1029/2003JD003597

[29] Repplinger C., Sellen S., Kedziora S., et al. (2024). Material modeling for numerical simulation of elastomer O-rings with experimental verification at low temperatures. Int. J. Hydrogen Energy 80:1046-1061. DOI:10.1016/j.ijhydene.2024.06.427

[30] Li X., Wang X., Lu W., et al. (2023). Design for in-situ water ice analysis in the lunar polar region. J. Deep Space Explor. 10:618-630. DOI:10.15982/j.issn.2096-9287.2023.20230106

[31] Roush T.L., Colaprete A., Cook A., et al. (2021). The Volatiles Investigating Polar Exploration Rover (VIPER) Near Infrared Volatile Spectrometer System (NIRVSS). 52nd Lunar Planet. Sci. Conf., abstract 1678.

[32] Baldridge A.M., Hook S.J., Grove C.I., et al. (2009). The ASTER spectral library version 2.0. Remote Sens. Environ. 113:711-715. DOI:10.1016/j.rse.2008.11.007

[33] Aguilar Ayala R., Hancock M.L., Jarnot A.W., et al. (2023). Mass Spectrometer Observing Lunar Operations (MSolo). 71st ASMS Conf. Mass Spectrom. Allied Topics, Houston, TX.

[34] Colaprete A. (2021). Volatiles Investigating Polar Exploration Rover (VIPER). NASA Technical Reports Server, Document ID 20210015009.

[35] Chumikov A.E., Cheptsov V.S., Wurz P., et al. (2021). Design, characteristics and scientific tasks of the LASMA-LR laser ionization mass spectrometer onboard Luna-25 and Luna-27 space missions. Int. J. Mass Spectrom. 469:116676. DOI:10.1016/j.ijms.2021.116676

[36] Meshcherinov V., Gazizov I., Kazakov V., et al. (2024). Spectrometer to explore isotopologues of lunar volatiles on Luna-27 lander. Planet. Space Sci. 248:105935. DOI:10.1016/j.pss.2024.105935

[37] Verchovsky A.B., Anand M., Barber S.J., et al. (2020). A quantitative evolved gas analysis for extra-terrestrial samples. Planet. Space Sci. 181:104830. DOI:10.1016/j.pss.2019.104830

[38] Straus S. and Madorsky S.L. (1956). Thermal degradation of unvulcanized and vulcanized rubber in vacuum. Ind. Eng. Chem. 48:1212-1219. DOI:10.1021/ie50559a036

[39] Losekamm M.J., Barber S., Biswas J., et al. (2021). LUVMI-X: A versatile platform for resource prospecting on the Moon. In Earth and Space 2021, pp. 289-299. DOI:10.1061/9780784483374.029

[40] Morse A., Mousis O., Sheridan S., et al. (2015). Low CO/CO2 ratios of comet 67P measured at the Abydos landing site by the Ptolemy mass spectrometer. Astron. Astrophys. 583:A42. DOI:10.1051/0004-6361/201526624

[41] Chen R., Lu W., Li X., et al. (2024). Chang'E-7 Lunar Soil Water Molecule Analyzer (LSWMA) prototype for high-precision measurement of water content and hydrogen isotope ratio. J. Earth Sci. 35:2180-2182. DOI:10.1007/s12583-024-2023-7

[42] Li X., Lu W., Qiu Z., et al. (2026). Ground calibration test method for Chang'E-7 Lunar Soil Water Molecule Analyzer (in Chinese). Chin. J. Space Sci. 46:465-474. DOI:10.11728/cjss2026.02.2025-0151

[43] Chen R., Lu W., Li X., et al. (2026). A high-precision lunar soil water content estimation method designed for the Chang'E-7 Lunar Soil Water Molecule Analyzer (LSWMA). Planet 2:26011. DOI:10.15302/planet.2026.26011

[44] Vorholz J., Harismiadis V.I., Rumpf B., et al. (2000). Vapor-liquid equilibrium of water, carbon dioxide, and the binary system water-carbon dioxide, from molecular simulation. Fluid Phase Equilib. 170:203-234. DOI:10.1016/S0378-3812(00)00315-0

[45] L'vov B.V. (2002). Mechanism and kinetics of thermal decomposition of carbonates. Thermochim. Acta 386:1-16. DOI:10.1016/S0040-6031(01)00757-2

[46] Jurczyk J., Glessi C., Madajska K., et al. (2022). Vacuum versus ambient pressure inert gas thermogravimetry: A study of silver carboxylates. J. Therm. Anal. Calorim. 147:2187-2195. DOI:10.1007/s10973-021-10616-6

[47] Shamsipur M., Pourmortazavi S.M., Hajimirsadeghi S.S., et al. (2013). Facile synthesis of zinc carbonate and zinc oxide nanoparticles via direct carbonation and thermal decomposition. Ceram. Int. 39:819-827. DOI:10.1016/j.ceramint.2012.07.003

[48] Genchi G., Sinicropi M.S., Lauria G., et al. (2020). The effects of cadmium toxicity. Int. J. Environ. Res. Public Health 17:3782. DOI:10.3390/ijerph17113782

[49] Paustenbach D.J., Tvermoes B.E., Unice K.M., et al. (2013). A review of the health hazards posed by cobalt. Crit. Rev. Toxicol. 43:316-362. DOI:10.3109/10408444.2013.779633

[50] Cheng L., Li W., Li Y., et al. (2019). Thermal analysis and decomposition kinetics of the dehydration of copper sulfate pentahydrate. J. Therm. Anal. Calorim. 135:2697-2703. DOI:10.1007/s10973-018-7595-y

[51] Paulik F., Paulik J., and Arnold M. (1992). Thermal decomposition of gypsum. Thermochim. Acta 200:195-204. DOI:10.1016/0040-6031(92)85115-C

[52] Fukuda M., Favergeon L., and Koga N. (2019). Universal kinetic description for thermal decomposition of copper(II) hydroxide over different water vapor pressures. J. Phys. Chem. C 123:20903-20915. DOI:10.1021/acs.jpcc.9b04704

[53] Kan R.F., Cao N.L., Chen R., et al. (2025). A solid calibration material for hydrogen isotopes and its preparation method. China Patent CN 119935668 B, September 30, 2025.

[54] Hynes J.T. (1985). Chemical reaction dynamics in solution. Annu. Rev. Phys. Chem. 36:573-597. DOI:10.1146/annurev.pc.36.100185.003041

[55] Kendall C. and Caldwell E.A. (1998). Fundamentals of isotope geochemistry. In Isotope Tracers in Catchment Hydrology, Kendall C. and McDonnell J.J., eds. (Elsevier), pp. 51-86. DOI:10.1016/B978-0-444-81546-0.50009-4

[56] Cole D.R. and Chakraborty S. (2001). Rates and mechanisms of isotopic exchange. Rev. Mineral. Geochem. 43:83-224. DOI:10.2138/rmg.2001.43.2

[57] Schmidt M., Maseyk K., Lett C., et al. (2010). Concentration effects on laser-based δ18O and δ2H measurements and implications for the calibration of vapour measurements with liquid standards. Rapid Commun. Mass Spectrom. 24:3553-3561. DOI:10.1002/rcm.4813

[58] Tremoy G., Vimeux F., Cattani O., et al. (2011). Measurements of water vapor isotope ratios with wavelength-scanned cavity ring-down spectroscopy technology: New insights and important caveats for deuterium excess measurements in tropical areas in comparison with isotope-ratio mass spectrometry. Rapid Commun. Mass Spectrom. 25:3469-3480. DOI:10.1002/rcm.5252

[59] Li H. and Feng L. (2019). A rapid method for determination of the hydrogen isotopes of H2O in micro-inclusions by chromium-filled elemental analyzer/isotope ratio mass spectrometry. Rapid Commun. Mass Spectrom. 33:946-950. DOI:10.1002/rcm.8430

[60] Zhao C., Zhang L., Lu S., et al. (2025). Research and prospect of ground-penetrating radar on

the Moon. J. Geophys. Eng. 22:1431-1447. DOI:10.1093/jge/gxaf084

FUNDING AND ACKNOWLEDGEMENTS

This study was co-supported by the Science and Technology Development Fund of Macau (Nos. 0002/2025/AKP, 0052-2024-RIA1, 0021/2024/RIA1, 0158/2024/AFJ, 0002/2024/SKL, and 0034/2024/AMJ), the National Key Research and Development Program of China (No. 2024YFE0201000), the National Natural Science Foundation of China (Nos. 62205346, 42201389, 42104141, and W2541013), the Shanghai Pujiang Program (No. 25PJA138), the Postdoctoral Fellowship Program of CPSF (No. GZC20241751), and the Anhui Postdoctoral Scientific Research Program Foundation (No. 2024B831). The authors thank the Stable Isotope Laboratory of the Institute of Geology and Geophysics, Chinese Academy of Sciences, for conducting the Cr-EA/IRMS analyses of the synthesized solid samples. We also sincerely thank the two anonymous reviewers and the editor for their constructive comments and suggestions, which helped improve the quality and clarity of the manuscript. **The funders had no role in study design, data collection and analysis, decision to publish, or preparation of the manuscript.**

AUTHOR CONTRIBUTIONS

Rui Chen contributed to the proposal of the methodology, experimental design, construction of the experimental platform, conduction of experiments, data processing, and manuscript writing. Xiang Li and Wenzhen Lu contributed to the construction of the experimental platform, conduction of experiments, and data processing. Waikei Ng, Kan Chen, and Zhenping Sui contributed to the construction of the experimental platform. Xindong Meng, Renrui Liu, Honkuan Wong, Rongji Li, Yun Qin, and Ling Zhang were responsible for the verification and processing of experimental data. Yi Xu, Nailiang Cao, Hejiu Hui, Qiquan Yang, Xiaoping Zhang, Zhenyu Xu, Ruifeng Kan, Meiru Guo, and Rui Gao provided the experimental facilities, instruments, and revision suggestions for this manuscript. **All authors contributed to the manuscript and approved the final version.**

DECLARATION OF INTERESTS

Qiquan Yang is an Editorial Board member of *The Innovation Informatics* and was blinded from reviewing or making final decisions on the manuscript. Peer review was handled independently of this member and their research group. The other authors declare no conflicts of interest.

DATA AND CODE AVAILABILITY

The data that support the findings of this study are available from the corresponding authors upon reasonable request.

ETHICAL STATEMENT AND PATIENT CONSENT

Not applicable.

SUPPLEMENTAL INFORMATION

It can be found online at https://doi.org/10.59717/j.xinn-inform.2026.1000xx

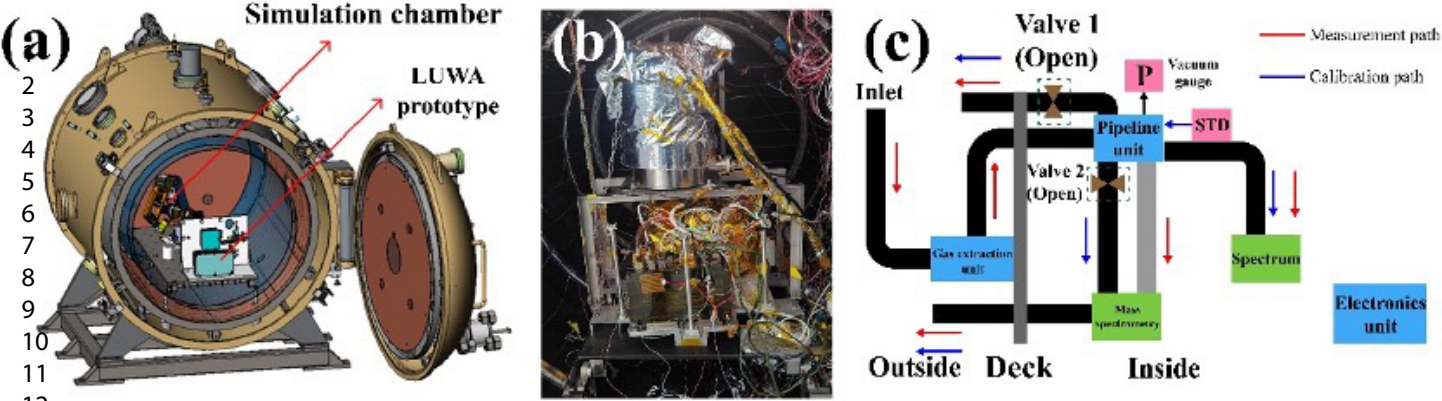
(a)
Simulation chamber
LUWA
prototype
(b)
(c)
Valve 1
(Open)
Inlet
P
Vacuum
gauge
Measurement path
Calibration path
Pipeline
unit
STD
Valve 2
(Open)
Gas extraction
unit
Spectrum
Mass
spectrometry
Electronics
unit
Outside
Deck
Inside

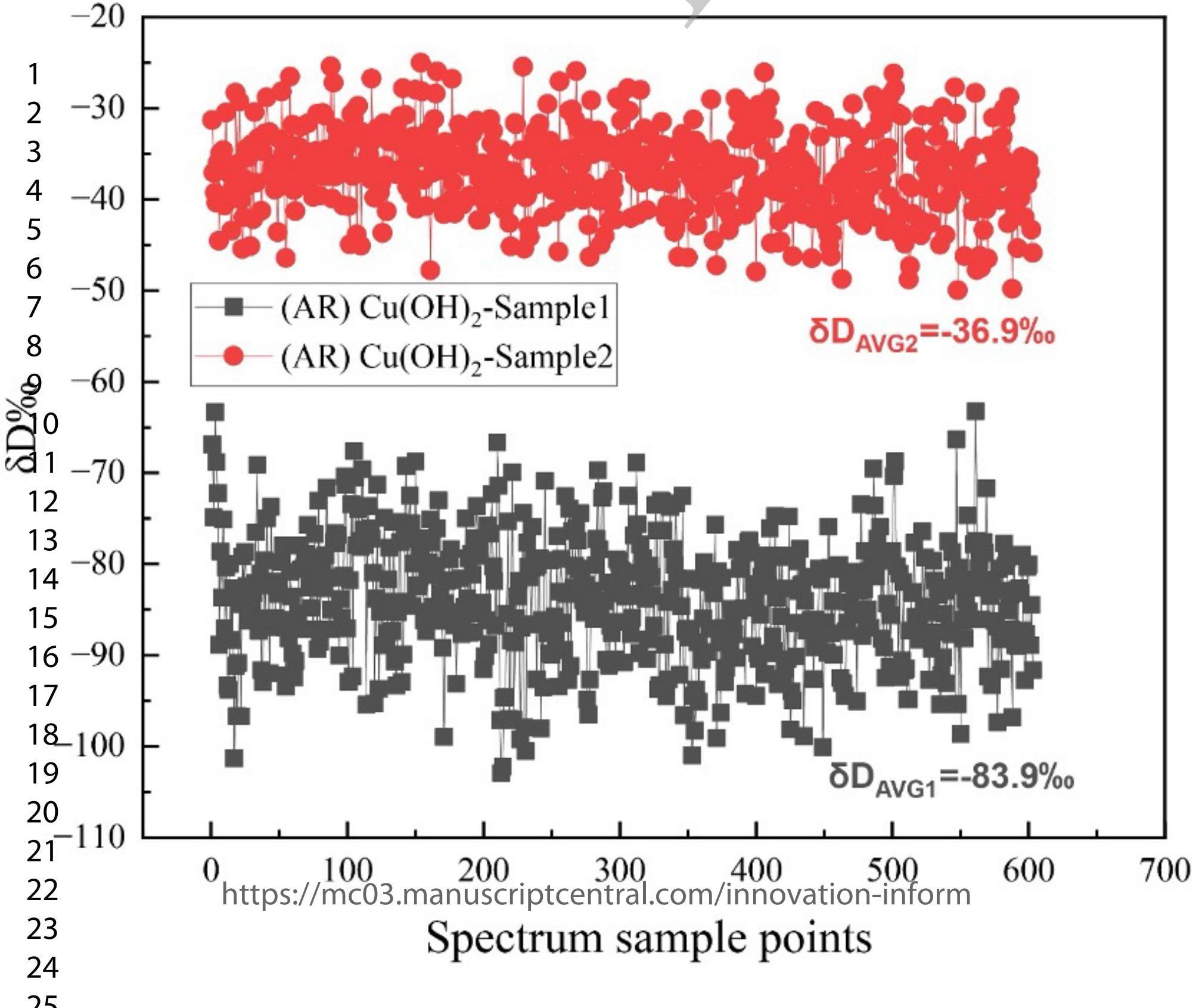
−20
−30
−40
−50
−60
−70
−80
−90
−100
−110
δD‰
(AR) Cu(OH)2-Sample1
(AR) Cu(OH)2-Sample2
δDAVG2=-36.9‰
δDAVG1=-83.9‰
0
100
200
300
400
500
600
700
Spectrum sample points

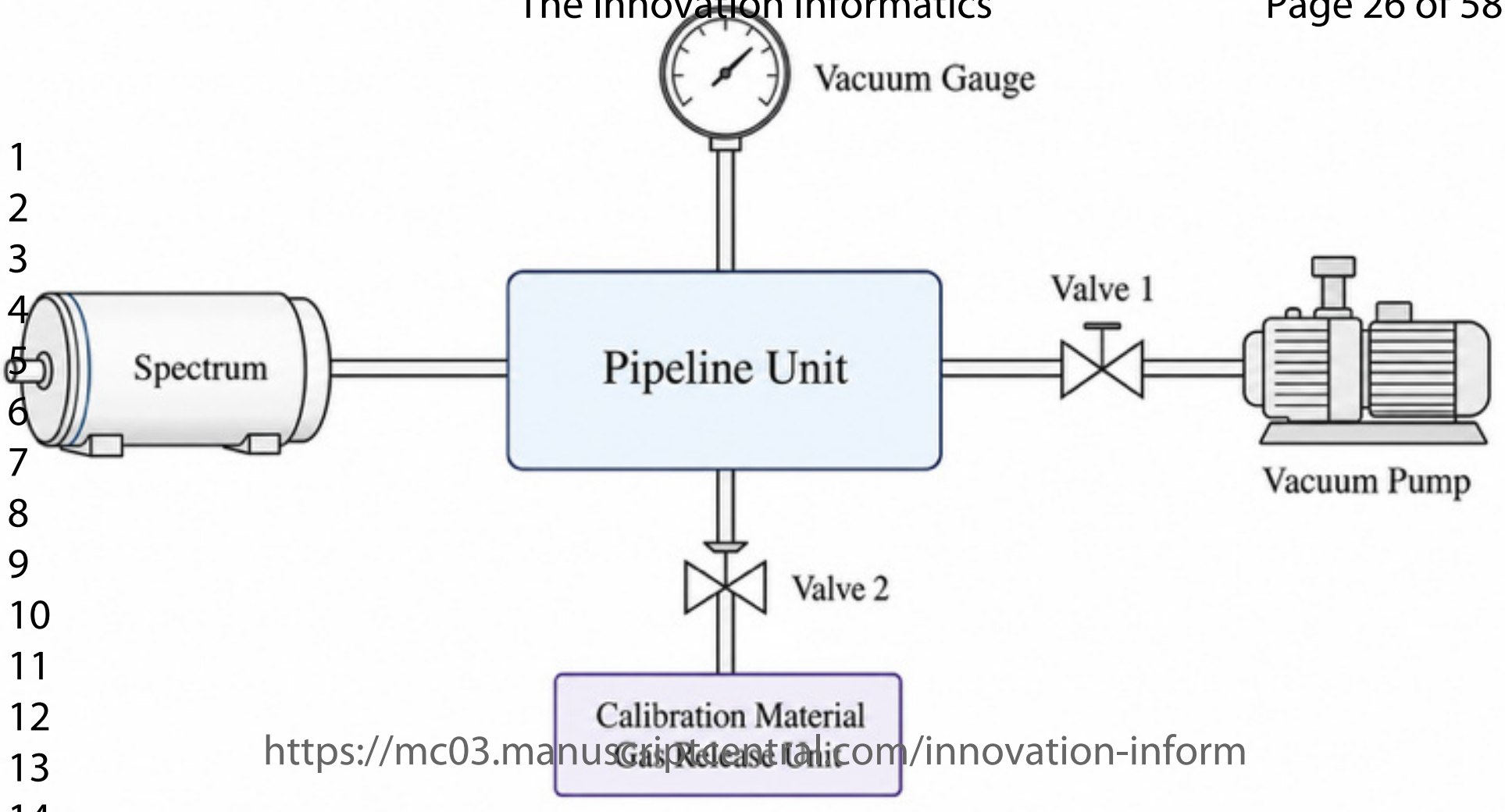

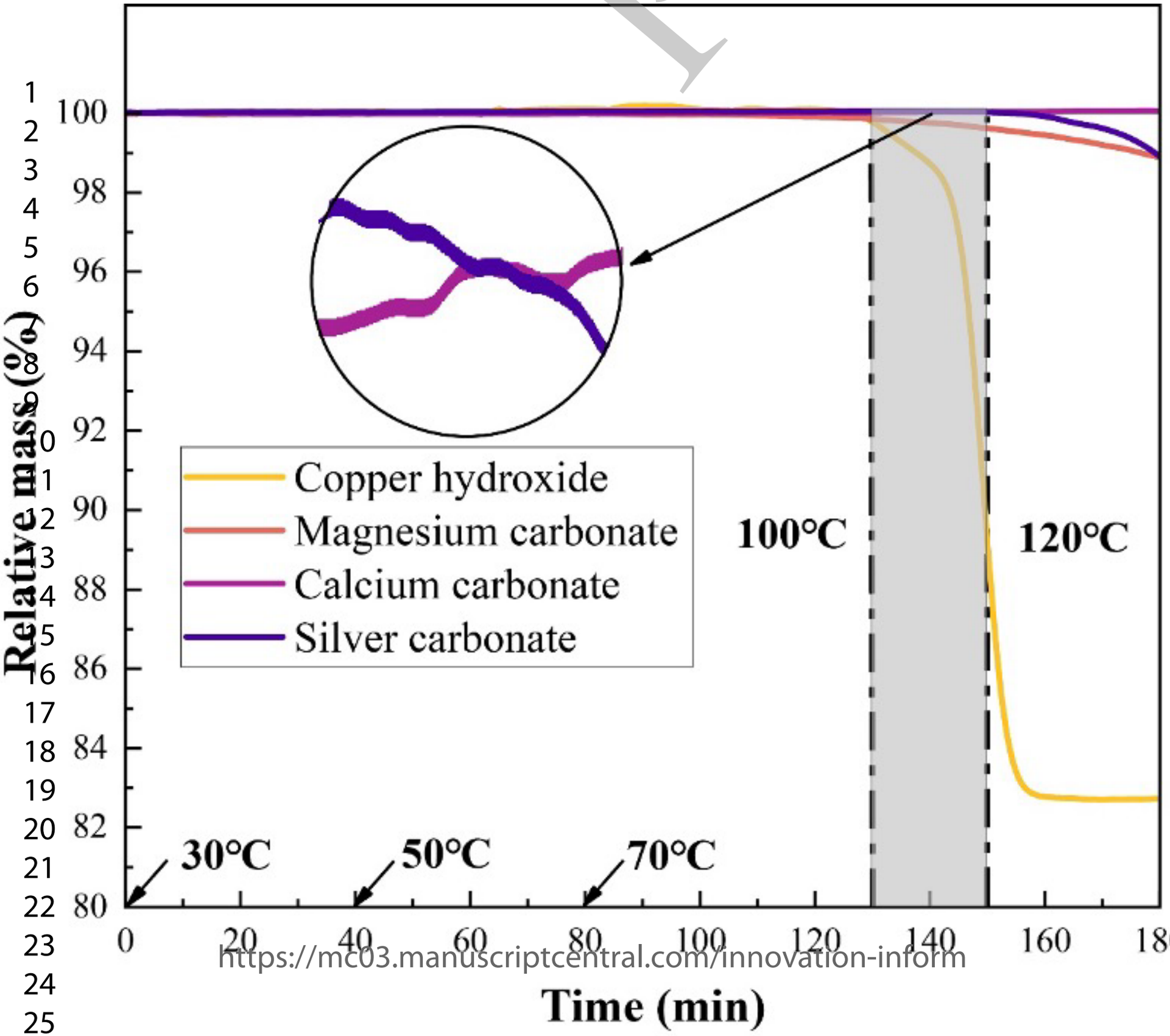

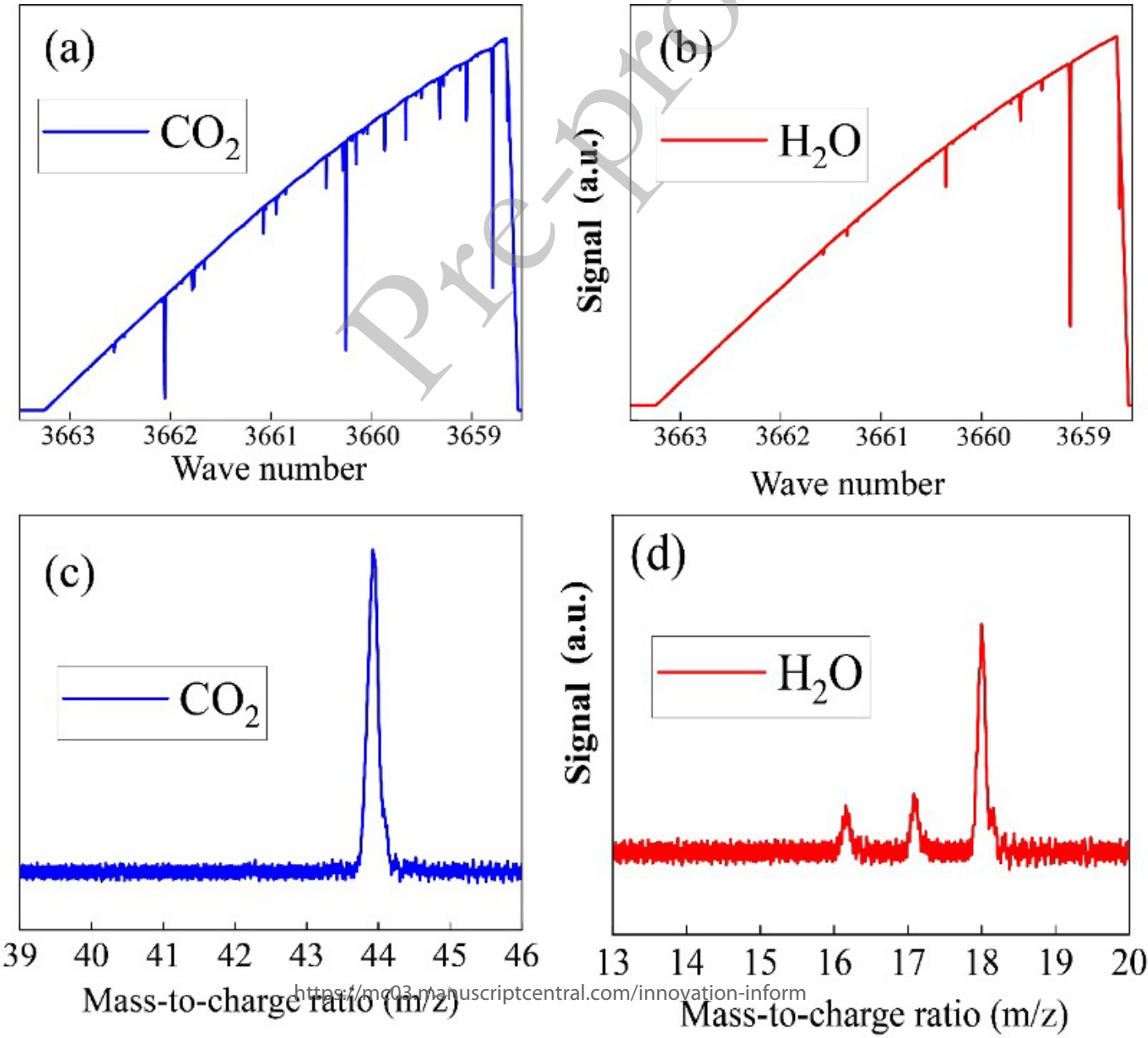
(a)
CO2
Signal (a.u.)
3663
3662
3661
3660
3659
Wave number
(b)
H2O
Signal (a.u.)
3663
3662
3661
3660
3659
Wave number
(c)
CO2
Signal (a.u.)
39
40
41
42
43
44
45
46
Mass-to-charge ratio (m/z)
(d)
H2O
Signal (a.u.)
13
14
15
16
17
18
19
20
Mass-to-charge ratio (m/z)

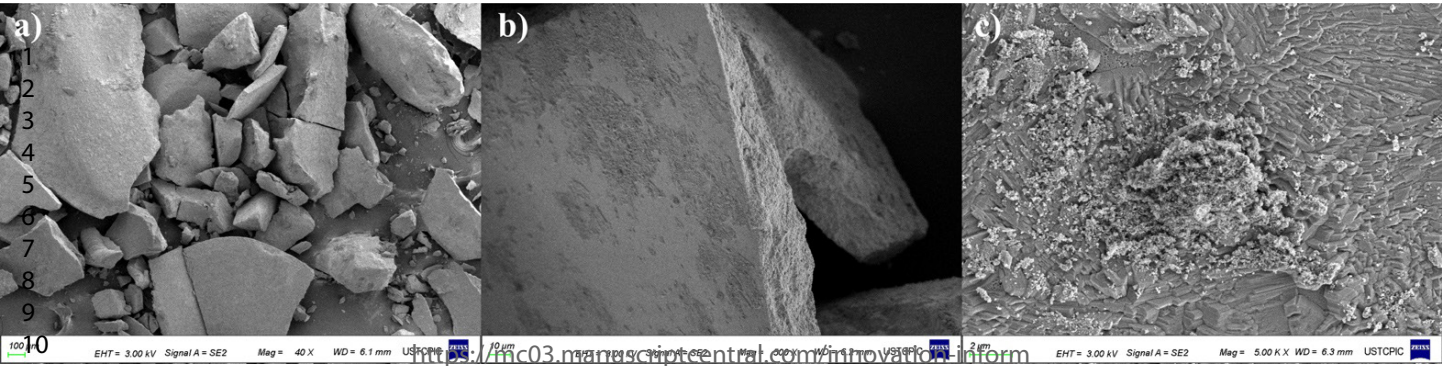

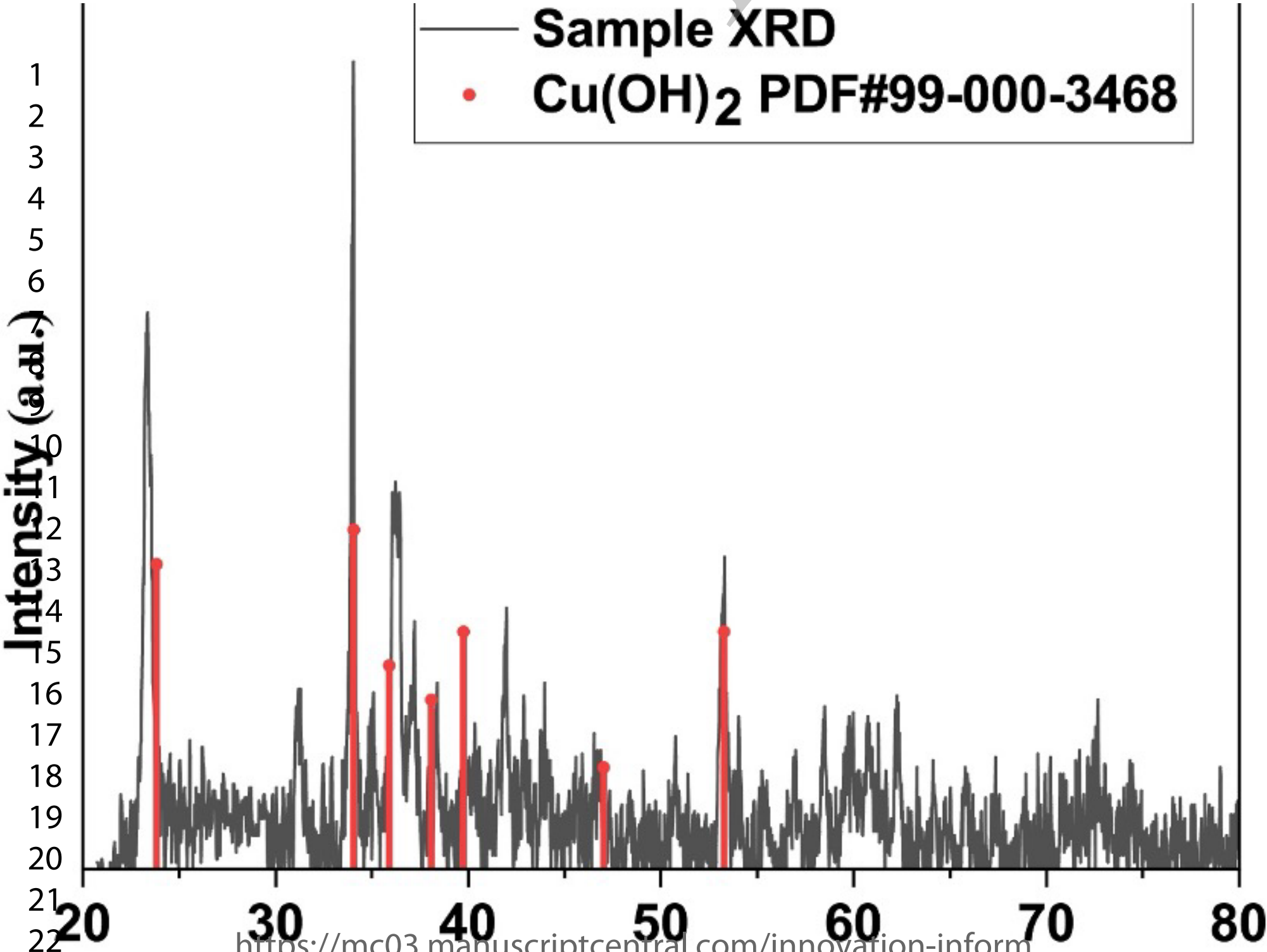
Sample XRD
Cu(OH)2 PDF#99-000-3468
Intensity (a.u.)
20
30
40
50
60
70
80

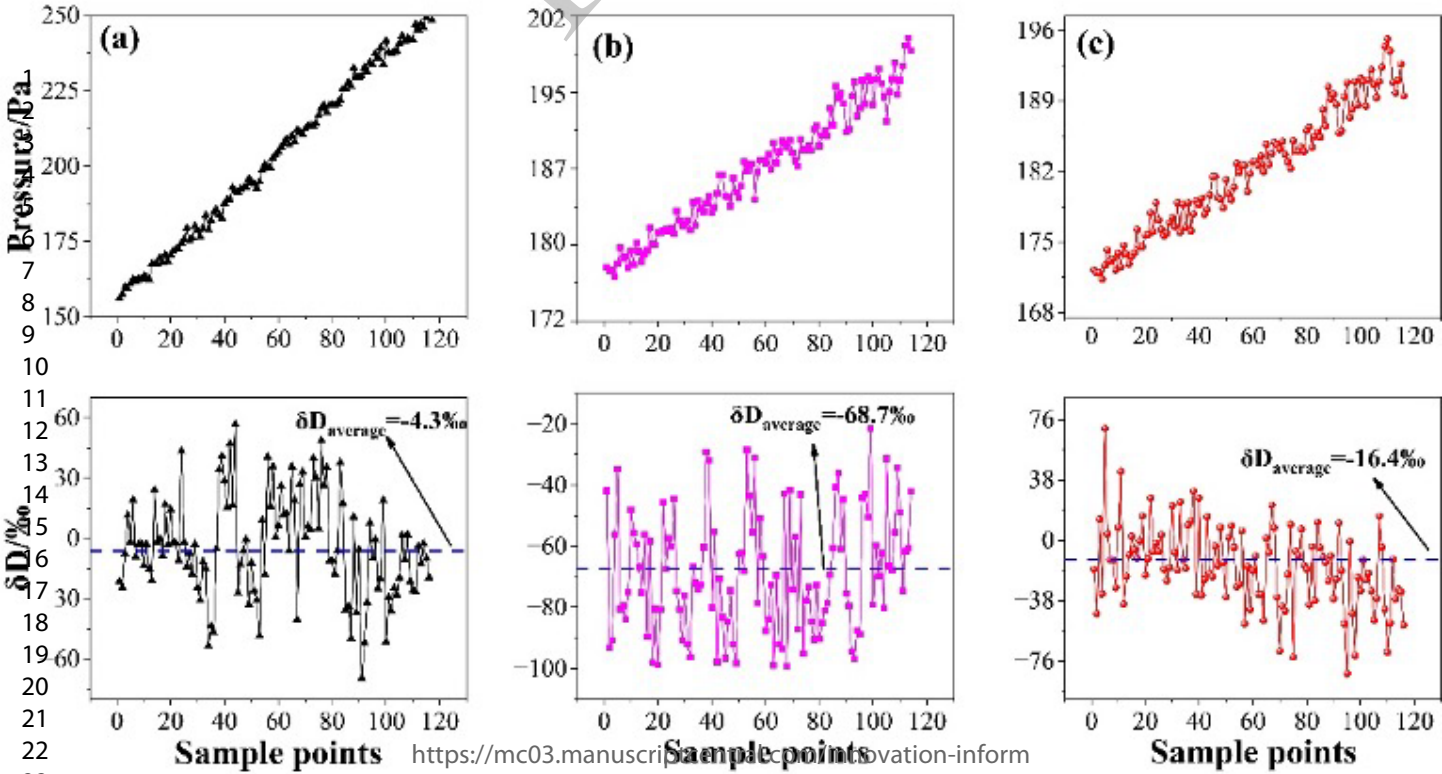

A dual-role solid calibration strategy for Chang'E-7 LUWA: Onboard CO_2 referencing and ground-based H_2O/δD validation

Rui Chen,[1,2,8] Xiang Li,[2,8] Wenzhen Lu,[1,2] Yi Xu,[1] Nailiang Cao,[2] Hejiu Hui,[3] Qiquan Yang,[4] Waikei Ng,[1] Xiaoping Zhang,[1] Kan Chen,[2] Zhenping Sui,[2,5] Zhenyu Xu,[2] Xindong Meng,[1] Renrui Liu,[1] Honkuan Wong,[1] Rongji Li,[2] Yun Qin,[1] Ling Zhang,[6] Ruifeng Kan,[2] Meiru Guo,[7] and Rui Gao[6]

*Correspondence: yixu@must.edu.mo (Y.X.); nlcao@aiofm.ac.cn (C.N.)

(The title should contain no more than **130** characters, including spaces.)

GRAPHICAL ABSTRACT

PUBLIC SUMMARY

- Chang'E-7's LUnar soil Water molecule Analyzer (LUWA) will measure lunar polar water and hydrogen isotopes.
- Solid materials were developed to release CO_2 or H_2O under vacuum with modest heating.
- Ag_2CO_3 enables repeated onboard CO_2 referencing through controlled partial gas release.
- Traceable $Cu(OH)_2$ provides an H_2O and hydrogen-isotope reference for ground calibration.
- These solid references support calibration of LUWA water and hydrogen-isotope measurements.

Key Words: Chang'E-7, LUnar soil Water molecule Analyzer (LUWA), Hydrogen isotope measurement, Multi-payload detection framework; Lunar polar water ice

A dual-role solid calibration strategy for Chang'E-7 LUWA: Onboard CO_2 referencing and ground-based H_2O/δD validation

Rui Chen,[1,2,8] Xiang Li,[2,8] Wenzhen Lu,[1,2] Yi Xu,[1] Nailiang Cao,[2] Hejiu Hui,[3] Qiquan Yang,[4] Waikei Ng,[1] Xiaoping Zhang,[1] Kan Chen,[2] Zhenping Sui,[2,5] Zhenyu Xu,[2] Xindong Meng,[1] Renrui Liu,[1] Honkuan Wong,[1] Rongji Li,[2] Yun Qin,[1] Ling Zhang,[6] Ruifeng Kan,[2] Meiru Guo,[7] and Rui Gao[6]

[1]The State Key Laboratory of Lunar and Planetary Science/Space Science Institute, Macau University of Science and Technology, Macau 999078, China
[2]Anhui Institute of Optics and Fine Mechanics, Hefei Institutes of Physical Science, Chinese Academy of Sciences, Hefei 230031, China
[3]The State Key Laboratory of Critical Earth Material Cycling and Mineral Deposits & Lunar and Planetary Science Institute, School of Earth Sciences and Engineering, Nanjing University, Nanjing 210023, China
[4]College of Surveying & Geo-Informatics, Tongji University, Shanghai 200092, China
[5]Jianghuai Advance Technology Center, Hefei 230000, China
[6]School of Earth Science and Engineering, Sun Yat-Sen University, Guangzhou 510275, China
[7]Lanzhou Institute of Physics, CAST, Lanzhou 730000, China
[8]The authors have the same contribution
*Correspondence: yixu@must.edu.mo (Y.X.); nlcao@aiofm.ac.cn (C.N.)

ABSTRACT

Lunar polar water ice is a key target of the Chang'E-7 mission because its abundance, physical state, and origin remain insufficiently constrained. Within the Chang'E-7 multi-payload framework, the LUnar soil Water molecule Analyzer (LUWA) is designed to measure H_2O abundance and hydrogen isotopic composition in permanently shadowed regions. Reliable measurements require calibration compatible with high vacuum, low power consumption, limited sealing capability, and restricted heating temperatures, conditions under which conventional gas- and liquid-phase standards are poorly suited. Here, we develop and validate two complementary solid reference materials for LUWA. Vacuum thermogravimetric analysis showed that Ag_2CO_3 and $Cu(OH)_2$ decompose at approximately 100-120 °C, releasing CO_2 and H_2O, respectively. Spectroscopic and mass-spectrometric measurements identified the expected dominant signals, with no obvious interfering gaseous species detected within the measured ranges. In the current LUWA implementation, Ag_2CO_3 was selected as the onboard CO_2 reference material for in situ calibration, whereas traceable $Cu(OH)_2$ was developed primarily for ground-based H_2O and δD calibration, prototype testing, end-to-end validation, and controlled regolith-simulant experiments. $Cu(OH)_2$ synthesized from precursor waters with known δD values preserved the mean isotopic information of the water source, with absolute differences between precursor-water and solid-derived vapor means within 10‰. Independent Cr-EA/IRMS measurements further supported the isotope-measurement workflow. Beyond its current role, traceable $Cu(OH)_2$ can serve as a solid isotope standard for validating heating, gas release, transfer, pressure measurement, and spectroscopic or mass-spectrometric detection. It also provides a controllable H_2O and δD source for regolith simulants with known water contents and for future characterization of adsorption–desorption memory effects, baseline drift, and pressure-dependent isotope response. With further storage, contamination-control, and flight-qualification studies, $Cu(OH)_2$-type materials may support future planetary payloads requiring controlled H_2O and hydrogen-isotope references. Together, these results establish a dual-role solid calibration strategy for LUWA.

-INTRODUCTION

The significance of lunar water exploration

Lunar water serves two fundamental roles. Scientifically, it provides critical insights into the Moon's evolutionary history. As a key volatile, water records the delivery of extraterrestrial materials from multiple sources and constrains the thermal and

geochemical evolution of the lunar interior and surface. As a resource, it enables sustainable bases through in-situ resource utilization (ISRU), reduces the costs of deep-space mission, and promotes the development of a cislunar economy. The Moon was initially regarded as a dry body.[1] However, subsequent studies demonstrated that the Moon's small obliquity allows certain polar regions to remain in permanent shadow, forming permanently shadowed regions (PSRs).[2] These regions maintain cryogenic temperatures low enough for water ice to persist over geological timescales.[3] Under such conditions, the sublimation rate of exposed water ice can be lower than 1 m per billion years. The scientific and resource potential of lunar polar water ice, however, can only be fully realized when its abundance, physical state, and origin are constrained.

The history of orbiter remote sensing exploration

Previous lunar missions have provided multiple lines of evidence for the presence and stability of water or hydrogen-bearing species in the lunar polar regions, but remote-sensing approaches have limitations. Thermal observations from the Diviner radiometer onboard the Lunar Reconnaissance Orbiter (LRO) demonstrate that temperatures in permanently shadowed regions (PSRs) can remain sufficiently low for water ice to be stable over geological timescales.[4] Radar observations also provided indications of possible polar ice. The Clementine bistatic radar experiment detected signals consistent with the presence of water ice within PSRs,[5] and subsequent polarimetric radar observations, such as Mini-RF, reported Circular Polarization Ratio (CPR) anomalies.[6] However, CPR is also affected by surface roughness, rock abundance, and viewing geometry, rendering radar anomalies alone insufficient for unambiguous water-ice identification.

Neutron spectroscopy has provided an additional constraint. The Lunar Exploration Neutron Detector (LEND) aboard LRO detected enhanced hydrogen abundances in polar regions,[7] but neutron data cannot discriminate between molecular water ice, hydroxyl-bearing minerals and solar-wind-implanted hydrogen. Spectral observations further reveal widespread hydration signatures: the Moon Mineralogy Mapper (M^3) aboard Chandrayaan-1 detected OH/H_2O-related absorption features in sunlit regions.[8,9] Molecular water detected near 6 μm has primarily been observed in illuminated terrains and is commonly associated with surface processes, limiting its direct relevance to PSR ice reservoirs.[10] The LCROSS impact experiment provided the most direct evidence for polar volatiles by detecting water in the ejecta plume from Cabeus crater,[11] yet impact-induced sublimation and excavation dynamics limit its ability to determine the undisturbed abundance and physical state of water ice in PSR regolith.

Therefore, although orbital and impact observations strongly support the presence of polar volatiles, they are insufficient to independently resolve the abundance, physical state, burial depth, stratification, and origin of lunar water ice. In particular, Mini-RF identifies dielectric or roughness anomalies but lacks the capability to constrain subsurface structure, ice-layer thickness, burial depth, and lateral continuity, which can be addressed by the Lunar Penetrating Radar (LPR).[12,13] These limitations highlight the necessity for in-situ measurements combined with multi-payload data integration, in which direct H_2O and hydrogen-isotope measurements are integrated with radar-derived structural constraints.

The rationale for in situ detection

The origin of lunar water remains a central scientific question and can be constrained through hydrogen isotopic analysis. Three major source mechanisms have been proposed: delivery by asteroidal impacts, particular carbonaceous chondrites;[14,15] contribution from cometary impacts;[16] and solar-wind hydrogen implantation followed by reactions with oxygen-bearing lunar surface materials.[17] These sources are expected to produce distinct hydrogen isotopic signatures. Terrestrial mantle water and many carbonaceous chondrites exhibit broadly similar D/H ratios, typically corresponding to intermediate, δD range (-126 to 46‰),[18,19] whereas solar-wind hydrogen is characterized by extremely low D/H ratios, with δD values lower than -980‰.[20] Accordingly, hydrogen isotope measurements provide a powerful diagnostic for constraining the relative contributions of different water sources.[14,17]

Previous isotope studies have mainly relied on returned samples and terrestrial laboratory analyses. Lunar sample measurements are commonly conducted using ion microprobe or secondary ion mass spectrometry methods,[16] while terrestrial materials can be measured through thermal extraction coupled with infrared spectroscopy and mass spectrometry.[21] However, returned lunar samples are susceptible to terrestrial contamination during collection, curation, transport, and laboratory processing, particularly for trace water and hydrogen isotopes. In addition, solar-wind-implanted hydrogen may interact with indigenous lunar materials, complicating the interpretation of returned-sample D/H data. These limitations highlight the importance of in-situ measurements for minimizing contamination and direct measurement of the isotopic composition of lunar polar volatiles.

Nevertheless, in-situ H_2O and δD measurements alone are insufficient to fully resolve the abundance, physical state, and origin of lunar polar water ice. Within the Chang'E-7 framework, LUWA provides calibrated point-scale measurements of water abundance and hydrogen isotopic composition,[22] while complementary constraints must be obtained from other payloads. Orbital Miniature Synthetic Aperture Radar (MSAR) can identify polarization anomalies and dielectric heterogeneity over broader polar terrains,[13,23] and rover-mounted LPR can further constrain local subsurface profiles, including possible burial

depth, stratification, and lateral continuity. [24, 25] These observations, combined with mineralogical context from infrared and Raman spectroscopy, enable integrated interpretation of polar ice occurrence. In this context, LUWA-derived H_2O and δD measurements function as traceable point-scale anchors within a broader Chang'E-7 multi-payload information chain, rather than as a standalone solution to the characterization of lunar water-ice.

The importance of Chang'E-7 and calibration materials

The Chang'E-7 mission targets PSRs in the lunar south polar region, where LUWA aboard a mini-flying probe will perform in-situ measurements of water abundance and hydrogen isotopic composition. These point-scale data require integration with observations from other Chang'E-7 payloads to constrain the distribution and origin of lunar polar water ice.

LUWA combines Tunable Diode Laser Absorption Spectroscopy (TDLAS) with mass spectrometry to achieve high-precision compositional analysis. [26] Its operational sequence includes system preparation, bake-out and purge, calibration, sample collection, sealed heating, gas analysis, and sample disposal. Operation in PSRs requires additional thermal control to ensure instrument stability. Because LUWA derives quantitative H_2O abundance and δD values from gases released during soil heating, accurate and traceable calibration is essential for ensuring the reliability of the entire measurement chain.

Conventional terrestrial calibration approaches are not well suited to lunar in-situ conditions. Standard gases are difficult to store and deliver under high vacuum, mass-limited, and sealing-constrained conditions, while also introducing potential leakage risks. Liquid water, although widely used for hydrogen-isotope calibration on Earth, requires sampling, vaporization, and transfer procedures that may introduce adsorption and isotope-fractionation effects.[27,28]These limitations are particularly critical under lunar operating conditions, where calibration opportunities, heating power, and operational time are limited.

Accordingly, LUWA requires compact, stable, and traceable solid calibration materials capable of releasing well-defined calibration gases under controlled heating. Such materials reduce storage and sealing risks, simplify the calibration procedure, and provide a metrological basis for converting LUWA spectral and mass-spectrometric signals into reliable in-situ water and isotope information. This study therefore focuses on the development, synthesis, and validation of solid calibration materials as a prerequisite for robust LUWA measurements within the Chang'E-7 multi-payload water-ice detection framework. Within this multi-payload framework, the scientific value of LUWA-derived measurements ultimately depends on the reliability of its calibration. Without traceable calibration materials compatible with lunar operational constraints, point-scale H_2O and δD data cannot be confidently integrated with radar-derived structural constraints or orbital observations for comprehensive water-ice interpretation. This requirement motivates the development of solid calibration materials described in this study.

The state-of-the-art and limitations of calibration material studies

Calibration for in-situ lunar water and isotope measurements faces multiple coupled constraints, including high vacuum, large temperature variations, limited sealing performance, restricted heating power, and short operational time. Under low-temperature conditions, polymer seals may lose elasticity and increase leakage risks, while elevated temperatures and vacuum conditions can reduce the effective volatilization or decomposition thresholds of calibration materials.[29] Over multi-week operations, even minor leakage or adsorption can alter the amount and isotopic composition of calibration gases. In addition, the limited battery budget and thermal-control capability of the mini-flying probe constrain calibration temperature to a relatively low range, typically around 80-120 °C.[30] These factors require calibration materials that are compact, vacuum-stable, chemically well defined, and capable of releasing calibration gases under modest heating.

Existing lunar volatile exploration payloads and calibration strategies do not fully satisfy these requirements for LUWA. For example, VIPER's Near Infrared Volatile Spectrometer Subsystem (NIRVSS) infers volatile content indirectly from reflectance spectra and cannot directly quantify hydrogen isotopic composition.[31, 32] Its Mass Spectrometer Observing Lunar Operations (MSolo) relies on pressurized gas standards stored in an onboard calibration gas system, which remain susceptible to leakage and temperature-dependent pressure fluctuations during long-duration spaceflight.[28,33,34] Luna-27's LASMA-LR laser ionization mass spectrometer is primarily designed for elemental and isotopic composition analysis of solid regolith, and does not employ calibration strategies optimized for in-situ water abundance and hydrogen-isotope measurement[35]. Although the accompanying DLS-L spectrometer targets D/H and oxygen isotope analysis via TDLAS, its calibration relies on liquid water and gaseous CO_2 standards that are susceptible to isotopic fractionation during long-duration spaceflight storage and transfer[36]. The PROSPECT/ProSPA package validates its evolved gas analysis using compounds such as $CaCO_3$, whose decomposition temperature of approximately 550–750°C is incompatible with the low-power and thermally constrained operating conditions required for LUWA in PSRs.[37,38]. LUMVI-X uses perfluorotributylamine as a calibrant, but its limited mass resolution restricts its ability to distinguish hydrogen isotopic signature relevant to D/H analysis.[39,40]

These limitations indicate that the key challenge lies not only in detecting water-related signals, but in converting such

signals into traceable and quantitatively reliable water and isotope information under lunar operational constraints. For LUWA, an ideal calibration material should remain stable during storage, release a single and identifiable calibration gas under vacuum at approximately 80-120 °C, minimize adsorption and isotope-fractionation effects, and provide a known reference for both spectroscopic and mass-spectrometric measurements. These requirements motivate the development of solid, traceable calibration materials for reliable in-situ water and isotope information acquisition.

1.6 The innovation and significance

The LUWA onboard Chang'E-7 is designed to provide direct in-situ information on water abundance and hydrogen isotopic composition in lunar polar environments. Prototype testing has demonstrated its capability for water-vapor pressure and hydrogen-isotope measurements under laboratory conditions.[41-43] However, the scientific value of LUWA-derived H_2O and δD data depends not only on instrument sensitivity, but also on the availability of calibration materials that are stable, traceable, and compatible with lunar operational constraints. Without reliable calibration, point-scale measurements from LUWA cannot be confidently integrated with other Chang'E-7 observations for broader water-ice interpretation.

The innovation of this study lies in developing traceable solid calibration materials that convert a difficult in-situ calibration problem into a controlled solid-to-gas release process. By screening candidate materials under vacuum, identifying Ag_2CO_3 and $Cu(OH)_2$ as low-temperature gas-release materials, characterizing the evolved CO_2 and H_2O signals using spectroscopic and mass-spectrometric measurements, and assessing the hydrogen-isotope fidelity of synthesized $Cu(OH)_2$, this work establishes a practical and traceable calibration basis for LUWA.

The significance of this work is twofold. From an engineering perspective, the proposed solid calibration materials offer compact, vacuum-compatible, and low-power calibration sources for a resource-constrained lunar payload. From lunar scientific perspective, they improve the reliability and traceability of LUWA-derived water and isotope information, allowing these point-scale measurements to serve as calibrated anchors in the Chang'E-7 multi-payload framework. When combined with regional hydrogen mapping, radar-derived subsurface structure, mineralogical and spectral context, and complementary volatile measurements, such calibrated LUWA data contribute to constraining the abundance, physical state, and potential origin of lunar polar water ice.

METHODS

Ground calibration platform

After the vacuum tank has been evacuated for 72 hours to below 10^{-5} Pa, the instrument is held at 35 °C. With the gas-extraction furnace sealed and valves 1 and 2 closed in Fig. 1c, the electronics unit issues a heating command to the calibration gas unit, raising and maintaining its temperature at 100 °C. The mass spectrometer selects its intake path according to the measured pressure. If the pressure is below 100 Pa, open self-locking valve 2 and draw gas through the black pipeline. The main pipeline pressure is then checked with the vacuum gauge. If the main pipeline pressure rises above 200 Pa, close the self-locking valve 2 and switch sampling to the gray pipeline.

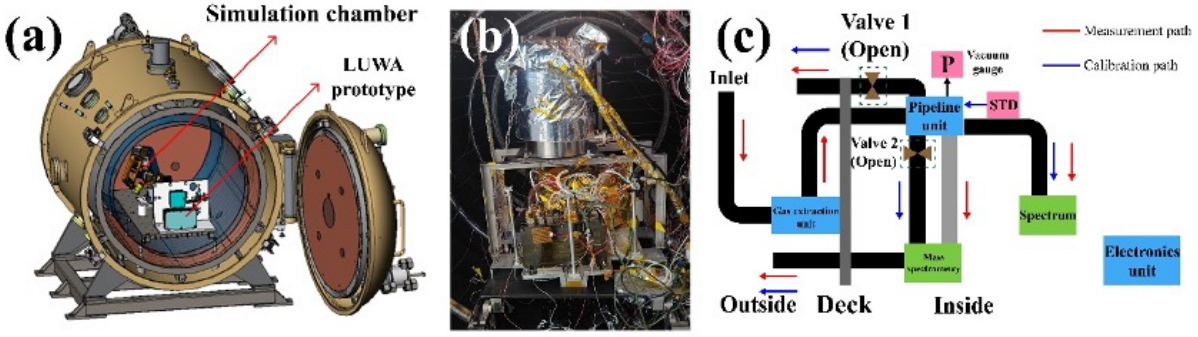

Figure 1. Ground calibration platform and LUWA prototype (A) LUWA prototype in the simulation chamber; (B) photograph of the prototype; and (C) internal pipeline configuration.

Standard material selection

LUWA incorporates two independent calibration units to support repeated calibration during lunar operation. An initial calibration is performed after landing to verify the instrument response following launch, transit, and landing, and additional calibrations can be conducted before individual in-situ measurements to establish contemporaneous references under the prevailing vacuum and thermal conditions. Each calibration unit can release the reference gas multiple times through controlled heating rather than being limited to a single use. During each calibration, an appropriate amount of gas is introduced into the analytical pathway, after which the gas is vented, and the calibration unit is isolated until the next calibration cycle.

Table 1. Decomposition temperatures of common carbonates.

Carbonate	Ag_2CO_3	$CdCO_3$	$ZnCO_3$	$MgCO_3$	$CaCO_3$	$SrCO_3$	$BaCO_3$
Td (°C)	147	240	250	441	661	615	942

Considering the complexity of binary systems [44] and the interaction between carbonate and metallic inner surfaces, the calibration materials were restricted to substances expected to release predominantly a single target gas upon heating (excluding bicarbonates, oxalates, etc.). Referring to the design specifications of the spectrometer and mass spectrometer in the analyzer, CO_2 and H_2O were selected as the target calibration gases and used in ground-based pre-experiments. [26] Because CO_2-releasing solid calibrants were of primary interest for onboard referencing, the initial screening focused on carbonates. Thermal decomposition temperatures of common carbonates at atmospheric pressure are listed in Table 1.[45]

Accounting for chemical-kinetic effects in vacuum, the onset temperature for thermal decomposition shifts downward;[46] Therefore, we targeted carbonates with vacuum-decomposition temperatures between 80 °C and 120 °C. In practice, this criterion encompasses minerals whose atmospheric-pressure decomposition occurs between 100 °C and 300 °C—such as magnesium carbonate ($MgCO_3$) and calcium carbonate ($CaCO_3$). Based on their thermal profiles (Table 1), the carbonates of cobalt ($CoCO_3$), zinc ($ZnCO_3$), cadmium ($CdCO_3$), and silver (Ag_2CO_3) emerged as the most promising candidates.

Among these candidates, zinc carbonate predominantly occurs as the basic hydrated form $2ZnCO_3 \cdot 3Zn(OH)_2 \cdot H_2O$, making it difficult to obtain pure $ZnCO_3$.[47] Its thermal decomposition releases both H_2O and CO_2, which would complicate calibration. Given the toxicity concerns associated with cobalt and cadmium compounds,[48,49] silver carbonate (Ag_2CO_3) was therefore chosen as the solid calibration substance for this temperature range.

CO_2 is suitable for pressure, spectroscopic, and mass-spectrometric referencing, but it cannot provide a hydrogen-isotope reference. We therefore additionally evaluated a water-releasing calibrant with a known hydrogen isotopic composition.

Therefore, we evaluated solid materials that release water upon heating, specifically hydrates and weakly basic compounds. However, common hydrates typically decompose below the 80-120 °C range, rendering them unsuitable for our in-situ calibration needs ,[50,51] and their decomposition onset shifts even lower in vacuum, making them unsuitable for in-orbit storage. Among weak bases, the readily available copper hydroxide ($Cu(OH)_2$) was selected, as it decomposes at approximately 150 °C under ambient pressure [52], and it is a practical candidate for producing a controlled water release for calibration.

Vacuum thermogravimetric analysis

Conventional thermogravimetric analysis (TGA) is typically conducted in controlled gas atmospheres (e.g., high-purity N_2 or O_2). The presence of a gas phase can influence the diffusion of decomposition products, modify reaction pathways, or chemically interact with the sample, thereby introducing confounding factors. To eliminate these confounding effects, vacuum thermogravimetric analysis (TGA) is required, since prior studies have shown that TGA curves obtained under inert-gas atmospheres can differ substantially from those measured in vacuum.[46]

To determine the decomposition temperatures of candidate calibration materials under orbital conditions and to establish the heating power and duration required for in-situ calibration, we performed vacuum TGA on $CaCO_3$, $MgCO_3$, Ag_2CO_3, and $Cu(OH)_2$. Measurements were carried out on a NETZSCH STA 2500 vacuum thermogravimetric analyzer (Supplementary Figure S2a), with the analysis chamber maintained below 1 Pa. The heating protocol applied a rate of 1 °C min^{-1}, including isothermal holds at 25 °C, 50 °C, and 70 °C for 20 min each to assess stability, followed by continuous heating to 150 °C. Each experiment was repeated twice, and the averaged results are reported. We then conducted end-to-end experiments with the two selected calibration materials, following the protocol detailed in Section 2.1. Before each sample measurement, the calibration routine described therein was executed to ensure consistency.

Approximately 50 mg of each material was used for each vacuum thermogravimetric measurement. Each material was measured twice under identical vacuum and heating conditions. The sample mass was normalized to its initial value, and the normalized curves from the two runs were averaged for data presentation.

Chemical synthesis

For CO_2 referencing, a carbonate with well-characterized composition and predominantly CO_2 release is required. In contrast, water-based calibration demands a reference material with a known hydrogen isotopic ratio to evaluate instrument performance and calibrate its isotope-measurement capability. We tested two samples (A and B) from the same batch of analytical-grade $Cu(OH)_2$. Each sample was vacuum-heated, and the released gases were introduced into a TDLAS spectrometer pre-calibrated with a liquid-water standard. The spectrometer recorded at 5 Hz, yielding over 500 δD measurements per sample. The mean δD values (Figure. 2) differ by approximately 50‰. This variability, attributable to untraceable hydrogen sources in $Cu(OH)_2$, indicates that commercially available analytical-grade copper hydroxide is unsuitable for direct use as an isotopic calibration standard.

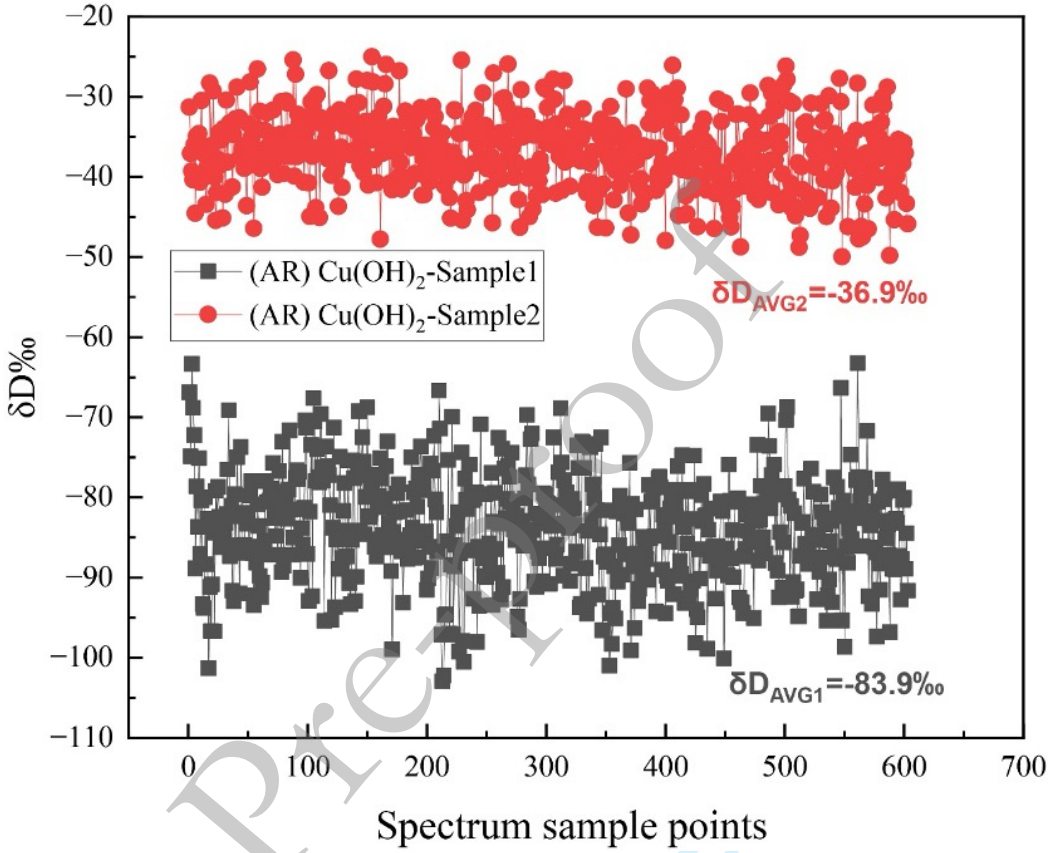

Figure 2. Time-resolved δD measurements of H_2O released from two commercial analytical-grade $Cu(OH)_2$ samples obtained from the same batch.

To address this issue, we developed a simple method for preparing $Cu(OH)_2$ with a traceable hydrogen isotopic composition as a solid reference material. A schematic overview of the synthesis procedure is provided in Supplementary Figure S1.[53]

The preparation method is guided by chemical reaction kinetics, the thermal stability of the products, and is designed according to the following chemical equations:

$$CuSO_4 + Na_2O + H_2O = Cu(OH)_2 \downarrow + Na_2SO_4 \quad (1)$$

During synthesis, we exploit the fact that chemical reaction rates are significantly faster than those of physical thermal fractionation processes.[28,54] Hydrogen sources were tightly controlled through elemental bookkeeping: copper was introduced as anhydrous copper sulfate, the base as high-purity sodium oxide, and all hydrogen in the product was derived from the added precursor water. During precipitation, hydrogen from the precursor water was incorporated into the structural hydroxyl groups of $Cu(OH)_2$. The final product was therefore a solid $Cu(OH)_2$ reference material with a traceable hydrogen isotopic composition. All operations were conducted in a glovebox under a high-purity nitrogen atmosphere.

We performed the entire preparation inside a high-purity nitrogen glovebox, ensuring that deionized water was the sole hydrogen source. The procedure comprised the following steps:

Prepare the copper solution: In the glove box, dissolve anhydrous copper sulfate (analytical grade) in deionized water to obtain a 0.1–0.3 mol/L solution.

Precipitate formation: Add high-purity Na_2O gradually in small portions until no further precipitate forms, yielding a mixed reaction suspension. Maintain the mass ratio of Na_2O to anhydrous copper sulfate at 1:(2–2.5).

Filtration and washing: Filter the suspension by suction. Wash the collected residue with anhydrous ethanol to remove soluble impurities. Use deionized water or anhydrous ethanol as required to assist the suction filtration.

Drying and storage: Dry the filtered precipitate under vacuum and then seal it in bottles inside the glove box under an inert gas atmosphere. After vacuum drying, a light-blue $Cu(OH)_2$ powder was obtained, as illustrated in Supplementary Figure S1.

To strictly control the hydrogen source to originate solely from precursor deionized water, analytical-grade anhydrous copper sulfate and high-purity Na_2O (containing ~20 wt% Na_2O_2 impurity) were used. To minimize adventitious hydrogen incorporation, all reagents and equipment were degassed in the glove box transition chamber prior to use. Heat-resistant apparatus was degassed at 150–200°C; other items were evacuated naturally for 1–2 days following the vacuum-degassing protocol.[27] All experimental operations were conducted in an inert gas glove box, and required reagents were opened and handled within the glove box.

Although chemical reaction rates are much higher than those of physical processes such as phase changes, thereby minimizing D/H fractionation associated with phase transitions, the mass difference between H and D leads to slightly different bond energies. In other words, compared to D, H is more likely to be incorporated into the product.[55]

This phenomenon can be calculated using Rayleigh fractionation:[55]

$$R_w = R_0 \cdot f^{\alpha-1} \tag{2}$$

Here, R_w is the isotopic value in the water. R_0 is the isotopic value in the initial reactant. f is the proportion of residual reactant, which is approximately equal to 1 due to the reaction being in the liquid water. α is the fractionation factor.[55] During precipitation, the liquid water reservoir was substantially larger than the amount of water (-OH) incorporated into the precipitate, such that the residual water fraction remained close to unity. According to the Rayleigh fractionation relationship, the isotopic composition of the residual water therefore changed only slightly throughout precipitation. Consequently, precipitates formed at different stages interacted with a water reservoir of nearly constant isotopic composition, limiting progressive Rayleigh-type fractionation and intraprecipitate isotopic heterogeneity. The bulk isotopic composition of the precipitate should thus mainly reflect the initial solid–water fractionation rather than substantial amplification caused by progressive depletion of the water reservoir.

However, kinetic equilibrium has not yet been reached. Before product filtration and drying, evaporation of the liquid phase will cause continuous isotopic changes.[28]These changes in the liquid phase isotope composition will further exchange with the product.[56] The influence of post-reaction kinetic equilibrium will be verified experimentally.

After preparation, the solid calibration material was subjected to a suite of compositional and performance tests; the details of these analyses are given in the next section.

Tests

Scanning electron microscopy was used to characterize the morphology and surface features of the synthesized $Cu(OH)_2$ particles. Measurements were performed using a ZEISS GeminiSEM 500 scanning electron microscope (Figure S2B). X-ray diffraction was used to identify the crystalline phases of the synthesized material. Measurements were performed using a Rigaku SmartLab diffractometer (Supplementary Figure S2C) over a 2θ range of 20–80°, and the measured diffraction pattern was compared with the reference pattern of $Cu(OH)_2$. SEM was used for morphological characterization, whereas XRD provided qualitative crystalline-phase identification.

The critical test for the calibration material is the hydrogen isotopic analysis, which verifies whether the synthesized solid can serve as a hydrogen-isotope calibrant. Before synthesis, 100 mL of each precursor water was reserved for hydrogen-isotope analysis. The detailed procedures for precursor-water calibration, solid-derived vapor measurement, and independent Cr-EA/IRMS validation are described in Section 2.6.

Because the isotope measurement system analyzes gaseous H_2O rather than the solid material directly, the LUWA prototype was modified to accommodate thermal release from solid samples (Figure 3). $Cu(OH)_2$ powders were synthesized from three precursor waters with distinct hydrogen isotopic compositions.

Before isotope measurement, the synthesized $Cu(OH)_2$ samples were stored in sealed containers inside the glovebox under

an inert atmosphere for 7 days. The measurement assembly was placed in a vacuum chamber and valves 1 and 2 were opened. The chamber was evacuated for 72 hours until the vacuum gauge read $<10^{-5}$ Pa. Valve 1 was then closed, and the gas-generation/calibration component was heated to release the sample's water vapor for analysis. To avoid concentration-dependent isotope effects,[57,58] the gas pressure in the measurement line was kept below 250 Pa. The hydrogen isotopic composition of the evolved gas was then recorded.

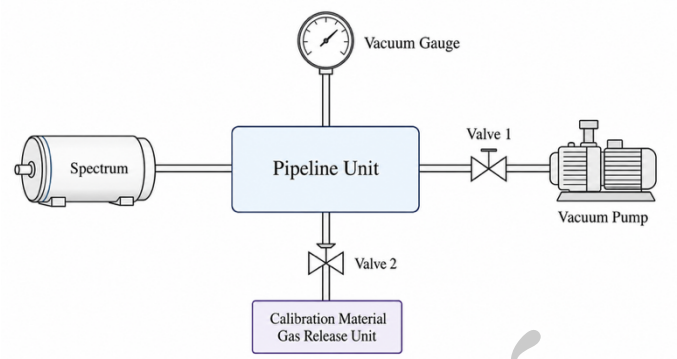

Figure 3. Solid-isotope measurement platform based on the LUWA prototype.

Hydrogen isotope analysis protocol

Hydrogen isotope compositions are reported as δD values relative to the VSMOW scale, defined as δD = [(D/H)sample/(D/H)VSMOW − 1] × 1000‰. The isotope protocol comprised three analytical steps: determination of the δD values of precursor waters using a Picarro L2130i system, gas-phase δD measurement of H_2O released from synthesized $Cu(OH)_2$ using the LUWA prototype TDLAS system, and independent Cr-EA/IRMS validation of representative synthesized $Cu(OH)_2$ solid standards.

The hydrogen isotopic compositions of the precursor waters were determined using a Picarro L2130i cavity ring-down spectrometer (Figure S2D) coupled with an automated PAL LSI liquid sample injector (Figure S2E). The analytical procedure followed the laser absorption spectroscopy protocol for hydrogen and oxygen isotope analysis of water samples specified in DZ/T 0184.36—2024. For each analytical batch, the Picarro analyzer was calibrated immediately before sample measurements using three national certified reference waters with distinct δD values: GBW04458, GBW04459, and GBW04460. Their certified δD values are −1.7 ± 0.4‰, −63.4 ± 0.6‰, and −144.0 ± 0.8‰, respectively (Table 2). According to the certificates, these reference waters are traceable to international isotope standards, including VSMOW2 and SLAP2, and their δ values are reported relative to the VSMOW scale. A batch-specific linear calibration was established between the raw instrumental values and the certified values, and this calibration was applied to the precursor-water measurements.

Each precursor-water sample was measured by ten consecutive injections. To minimize carryover and memory effects, the first six injections were excluded, and the reported value was calculated from the final four injections. The same procedure was applied to both reference waters and unknown precursor-water samples. Short-term instrumental precision was evaluated from repeated measurements of the reference waters immediately before sample analysis. Under the analytical conditions used in this study, the δD repeatability was better than 0.1‰. This calibration and replicate-measurement procedure provided the traceability and analytical precision required for evaluating the isotopic offsets between the precursor waters and the synthesized $Cu(OH)_2$-derived water.

For gas-phase measurements of the synthesized solid standards, $Cu(OH)_2$ samples were heated to release H_2O vapor, which was then introduced into the LUWA prototype TDLAS system for isotope analysis. In the solid-standard measurements, H_2O vapor was first generated by thermal decomposition of $Cu(OH)_2$ and then analyzed by the same laser absorption spectroscopic principle. For each synthesized $Cu(OH)_2$ sample, one independent thermal release was performed. The mean δD value and standard deviation were calculated from the accepted time resolved measurements collected during the continuous release. The resulting standard deviation represents within-release temporal variability under evolving gas pressure conditions and should not be interpreted as analytical uncertainty or release-to-release reproducibility. This procedure allowed the isotopic composition of water vapor released from the synthesized solid standard to be evaluated on the same VSMOW-referenced scale. The LUWA prototype TDLAS system was independently calibrated using standard waters, and the precursor waters were also measured to verify consistency between the Picarro and TDLAS measurement scales.

To independently evaluate the isotope consistency of the synthesized $Cu(OH)_2$ solid standards, representative samples prepared using the same synthesis protocol were analyzed by Cr-EA/IRMS.[59] This analysis was designed to provide an

orthogonal mass-spectrometric validation of the TDLAS-based gas-phase measurement of H_2O vapor released from the solid standards. Continuous-flow analyses were carried out using a Flash 2000HT elemental analyzer with a MAS 200R autosampler coupled to a Delta V Advantage isotope ratio mass spectrometer via a ConFlo IV interface. Approximately 4–5 mg of each solid sample was reacted with chromium chips and chromium powder at 1050 °C to generate H_2, which was then carried by helium into the isotope ratio mass spectrometer for analysis. USGS57 and USGS58 were used for data linear regression, and the analytical accuracy was better than 2‰. This Cr-EA/IRMS procedure provided an independent check on the hydrogen isotopic composition of the synthesized $Cu(OH)_2$ standards and on the reliability of the solid-derived vapor isotope measurement workflow.

Table 2. Certified reference waters used for δD calibration.

Reference water	Certified δD value	Uncertainty	Scale
GBW04458	−1.7‰	±0.4‰	VSMOW
GBW04459	−63.4‰	±0.6‰	VSMOW
GBW04460	−144.0‰	±0.8‰	VSMOW

RESULTS

Figure 4 presents the averaged vacuum thermogravimetric curves obtained from two independent measurements of each candidate material, with an initial sample mass of approximately 50 mg in each experiment. The two measurements showed nearly overlapping thermal behavior, indicating good repeatability under the applied vacuum and heating conditions.

Under vacuum, $Cu(OH)_2$ underwent its principal mass loss between approximately 100 °C and 120 °C. The measured mass loss was approximately 18.2 wt%, consistent with the theoretical H_2O mass fraction of 18.47 wt% for complete decomposition to CuO and H_2O. This agreement indicates that $Cu(OH)_2$ was nearly completely decomposed within the investigated temperature range.

Ag_2CO_3 began to decompose gradually at approximately 100 °C and continued to lose mass up to the maximum investigated temperature of 150 °C, without reaching a clear plateau. Therefore, a decomposition completion temperature could not be assigned. The theoretical mass loss for complete conversion of Ag_2CO_3 to Ag_2O and CO_2 is 15.96 wt%. The reaction remained incomplete within the investigated temperature range.

$MgCO_3$ began to decompose slowly at approximately 70 °C, indicating insufficient thermal stability, whereas $CaCO_3$ showed no identifiable decomposition within the investigated temperature range. Based on the criteria outlined in Section 2.2, Ag_2CO_3 and $Cu(OH)_2$ were selected for subsequent full process tests as candidate CO_2 and H_2O reference materials, respectively.

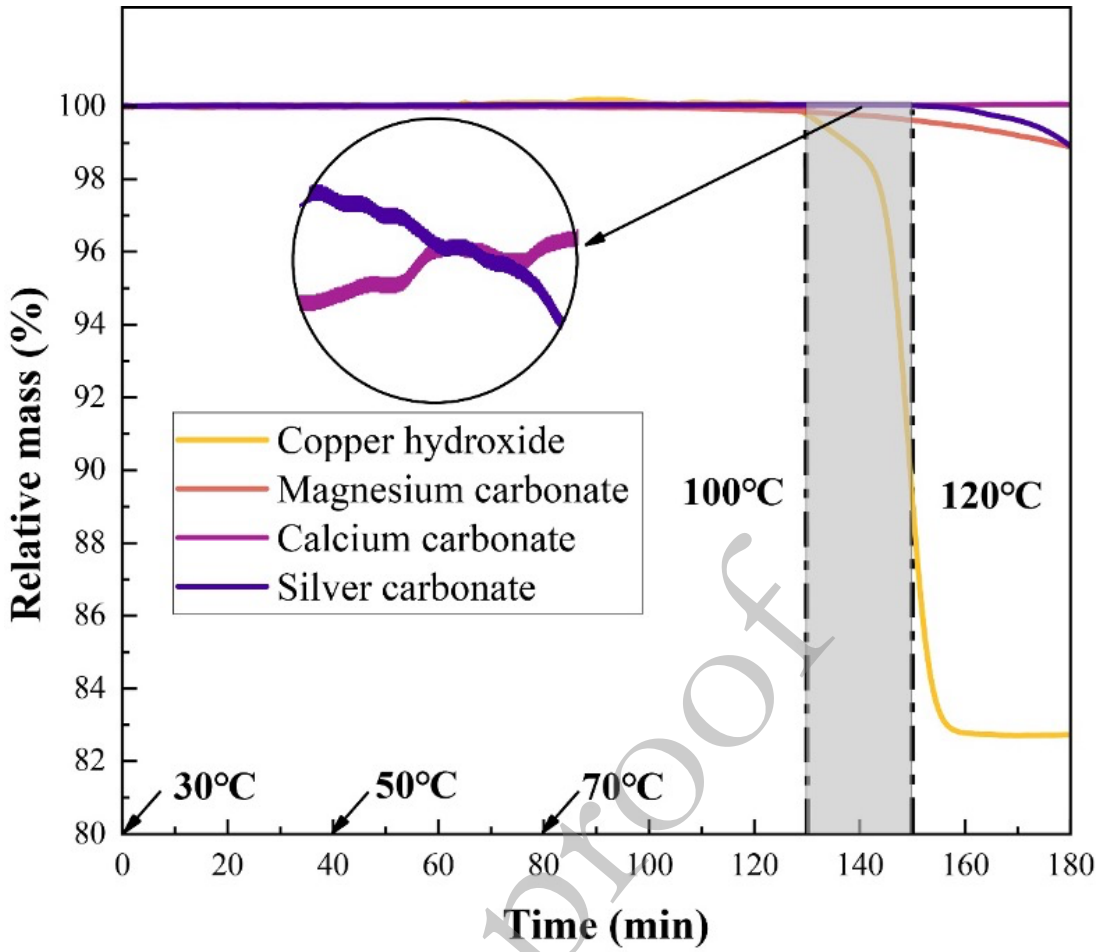

Figure 4. Averaged vacuum thermogravimetric curves obtained from two independent measurements of $CaCO_3$, $MgCO_3$, Ag_2CO_3, and $Cu(OH)_2$.

During the full process tests, Ag_2CO_3 and $Cu(OH)_2$ were used as the CO_2- and H_2O-releasing materials, respectively. Figure 5 shows the spectroscopic and mass-spectrometric results obtained from the evolved gases at a vacuum-gauge pressure of approximately 137 Pa. The spectroscopic measurements show clear absorption features attributable to CO_2 and H_2O vapor. The mass spectra likewise display the expected dominant molecular-ion signals, together with fragment signals at m/z 16 and 17 for H_2O. These fragment peaks arise from facile H–O bond cleavage during ionization, producing O (mass number of 16) and OH (mass number of 17) species. No obvious interfering gaseous species were observed within the measured spectroscopic and mass-to-charge ranges. These results demonstrate the feasibility of using Ag_2CO_3 and $Cu(OH)_2$ as controlled sources of CO_2 and H_2O reference signals for LUWA calibration and validation.

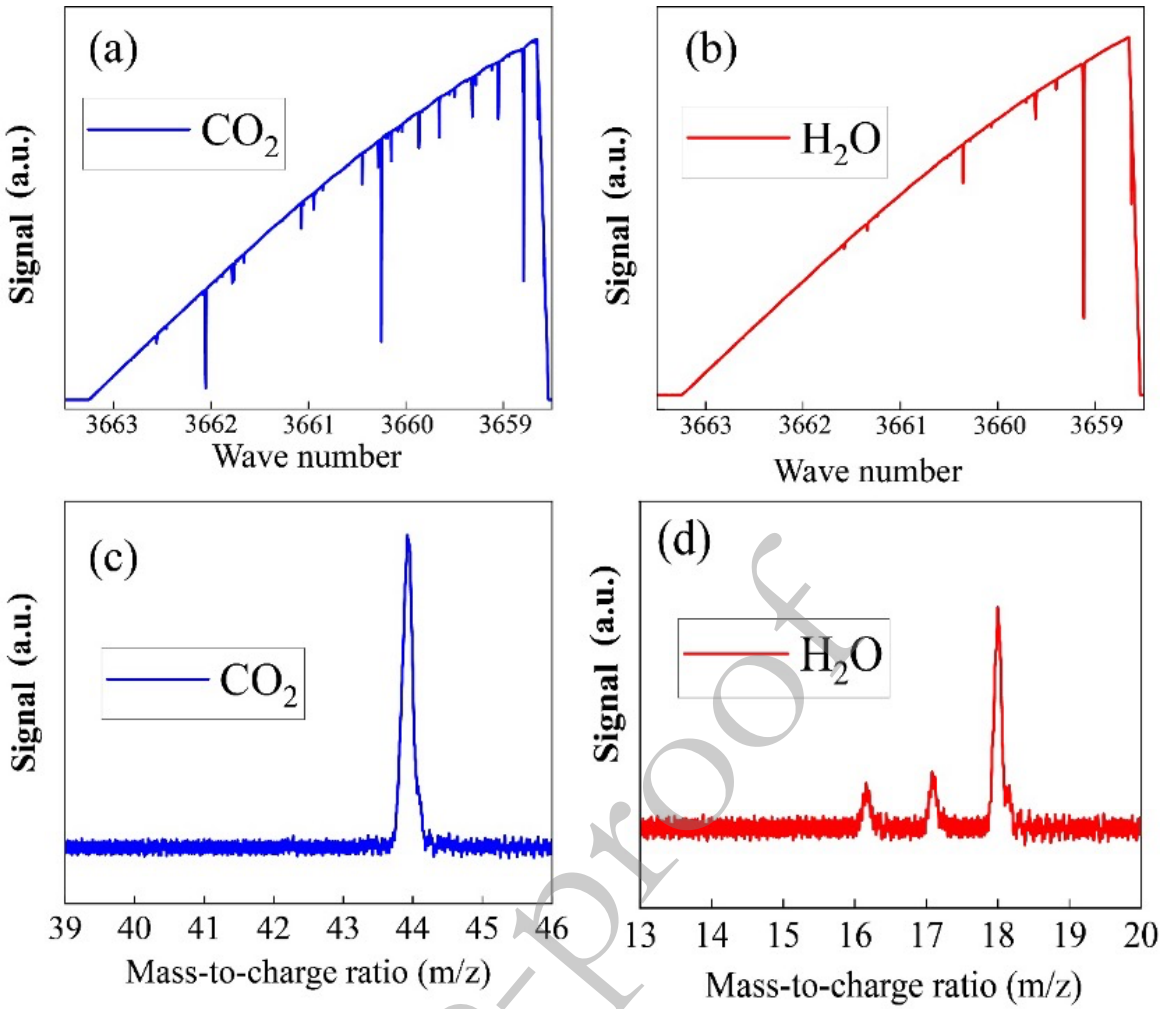

Figure 5. Spectroscopic and mass-spectrometric signals of gases evolved from Ag_2CO_3 and $Cu(OH)_2$ (A) CO_2 absorption spectrum from Ag_2CO_3; (B) H_2O absorption spectrum from $Cu(OH)_2$; (C) mass spectrum of gas evolved from Ag_2CO_3; and (D) mass spectrum of gas evolved from $Cu(OH)_2$.

During the full process tests, $Cu(OH)_2$ released H_2O rapidly and underwent nearly complete decomposition within the applied heating range. The amount of H_2O inferred from the measured partial pressure was consistent with the theoretical water content of $Cu(OH)_2$, approximately 18 wt%. Nearly complete decomposition ensured that the evolved H_2O represented the bulk hydrogen isotope composition of the material and minimized potential isotope fractionation associated with partial release.

Ag_2CO_3 exhibited a slower and more gradual CO_2 release. A pressure above approximately 50 Pa was sufficient to provide spectroscopic and mass spectrometric reference signals, after which the inlet valve was closed and gas introduction was terminated without requiring complete decomposition of the loaded material. No signal at m/z 32 was detected in the full mass scan (not shown), providing no evidence for substantial O_2 release or further decomposition of the Ag_2O product under the applied conditions. The remaining Ag_2CO_3 could therefore be retained for subsequent controlled gas releases.

The full process tests involved vibration, long-term storage (> 4 month) and thermal-cycling procedures. Following these procedures, the tested units remained operational and retained their ability to generate the target-gas reference signals required for calibration.

Considering the gas release characteristics observed in the full process tests together with the current LUWA mission requirements, Ag_2CO_3 was selected as the reference material for the two onboard calibration units. The pressure controlled partial release strategy allows the remaining material to be used in subsequent calibration cycles. With a nominal material loading volume of approximately 1 cm^3 per unit, the two calibration units are designed to support approximately four to five calibrations in total, including an initial calibration after landing and additional calibrations before individual in-situ measurements.

Traceable $Cu(OH)_2$ was assigned primarily to ground H_2O and δD calibration, prototype testing, full process validation, and controlled regolith simulant experiments. This assignment reflects the operational requirements and calibration strategy of

the current mission rather than an intrinsic restriction on the possible flight use of $Cu(OH)_2$.

Figure 6 presents SEM images of the synthesized $Cu(OH)_2$. The sample consists predominantly of plate-like and elongated particles with a heterogeneous particle-size distribution. Higher-magnification images reveal textured surface features on the particles. These observations characterize the morphology of the synthesized material.

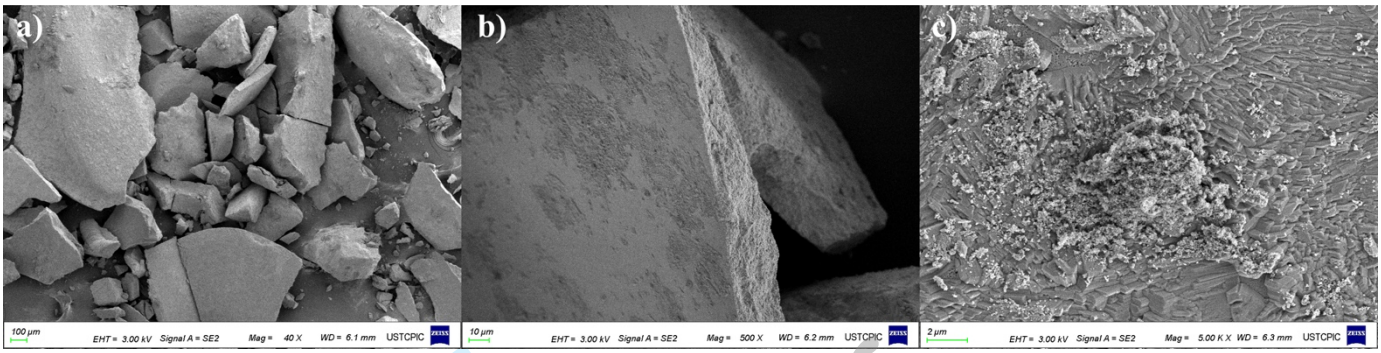

Figure 6. SEM images of synthesized $Cu(OH)_2$ at scale bars of (A) 100 µm, (B) 10 µm, and (C) 2 µm.

Figure 7 presents the XRD pattern of the synthesized material together with the reference pattern of $Cu(OH)_2$ (PDF#99-000-3468). The principal diffraction peaks at approximately 23.8°, 34.0°, and 53.3°, together with secondary peaks at approximately 35.9°, 38.1°, and 39.7°, are consistent with the reference peak positions of crystalline $Cu(OH)_2$. No prominent additional crystalline peaks were observed within the investigated 2θ range. These results identify $Cu(OH)_2$ as the dominant crystalline phase of the synthesized material.

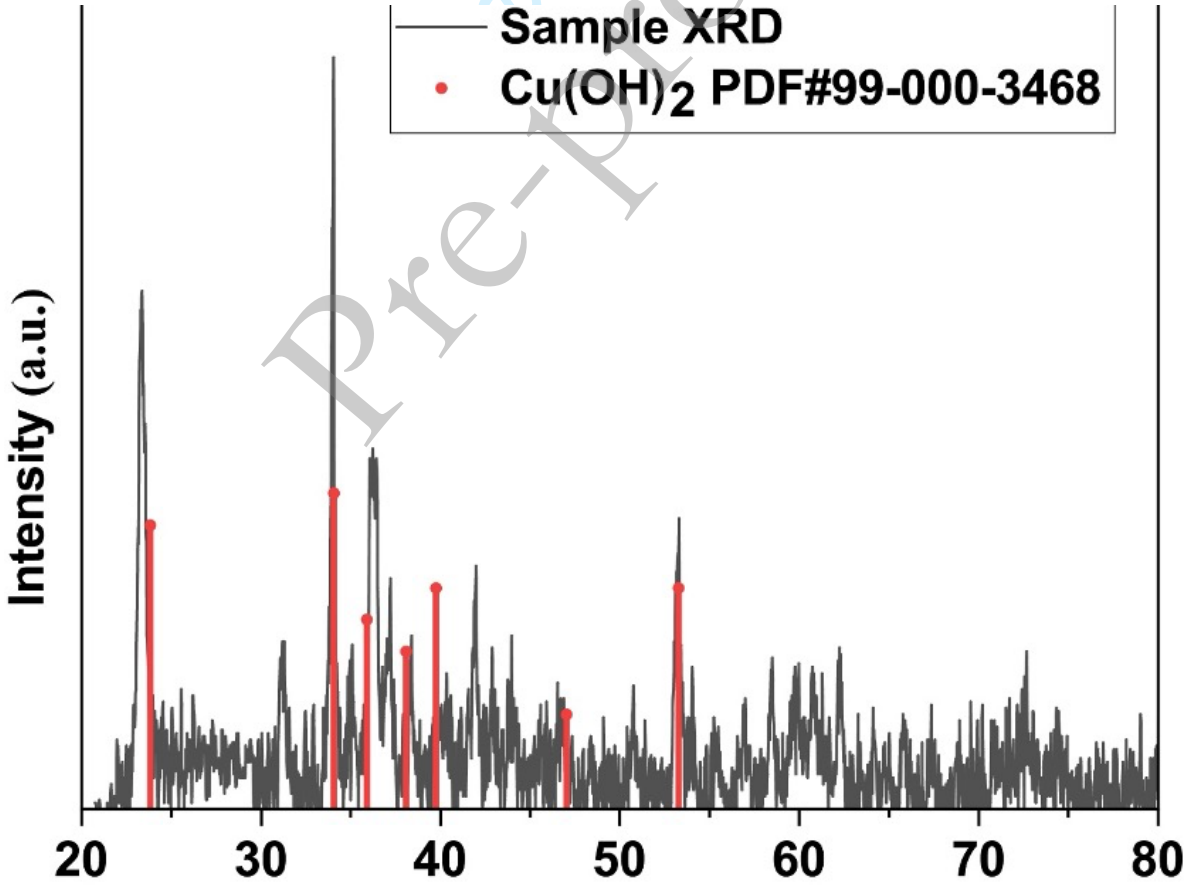

Figure 7. XRD pattern of the synthesized material compared with the reference diffraction pattern of $Cu(OH)_2$ (PDF#99-000-3468).

The spectroscopic isotope signal approached its lower detection limit at an H_2O partial pressure of approximately 150 Pa. The hydrogen isotope results are summarized in Supplementary Table S1. The precursor waters had δD values of +4.0‰, −74.0‰, and −24.0‰. The corresponding H_2O released from synthesized $Cu(OH)_2$ yielded mean δD values of −4.3 ± 25.30‰, −68.7 ± 19.64‰, and −16.4 ± 25.21‰, based on 116, 114, and 116 accepted time-resolved measurements, respectively (Fig. 8).

One independent thermal release was performed for each synthesized $Cu(OH)_2$ sample. The reported standard deviations therefore represent temporal variability during an individual dynamic release rather than release-to-release reproducibility. This variability reflects the continuously changing H_2O partial pressure and signal intensity during decomposition and may also include contributions from pressure-dependent isotope response, adsorption and desorption within the analytical pathway, and reduced signal quality near the isotope detection limit.

The absolute differences between the mean precursor-water and solid-derived vapor values were 8.3‰, 5.3‰, and 7.6‰, respectively. These differences remained within 10‰, indicating that the overall synthesis, drying, thermal release, gas-transfer, and measurement workflow preserved the mean isotope information of the precursor waters within the investigated accuracy range. Given the analytical uncertainty and within-release temporal variability, these differences should not be interpreted as a resolved or systematic isotope-fractionation factor.

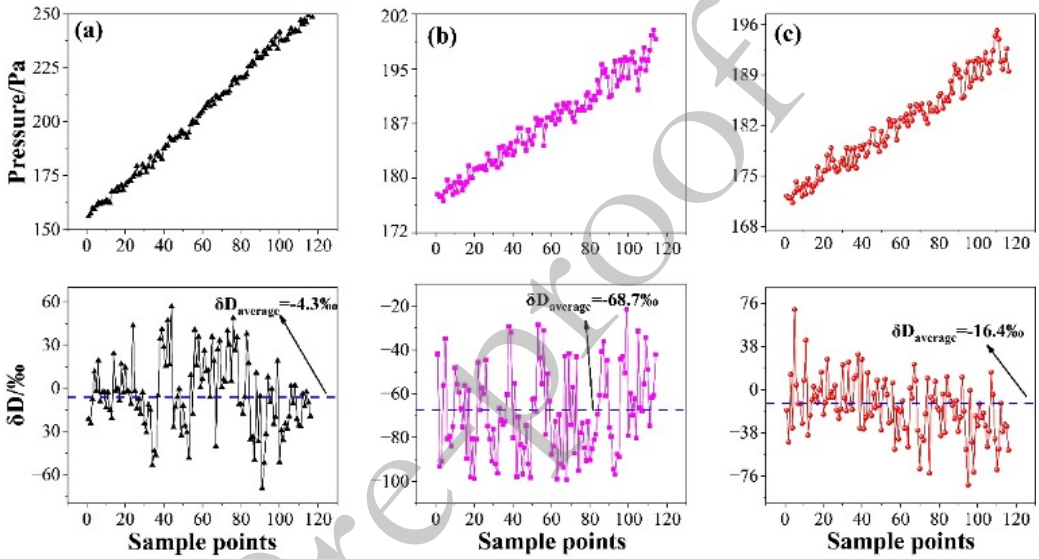

Figure 8. Time-resolved δD measurements of H_2O released from synthesized $Cu(OH)_2$ samples prepared using three precursor waters with different hydrogen isotopic compositions.

A separate batch of $Cu(OH)_2$ was synthesized using the same protocol for the Cr-EA/IRMS cross-method comparison. This cross-method comparison was designed to evaluate the consistency of the solid-derived vapor isotope measurement workflow against an independent mass-spectrometric method. The Cr-EA/IRMS measurements yielded a mean δD value of −113.98 ± 0.36‰ (n = 5), whereas the TDLAS gas-phase measurements yielded −121.45 ± 4.06‰ (n = 5). The mean difference between the two methods was approximately 7.47‰, which is substantially smaller than the current isotope precision of the LUWA prototype. This result supports the reliability of the gas-phase isotope measurement workflow for LUWA-related ground calibration and prototype testing.

DISCUSSION

Solid calibration materials provide a practical alternative to conventional gaseous or liquid isotope standards for in-situ planetary measurements. Their main advantage is the ability to generate calibration gases on demand through controlled thermal decomposition, thereby reducing the complexity of storing and handling volatile standards under spaceflight conditions.

Material selection was determined not only by decomposition temperature and gas composition, but also by the different operational requirements of onboard calibration and ground validation. Ag_2CO_3 and $Cu(OH)_2$ therefore serve complementary roles in the current LUWA calibration and validation framework.

Ag_2CO_3 was selected as the reference material for the two onboard calibration units. Its comparatively gradual CO_2 release

is advantageous for controlled calibration because complete decomposition of the material is not required during a single operation. Instead, an appropriate amount of CO_2 can be released through controlled heating, and the calibration unit can be isolated after the required reference pressure is reached. The remaining material can then support subsequent calibration cycles. This operating mode enables an initial calibration after landing and additional calibrations before individual in-situ measurements.

Traceable $Cu(OH)_2$ is used primarily for ground H_2O and δD calibration, prototype testing, full process validation, and controlled regolith simulant experiments. Its low decomposition temperature, rapid H_2O release, and known stoichiometric water content make it suitable for evaluating the complete LUWA process, including sample heating, gas release, transfer, pressure measurement, and spectroscopic and mass spectrometric detection. The synthesis route developed in this study links the mean hydrogen isotope composition of the released H_2O to that of the precursor water, with absolute differences between the mean values remaining within 10‰.

The uncertainty measures associated with the precursor waters and the solid-derived vapor have different statistical meanings. The uncertainty of the precursor-water values reflects the consistency of repeated calibrated liquid injections under relatively stable analytical conditions. In contrast, the standard deviation of the solid-derived vapor reflects temporal variability during a single dynamic thermal release, in which H_2O pressure and signal intensity changed continuously. The present results therefore demonstrate consistency between the mean isotope values rather than release-to-release precision of the synthesized solid reference.

The observed differences between the mean precursor-water and solid-derived vapor values may represent the cumulative effects of precipitation, filtration, vacuum drying, thermal decomposition, gas transfer, adsorption and desorption, measurement memory, pressure-dependent spectroscopic response, and instrumental uncertainty. Because these stages were not evaluated independently, their individual contributions cannot be quantitatively separated in the present study. Nearly complete decomposition of $Cu(OH)_2$ was used to reduce additional isotope bias associated with selective partial H_2O release, but it does not eliminate possible fractionation or measurement effects during the other stages.

The current role assigned to $Cu(OH)_2$ reflects the mission configuration and calibration strategy adopted for LUWA rather than an intrinsic limitation of the material for spaceflight. Within its current ground-based role, synthesized $Cu(OH)_2$ offers several broader methodological advantages for water isotope measurements. First, it can serve as a solid isotope transfer reference by incorporating hydrogen from precursor water with a known δD value into a stable solid phase. This enables repeated evaluation of the complete solid sample measurement process, including heating, gas release, transfer, and detection. Second, it can support end to end validation of LUWA like analytical systems by allowing controlled assessment of release kinetics, gas pathway adsorption, pressure dependent isotope response, measurement memory, and consistency between spectroscopic and mass spectrometric measurements. Third, because the H_2O content of $Cu(OH)_2$ is defined by its stoichiometry, it provides a practical means of preparing regolith simulants with known and reproducible water contents, avoiding the uncontrolled sublimation and redistribution that can occur when real ice is handled under laboratory conditions.

These capabilities also indicate potential applications beyond the present LUWA ground validation program. With further optimization of storage, packaging, contamination and background control, operational procedures, and flight qualification, traceable $Cu(OH)_2$ type materials may provide controlled H_2O and δD references for future planetary payloads. In particular, a solid reference with known water content and isotope composition could provide an intermittent anchor for characterizing adsorption and desorption memory effects in carrier gas free isotope measurement systems. However, this application has not yet been implemented in the current LUWA configuration and will require further development and validation.

Known limitations include adsorption and surface exchange with atmospheric moisture, the propensity of copper hydroxide to react with CO_2 and form carbonates if stored improperly, potential kinetic isotope effects during partial equilibration or concentration-dependent release, and instrument detection limits (in our tests, the spectrometer isotope signal reached its lower detection limit when evolved H_2O partial pressure fell to ~150 Pa).

Another important advantage of traceable solid calibration materials is their ability to provide reference anchors for correcting isotope memory effects during repeated measurements. Water-isotope analyses are particularly susceptible to memory effects because residual H_2O can adsorb on chamber walls, valves, transfer lines, and optical cells, causing the isotope signal of one measurement to influence subsequent analyses. This problem may become more pronounced in spaceborne instruments, where repeated purge, bake-out, and full replacement of the gas-handling pathway are constrained by power, time, and mechanical resources. A solid calibrant with a known H_2O content and δD value can therefore serve as an intermittent truth anchor in the measurement sequence. By inserting calibration releases before, between, or after sample analyses, the residual contribution from previous measurements can be quantified, allowing correction of baseline drift, adsorption–desorption effects, and carryover-induced isotope bias. In this sense, traceable $Cu(OH)_2$ is not only a calibration source for absolute δD assignment, but also a practical tool for maintaining isotope-data consistency during repeated LUWA-related ground validation and, after further qualification, for future planetary isotope-measurement workflows.

To mitigate these risks, calibration materials should be stored under inert, anhydrous conditions or in evacuated, gas-tight

containers, and where practical, thermally pre-cleaned, with an aliquot reserved for isotopic verification. Before measurement, samples must be evacuated to high vacuum (for example, below 10^{-5} Pa) and then subjected to controlled heating, ensuring that the partial pressure of evolved gases remains under the threshold for concentration-dependent isotope effects (approximately 250 Pa). Rigorous monitoring of background levels and reproducibility through blanks and replicate releases further safeguards measurement integrity.

The isotope precision of LUWA also defines the level of source discrimination that can be realistically achieved. For a single dominant source, the designed δD precision of LUWA, approximately 50‰, is sufficient to distinguish the solar-wind end-member (δD < −980‰) from the more D-enriched asteroidal/cometary end-members, but is not sufficient to resolve asteroidal vs. cometary mixtures when the solar-wind contribution is minor. Here, the 5.3–8.3‰ isotopic offsets observed for the synthesized $Cu(OH)_2$ calibrants are smaller than the instrumental design precision and therefore are not expected to dominate the current isotope error budget. However, source interpretation becomes less straightforward when lunar water ice represents a mixture of multiple reservoirs. In particular, if the solar-wind component is absent or minor, mixed asteroidal and cometary contributions may become difficult to distinguish using δD alone because their effective isotopic signatures can overlap depending on the mixing proportion. In such cases, isotope data should be combined with quantitative mixing models, constrained by the impact history, cold-trap evolution, and thermal history of the Moon, as well as by the spatial and structural information provided by other Chang'E-7 payloads.

The solid form factor reduces leakage and handling risks relative to pressurized gas and liquid standards and is compatible with the restricted heating capability of LUWA. Ag_2CO_3 supports repeated pressure-controlled partial release for onboard referencing, whereas $Cu(OH)_2$ provides a consumable H_2O and δD reference for ground validation. The tested calibration units retained their functional calibration capability after vibration, thermal cycling, and storage for more than four months. These results support the robustness of the solid calibration approach under the tested conditions, although longer-duration stability, shelf life, and formal flight qualification require further systematic evaluation.

Overall, Ag_2CO_3 and traceable $Cu(OH)_2$ provide complementary reference functions within the LUWA calibration and validation framework. The present results demonstrate controlled target-gas generation, repeated onboard CO_2 referencing capability, and consistency between the mean isotope compositions of precursor waters and solid-derived H_2O. It provides LUWA with a traceable calibration reference for acquiring reliable H_2O and δD information, which can contribute critical isotopic constraints for interpreting the origin of lunar water ice, particularly when integrated with subsurface structural information from in-situ radar sounding, including possible ice layer boundaries, burial depth, ice layer continuity, and dielectric heterogeneity, as well as orbital remote-sensing constraints on the spatial distribution and geological context of potential ice-bearing deposits[60]. Further work should quantify release-to-release reproducibility, gas recovery and instrumental response, long-term storage stability, and the feasibility of memory-effect correction using traceable solid H_2O references.

CONCLUSIONS

Accurate in-situ detection of lunar water ice requires reliable measurements of both water abundance and hydrogen isotopic composition. Deep-space operating conditions, including ultra-high vacuum, tight energy constraints, limited sealing capability, and extreme temperature variations, challenge conventional gas- and liquid-phase calibration methods and require calibration strategies compatible with lunar operational constraints.

To meet these requirements for the Chang'E-7 LUWA, we evaluated silver carbonate and copper hydroxide as solid calibration materials. Vacuum thermogravimetric analysis showed that both materials release calibration gases within an operationally feasible temperature range under vacuum. Full-process prototype validation further confirmed that Ag_2CO_3 and $Cu(OH)_2$ can generate identifiable CO_2 and H_2O signals, respectively, for spectral and mass-spectrometric calibration. These results demonstrate the feasibility of using solid materials as compact calibration sources for LUWA under simulated space-environment constraints.

For hydrogen-isotope calibration, we developed a synthesis route for $Cu(OH)_2$ with a traceable hydrogen isotopic signature derived from precursor water. The synthesized $Cu(OH)_2$ largely preserved the isotopic information of the precursor water, providing a route toward traceable solid-phase δD calibration. We then integrated this material into a prototype water-molecule analyzer and established a solid-phase hydrogen-isotope measurement workflow, demonstrating its applicability for LUWA-related H_2O release and isotope-detection experiments.

The two materials serve different calibration roles. Ag_2CO_3 provides a stable CO_2 calibration source and is suitable for both ground-based testing and final mission calibration. The synthesized $Cu(OH)_2$ developed in this study provides a traceable solid H_2O source for hydrogen-isotope-related calibration and validation under laboratory conditions. Although our synthesis strategy effectively controls the hydrogen source and overcomes the isotope-traceability issue of commercial $Cu(OH)_2$, introducing an additional H_2O-releasing material during in-situ lunar measurements could increase the background water signal

and interfere with the analysis of indigenous lunar water. Therefore, $Cu(OH)_2$ is used primarily for LUWA ground calibration, prototype testing, and controlled regolith-simulant experiments.

In the ground-based regolith experiments, $Cu(OH)_2$ was used as a controllable analogue for ice-bearing or "dirty-ice" regolith. This strategy allows the preparation of regolith simulants with known and reproducible water contents, while avoiding uncontrolled water loss caused by sublimation during sample preparation and storage. Because the hydrogen in the synthesized $Cu(OH)_2$ is chemically incorporated from precursor water with a known isotopic composition, the material also minimizes sublimation-driven isotope fractionation before measurement. It therefore provides a stable and traceable solid H_2O source for testing the LUWA heating-release and detection process under controlled laboratory conditions.

By establishing a traceable solid-calibration route, this work improves the reliability of the first step in the Chang'E-7 water-ice information chain: the conversion of released gas signals into quantitative H_2O abundance and δD data. They can provide ground-truth-like point constraints for evaluating radar- and remote-sensing-based interpretations of polar ice deposits. For example, in-situ radar sounding can reveal subsurface layering, burial geometry, and dielectric contrasts along the rover traverse, while orbital observations can place these local measurements within the broader spatial and geological setting of candidate ice-bearing regions. In this way, calibrated LUWA data can strengthen the joint assessment of where lunar polar water ice occurs, how it is stored in the regolith, and which source reservoirs may have contributed to its formation.

REFERENCES

[1] Nakajima M. and Stevenson D.J. (2018). Inefficient volatile loss from the Moon-forming disk: Reconciling the giant impact hypothesis and a wet Moon. Earth Planet. Sci. Lett. 487:117-126. DOI:10.1016/j.epsl.2018.01.026

[2] Arnold J.R. (1979). Ice in the lunar polar regions. J. Geophys. Res. Solid Earth 84:5659-5668. DOI:10.1029/JB084iB10p05659

[3] Watson K., Murray B., and Brown H. (1961). On the possible presence of ice on the Moon. J. Geophys. Res. 66:1598-1600. DOI:10.1029/JZ066i005p01598

[4] Paige D.A., Siegler M.A., Zhang J.A., et al. (2010). Diviner lunar radiometer observations of cold traps in the Moon's south polar region. Science 330:479-482. DOI:10.1126/science.1187726

[5] Nozette S., Lichtenberg C.L., Spudis P.D., et al. (1996). The Clementine bistatic radar experiment. Science 274:1495-1498. DOI:10.1126/science.274.5292.1495

[6] Fa W. and Cai Y. (2013). Circular polarization ratio characteristics of impact craters from Mini-RF observations and implications for ice detection at the polar regions of the Moon. J. Geophys. Res. Planets 118:1582-1608. DOI:10.1002/jgre.20110

[7] Sanin A.B., Mitrofanov I.G., Litvak M.L., et al. (2017). Hydrogen distribution in the lunar polar regions. Icarus 283:20-30. DOI:10.1016/j.icarus.2016.06.002

[8] Li S. and Milliken R.E. (2017). Water on the surface of the Moon as seen by the Moon Mineralogy Mapper: Distribution, abundance, and origins. Sci. Adv. 3:e1701471. DOI:10.1126/sciadv.1701471

[9] Li S., Lucey P.G., Milliken R.E., et al. (2018). Direct evidence of surface exposed water ice in the lunar polar regions. Proc. Natl. Acad. Sci. U.S.A. 115:8907-8912. DOI:10.1073/pnas.1802345115

[10] Honniball C.I., Lucey P.G., Li S., et al. (2021). Molecular water detected on the sunlit Moon by SOFIA. Nat. Astron. 5:121-127. DOI:10.1038/s41550-020-01222-x

[11] Colaprete A., Schultz P.H., Heldmann J.L., et al. (2010). Detection of water in the LCROSS ejecta plume. Science 330:463-468. DOI:10.1126/science.1186986

[12] Spudis P.D., Bussey D.B.J., Baloga S.M., et al. (2013). Evidence for water ice on the Moon: Results for anomalous polar craters from the LRO Mini-RF imaging radar. J. Geophys. Res. Planets 118:2016-2029. DOI:10.1002/jgre.20156

[13] Mo L., Xu J., Dong Z., et al. (2025). Water ice and the shallow regolith structure of the Shackleton Crater, the Moon: Implications for future Chang'E-7 in situ radar observation. Space Sci. Technol. 5:0225. DOI:10.34133/space.0225

[14] Saal A.E., Hauri E.H., Van Orman J.A., et al. (2013). Hydrogen isotopes in lunar volcanic glasses and melt inclusions reveal a carbonaceous chondrite heritage. Science 340:1317-1320. DOI:10.1126/science.1235142

[15] Barnes J.J., Kring D.A., Tartèse R., et al. (2016). An asteroidal origin for water in the Moon.

Nat. Commun. 7:11684. DOI:10.1038/ncomms11684

[16] Greenwood J.P., Itoh S., Sakamoto N., et al. (2011). Hydrogen isotope ratios in lunar rocks indicate delivery of cometary water to the Moon. Nat. Geosci. 4:79-82. DOI:10.1038/ngeo1050

[17] Liu Y., Guan Y., Zhang Y., et al. (2012). Direct measurement of hydroxyl in the lunar regolith and the origin of lunar surface water. Nat. Geosci. 5:779-782. DOI:10.1038/ngeo1601

[18] Hallis L.J. (2017). D/H ratios of the inner Solar System. Philos. Trans. R. Soc. A 375:20150390. DOI:10.1098/rsta.2015.0390

[19] Piani L., Nagashima K., Kawasaki N., et al. (2023). Hydrogen isotopic composition of hydrous minerals in asteroid Ryugu. Astrophys. J. Lett. 946:L43. DOI:10.3847/2041-8213/acc393

[20] Wiens R.C., Bochsler P., Burnett D.S., et al. (2004). Solar and solar wind isotopic compositions. Earth Planet. Sci. Lett. 226:549-565. DOI:10.1016/j.epsl.2004.07.011

[21] Moine B., Bolfan-Casanova N., Radu I., et al. (2020). Molecular hydrogen in minerals as a clue to interpret D variations in the mantle. Nat. Commun. 11:3604. DOI:10.1038/s41467-020-17442-8

[22] Li Y., Shen S., Lu W., et al. (2026). Calibration method and implementation for the Lunar Penetrating Radar on Chang'E-7 mission (in Chinese). Chin. J. Space Sci. 46:507-519. DOI:10.11728/cjss2026.02.2025-0102

[23] Wang C., Jia Y., Xue C., et al. (2024). Scientific objectives and payload configuration of the Chang'E-7 mission. Natl. Sci. Rev. 11:nwad329. DOI:10.1093/nsr/nwad329

[24] Shen S., Tang C., Li Y., et al. (2025). The Lunar Penetrating Radar on the Chang'E-7 Rover. Space Sci. Rev. 221:98. DOI:10.1007/s11214-025-01223-0

[25] Feng J., Siegler M.A., and White M.N. (2022). Dielectric properties and stratigraphy of regolith in the lunar South Pole-Aitken basin: Observations from the Lunar Penetrating Radar. Astron. Astrophys. 661:A47. DOI:10.1051/0004-6361/202143015

[26] Li X., Cao N.L., Kan R.F., et al. (2025). Miniaturized tunable laser spectrometer for the simultaneous detection of water ice and hydrogen-oxygen isotopes for the Chang'E-7 Lunar Soil Water Molecule Analyzer. ACS Sens. 10:4679-4686. DOI:10.1021/acssensors.5c01115

[27] Pfeiffer Vacuum. (2008). The Vacuum Technology Book. Pfeiffer Vacuum.

[28] Cappa C.D., Hendricks M.B., DePaolo D.J., et al. (2003). Isotopic fractionation of water during evaporation. J. Geophys. Res. Atmos. 108:4525. DOI:10.1029/2003JD003597

[29] Repplinger C., Sellen S., Kedziora S., et al. (2024). Material modeling for numerical simulation of elastomer O-rings with experimental verification at low temperatures. Int. J. Hydrogen Energy 80:1046-1061. DOI:10.1016/j.ijhydene.2024.06.427

[30] Li X., Wang X., Lu W., et al. (2023). Design for in-situ water ice analysis in the lunar polar region. J. Deep Space Explor. 10:618-630. DOI:10.15982/j.issn.2096-9287.2023.20230106

[31] Roush T.L., Colaprete A., Cook A., et al. (2021). The Volatiles Investigating Polar

Exploration Rover (VIPER) Near Infrared Volatile Spectrometer System (NIRVSS). 52nd Lunar Planet. Sci. Conf., abstract 1678.

[32] Baldridge A.M., Hook S.J., Grove C.I., et al. (2009). The ASTER spectral library version 2.0. Remote Sens. Environ. 113:711-715. DOI:10.1016/j.rse.2008.11.007

[33] Aguilar Ayala R., Hancock M.L., Jarnot A.W., et al. (2023). Mass Spectrometer Observing Lunar Operations (MSolo). 71st ASMS Conf. Mass Spectrom. Allied Topics, Houston, TX.

[34] Colaprete A. (2021). Volatiles Investigating Polar Exploration Rover (VIPER). NASA Technical Reports Server, Document ID 20210015009.

[35] Chumikov A.E., Cheptsov V.S., Wurz P., et al. (2021). Design, characteristics and scientific tasks of the LASMA-LR laser ionization mass spectrometer onboard Luna-25 and Luna-27 space missions. Int. J. Mass Spectrom. 469:116676. DOI:10.1016/j.ijms.2021.116676

[36] Meshcherinov V., Gazizov I., Kazakov V., et al. (2024). Spectrometer to explore isotopologues of lunar volatiles on Luna-27 lander. Planet. Space Sci. 248:105935. DOI:10.1016/j.pss.2024.105935

[37] Verchovsky A.B., Anand M., Barber S.J., et al. (2020). A quantitative evolved gas analysis for extra-terrestrial samples. Planet. Space Sci. 181:104830. DOI:10.1016/j.pss.2019.104830

[38] Straus S. and Madorsky S.L. (1956). Thermal degradation of unvulcanized and vulcanized rubber in vacuum. Ind. Eng. Chem. 48:1212-1219. DOI:10.1021/ie50559a036

[39] Losekamm M.J., Barber S., Biswas J., et al. (2021). LUVMI-X: A versatile platform for resource prospecting on the Moon. In Earth and Space 2021, pp. 289-299. DOI:10.1061/9780784483374.029

[40] Morse A., Mousis O., Sheridan S., et al. (2015). Low CO/CO2 ratios of comet 67P measured at the Abydos landing site by the Ptolemy mass spectrometer. Astron. Astrophys. 583:A42. DOI:10.1051/0004-6361/201526624

[41] Chen R., Lu W., Li X., et al. (2024). Chang'E-7 Lunar Soil Water Molecule Analyzer (LSWMA) prototype for high-precision measurement of water content and hydrogen isotope ratio. J. Earth Sci. 35:2180-2182. DOI:10.1007/s12583-024-2023-7

[42] Li X., Lu W., Qiu Z., et al. (2026). Ground calibration test method for Chang'E-7 Lunar Soil Water Molecule Analyzer (in Chinese). Chin. J. Space Sci. 46:465-474. DOI:10.11728/cjss2026.02.2025-0151

[43] Chen R., Lu W., Li X., et al. (2026). A high-precision lunar soil water content estimation method designed for the Chang'E-7 Lunar Soil Water Molecule Analyzer (LSWMA). Planet 2:26011. DOI:10.15302/planet.2026.26011

[44] Vorholz J., Harismiadis V.I., Rumpf B., et al. (2000). Vapor-liquid equilibrium of water, carbon dioxide, and the binary system water-carbon dioxide, from molecular simulation. Fluid Phase Equilib. 170:203-234. DOI:10.1016/S0378-3812(00)00315-0

[45] L'vov B.V. (2002). Mechanism and kinetics of thermal decomposition of carbonates. Thermochim. Acta 386:1-16. DOI:10.1016/S0040-6031(01)00757-2

[46] Jurczyk J., Glessi C., Madajska K., et al. (2022). Vacuum versus ambient pressure inert gas

thermogravimetry: A study of silver carboxylates. J. Therm. Anal. Calorim. 147:2187-2195. DOI:10.1007/s10973-021-10616-6

[47] Shamsipur M., Pourmortazavi S.M., Hajimirsadeghi S.S., et al. (2013). Facile synthesis of zinc carbonate and zinc oxide nanoparticles via direct carbonation and thermal decomposition. Ceram. Int. 39:819-827. DOI:10.1016/j.ceramint.2012.07.003

[48] Genchi G., Sinicropi M.S., Lauria G., et al. (2020). The effects of cadmium toxicity. Int. J. Environ. Res. Public Health 17:3782. DOI:10.3390/ijerph17113782

[49] Paustenbach D.J., Tvermoes B.E., Unice K.M., et al. (2013). A review of the health hazards posed by cobalt. Crit. Rev. Toxicol. 43:316-362. DOI:10.3109/10408444.2013.779633

[50] Cheng L., Li W., Li Y., et al. (2019). Thermal analysis and decomposition kinetics of the dehydration of copper sulfate pentahydrate. J. Therm. Anal. Calorim. 135:2697-2703. DOI:10.1007/s10973-018-7595-y

[51] Paulik F., Paulik J., and Arnold M. (1992). Thermal decomposition of gypsum. Thermochim. Acta 200:195-204. DOI:10.1016/0040-6031(92)85115-C

[52] Fukuda M., Favergeon L., and Koga N. (2019). Universal kinetic description for thermal decomposition of copper(II) hydroxide over different water vapor pressures. J. Phys. Chem. C 123:20903-20915. DOI:10.1021/acs.jpcc.9b04704

[53] Kan R.F., Cao N.L., Chen R., et al. (2025). A solid calibration material for hydrogen isotopes and its preparation method. China Patent CN 119935668 B, September 30, 2025.

[54] Hynes J.T. (1985). Chemical reaction dynamics in solution. Annu. Rev. Phys. Chem. 36:573-597. DOI:10.1146/annurev.pc.36.100185.003041

[55] Kendall C. and Caldwell E.A. (1998). Fundamentals of isotope geochemistry. In Isotope Tracers in Catchment Hydrology, Kendall C. and McDonnell J.J., eds. (Elsevier), pp. 51-86. DOI:10.1016/B978-0-444-81546-0.50009-4

[56] Cole D.R. and Chakraborty S. (2001). Rates and mechanisms of isotopic exchange. Rev. Mineral. Geochem. 43:83-224. DOI:10.2138/rmg.2001.43.2

[57] Schmidt M., Maseyk K., Lett C., et al. (2010). Concentration effects on laser-based δ18O and δ2H measurements and implications for the calibration of vapour measurements with liquid standards. Rapid Commun. Mass Spectrom. 24:3553-3561. DOI:10.1002/rcm.4813

[58] Tremoy G., Vimeux F., Cattani O., et al. (2011). Measurements of water vapor isotope ratios with wavelength-scanned cavity ring-down spectroscopy technology: New insights and important caveats for deuterium excess measurements in tropical areas in comparison with isotope-ratio mass spectrometry. Rapid Commun. Mass Spectrom. 25:3469-3480. DOI:10.1002/rcm.5252

[59] Li H. and Feng L. (2019). A rapid method for determination of the hydrogen isotopes of H2O in micro-inclusions by chromium-filled elemental analyzer/isotope ratio mass spectrometry. Rapid Commun. Mass Spectrom. 33:946-950. DOI:10.1002/rcm.8430

[60] Zhao C., Zhang L., Lu S., et al. (2025). Research and prospect of ground-penetrating radar on the Moon. J. Geophys. Eng. 22:1431-1447. DOI:10.1093/jge/gxaf084

FUNDING AND ACKNOWLEDGEMENTS

This study was co-supported by the Science and Technology Development Fund of Macau (Nos. 0002/2025/AKP, 0052-2024-RIA1, 0021/2024/RIA1, 0158/2024/AFJ, 0002/2024/SKL, and 0034/2024/AMJ), the National Key Research and Development Program of China (No. 2024YFE0201000), the National Natural Science Foundation of China (Nos. 62205346, 42201389, 42104141, and W2541013), the Shanghai Pujiang Program (No. 25PJA138), the Postdoctoral Fellowship Program of CPSF (No. GZC20241751), and the Anhui Postdoctoral Scientific Research Program Foundation (No. 2024B831). The authors thank the Stable Isotope Laboratory of the Institute of Geology and Geophysics, Chinese Academy of Sciences, for conducting the Cr-EA/IRMS analyses of the synthesized solid samples. We also sincerely thank the two anonymous reviewers and the editor for their constructive comments and suggestions, which helped improve the quality and clarity of the manuscript. **The funders had no role in study design, data collection and analysis, decision to publish, or preparation of the manuscript.**

AUTHOR CONTRIBUTIONS

Rui Chen contributed to the proposal of the methodology, experimental design, construction of the experimental platform, conduction of experiments, data processing, and manuscript writing. Xiang Li and Wenzhen Lu contributed to the construction of the experimental platform, conduction of experiments, and data processing. Waikei Ng, Kan Chen, and Zhenping Sui contributed to the construction of the experimental platform. Xindong Meng, Renrui Liu, Honkuan Wong, Rongji Li, Yun Qin, and Ling Zhang were responsible for the verification and processing of experimental data. Yi Xu, Nailiang Cao, Hejiu Hui, Qiquan Yang, Xiaoping Zhang, Zhenyu Xu, Ruifeng Kan, Meiru Guo, and Rui Gao provided the experimental facilities, instruments, and revision suggestions for this manuscript. **All authors contributed to the manuscript and approved the final version.**

DECLARATION OF INTERESTS

Qiquan Yang is an Editorial Board member of *The Innovation Informatics* and was blinded from reviewing or making final decisions on the manuscript. Peer review was handled independently of this member and their research group. The other authors declare no conflicts of interest.

DATA AND CODE AVAILABILITY

The data that support the findings of this study are available from the corresponding authors upon reasonable request.

ETHICAL STATEMENT AND PATIENT CONSENT

Not applicable.

SUPPLEMENTAL INFORMATION

It can be found online at https://doi.org/10.59717/j.xinn-inform.2026.1000xx

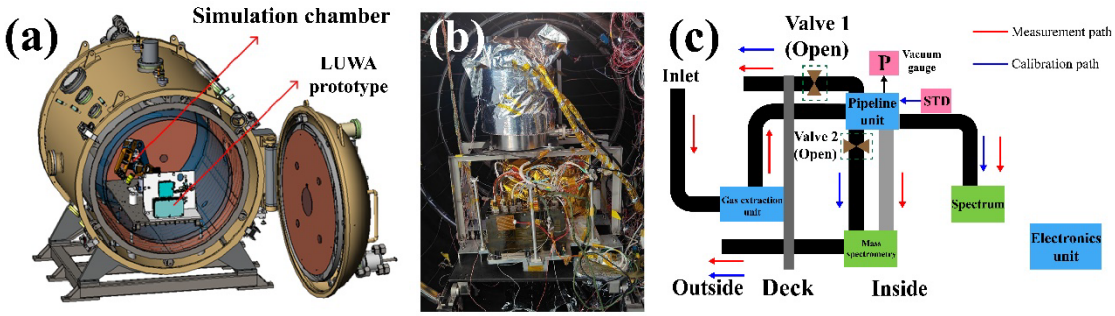

Figure 1. Ground calibration platform and LUWA prototype. (a) LUWA prototype in the simulation chamber; (b) photograph of the prototype; and (c) internal pipeline configuration.

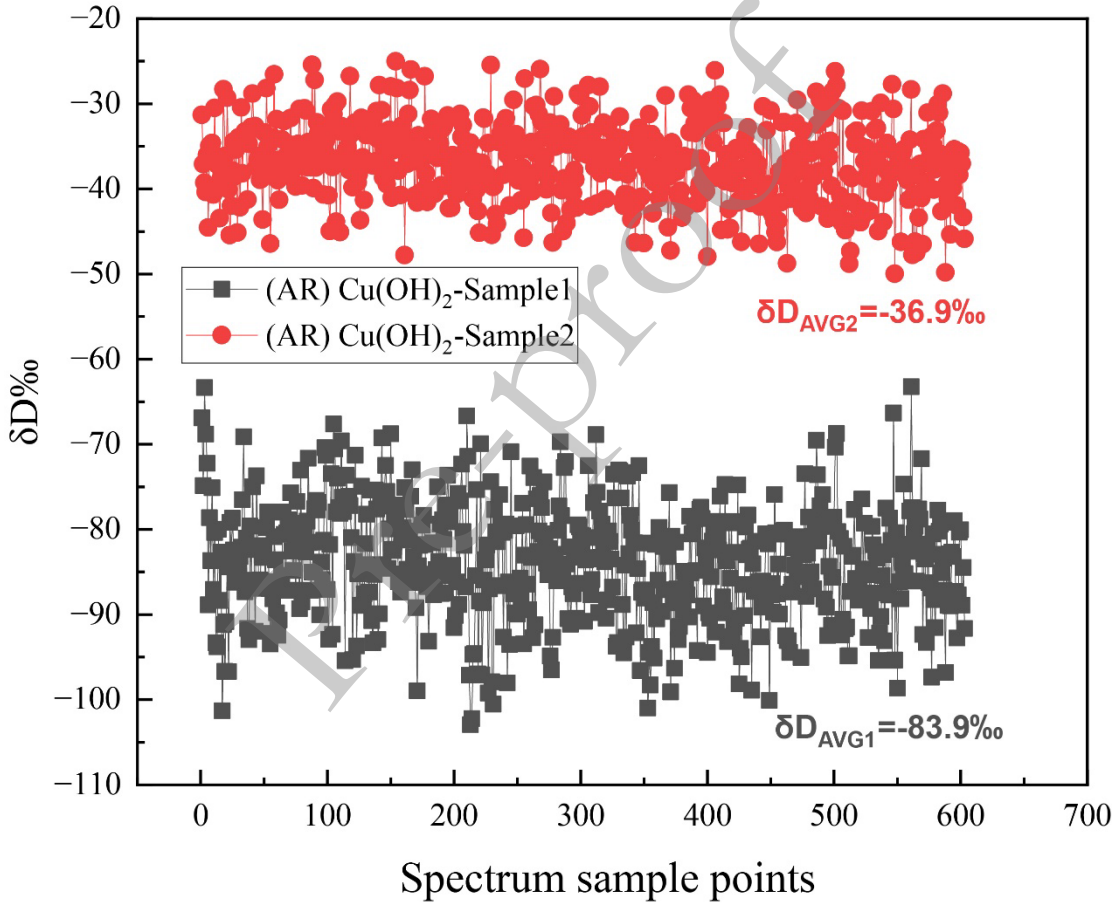

Figure 2. Time-resolved δD measurements of H_2O released from two commercial analytical-grade $Cu(OH)_2$ samples obtained from the same batch.

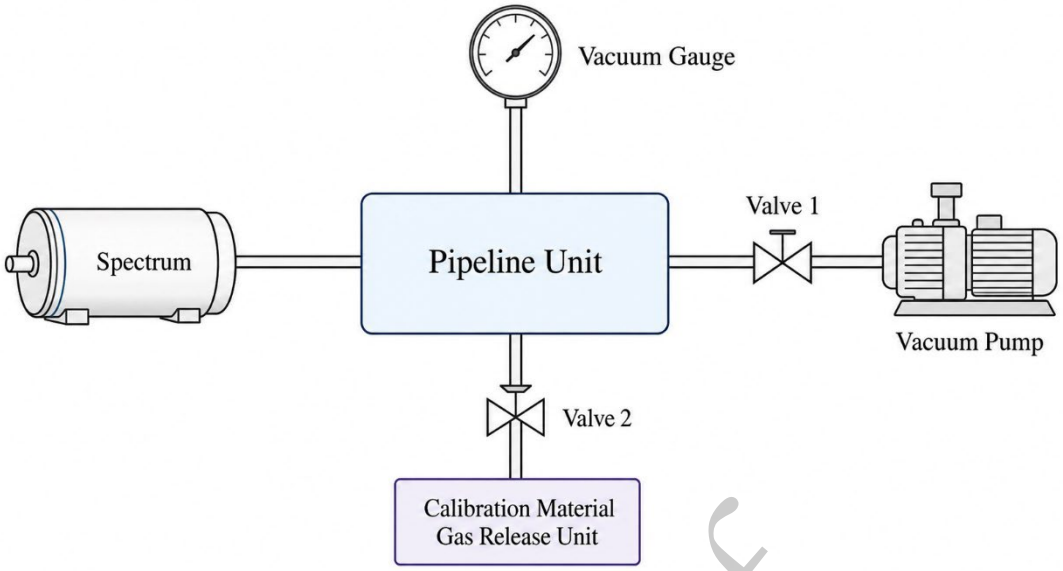

Figure 3. Solid-isotope measurement platform based on the LUWA prototype.

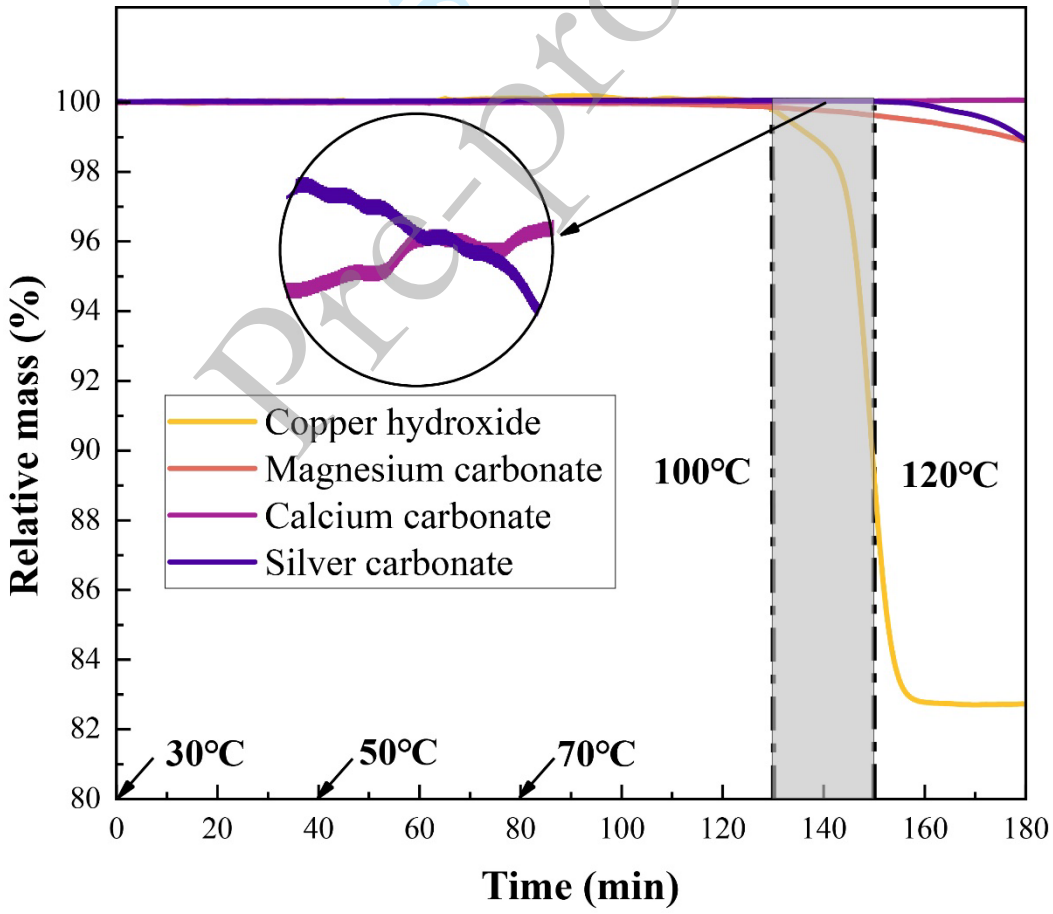

Figure 4. Averaged vacuum thermogravimetric curves obtained from two independent measurements of $CaCO_3$, $MgCO_3$, Ag_2CO_3, and $Cu(OH)_2$.

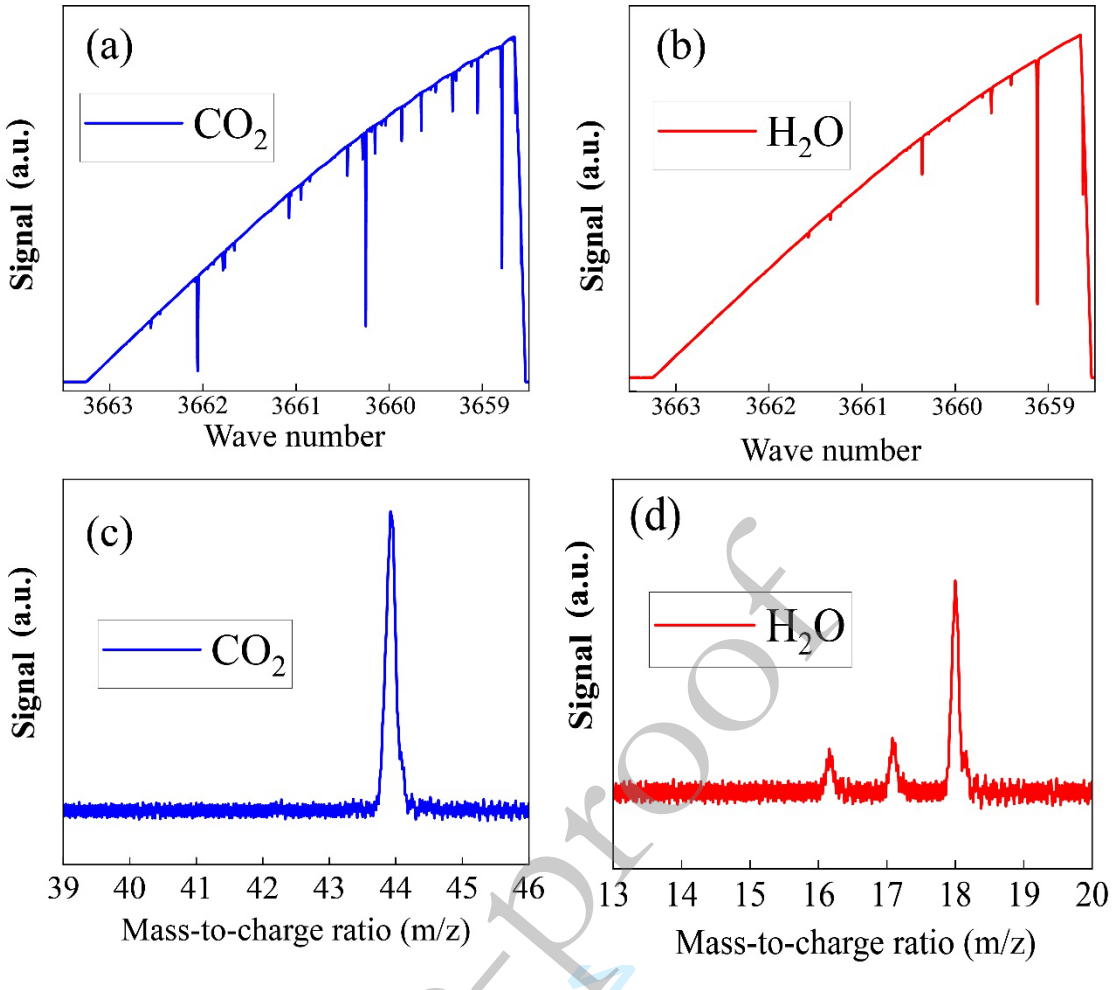

Figure 5 Spectroscopic and mass-spectrometric signals of gases evolved from Ag_2CO_3 and $Cu(OH)_2$: (a) CO_2 absorption spectrum from Ag_2CO_3; (b) H_2O absorption spectrum from $Cu(OH)_2$; (c) mass spectrum of gas evolved from Ag_2CO_3; and (d) mass spectrum of gas evolved from $Cu(OH)_2$.

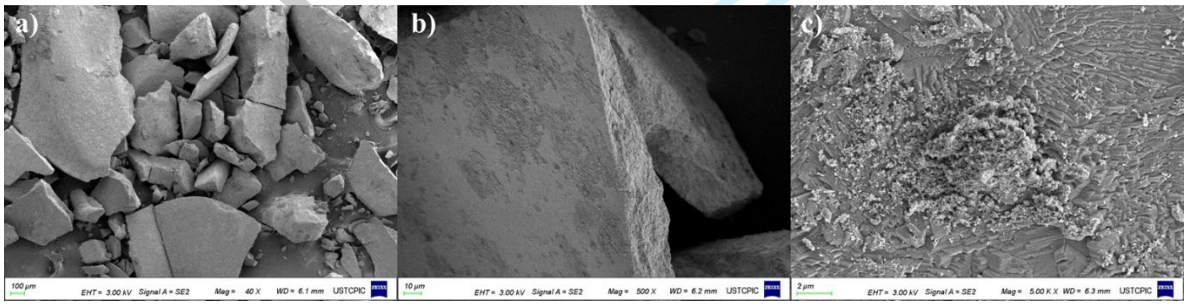

Figure 6. SEM images of synthesized $Cu(OH)_2$ at scale bars of (a) 100 μm, (b) 10 μm, and (c) 2 μm.

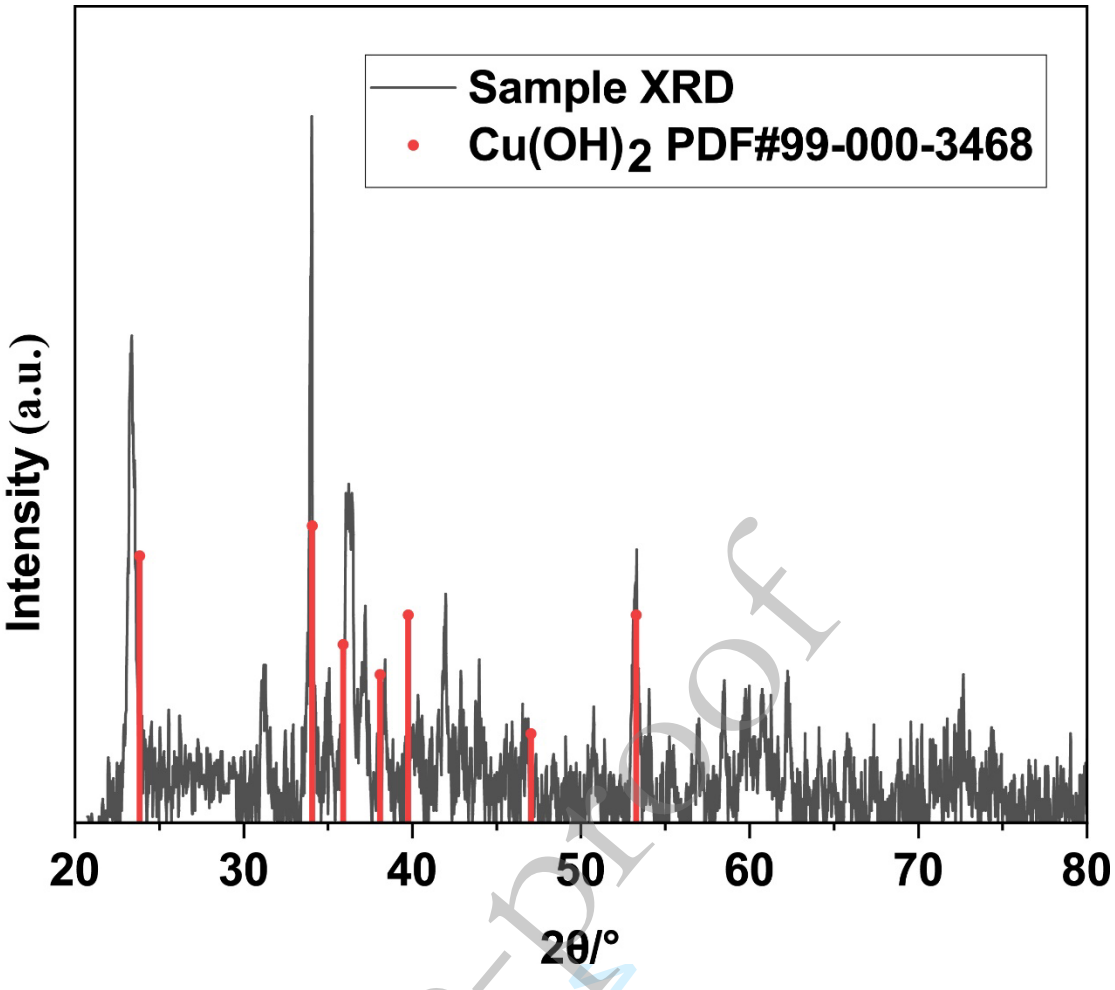

Figure 7. XRD pattern of the synthesized material compared with the reference diffraction pattern of $Cu(OH)_2$ (PDF#99-000-3468).

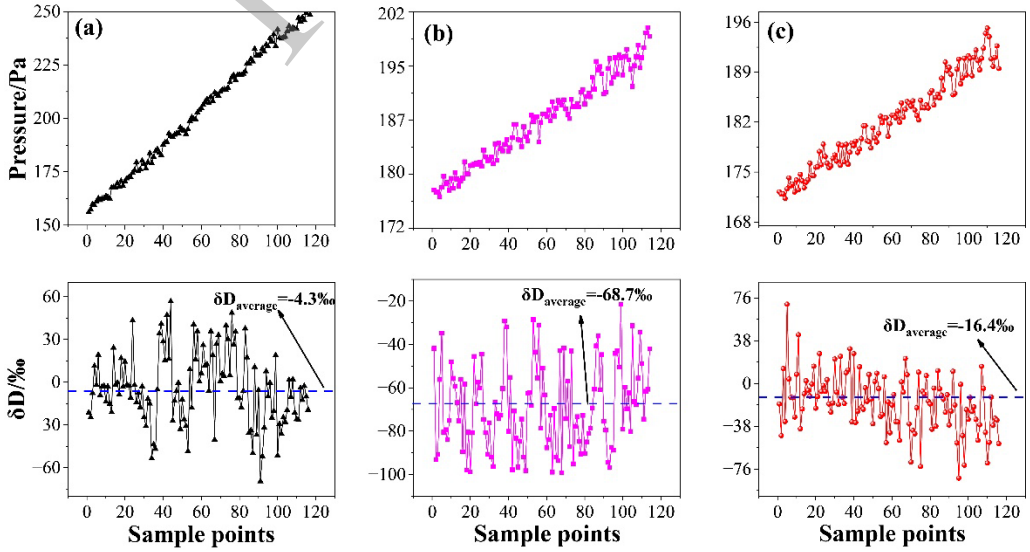

Figure 8. Time-resolved δD measurements of H_2O released from synthesized $Cu(OH)_2$ samples prepared using three precursor waters with different hydrogen isotopic compositions.

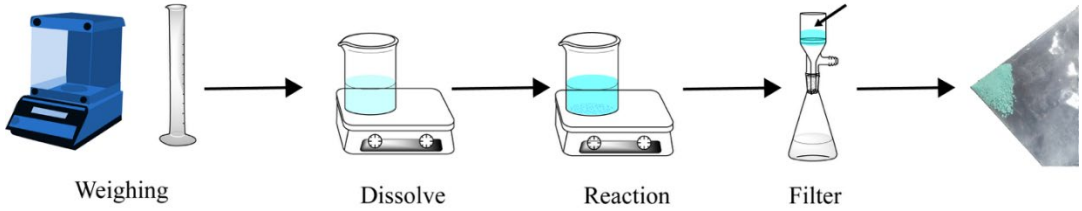

Figure S1. Schematic synthesis procedure for the traceable $Cu(OH)_2$ hydrogen-isotope reference material.

Figure S2. Instruments used in this study: (a) NETZSCH STA 2500 vacuum thermogravimetric analyzer; (b) ZEISS GeminiSEM 500 scanning electron microscope; (c) Rigaku SmartLab X-ray diffractometer; (d) Picarro L2130i hydrogen-isotope analyzer; and (e) PAL LSI automatic liquid-sample injector.

Table S1. Summary of hydrogen isotope measurements for precursor waters and H_2O released from synthesized $Cu(OH)_2$.

Sample	Precursor water δD, mean ± SD(‰)	Retained injections, n	$Cu(OH)_2$ derived H_2O δD, mean ±temporal SD(‰)	Independent releases, n	Time resolved points, n	Absolute offset (‰)
1	+4.0±0.1	4	−4.3±25.30	1	116	8.3
2	−74.0±0.1	4	−68.7±19.64	1	114	5.3
3	−24.0±0.1	4	−16.4±25.21	1	116	7.6

The precursor-water uncertainty represents the estimated analytical uncertainty of the calibrated liquid-injection procedure. The standard deviations reported for solid-derived H_2O represent temporal variability during one continuous thermal release and do not represent release-to-release reproducibility.